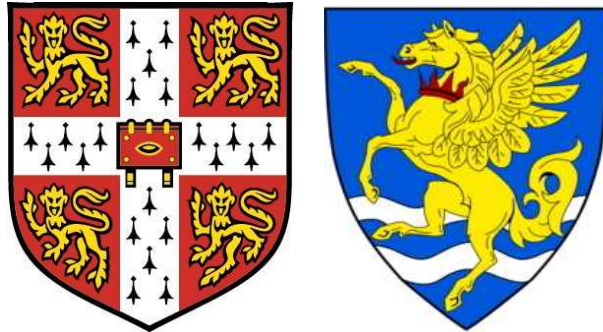# Theory of the Pearlite Transformation in Steels

By

Ashwin Suresh Pandit

Robinson College, Cambridge

University of Cambridge

Department of Materials Science and Metallurgy

Pembroke Street, Cambridge CB2 3QZ

A dissertation submitted for the

degree of Doctor of Philosophy

at the University of Cambridge

June 2011

Preface

This dissertation is submitted for the Doctor of Philosophy in Natural Sciences at the University of Cambridge. The research reported herein was conducted under the supervision of Professor H. K. D. H. Bhadeshia in the Department of Materials Science and Metallurgy, University of Cambridge, between June 2008 and June 2011.

This work is to the best of my knowledge original, except where acknowledgment and references are made to the previous work. Neither this, nor any substantially similar dissertation has been or is being submitted for any degree, diploma or other qualification at any other university or institution. This dissertation does not exceed the word limit of 60,000 words.

Some of the work described herein has been published:

1. A. S. Pandit and H. K. D. H. Bhadeshia, "Mixed Diffusion-Controlled Growth of Pearlite in Binary Steel", Proceedings of the Royal Society A 467, 508-521 (2011).

2. A. S. Pandit and H. K. D. H. Bhadeshia, "Diffusion-controlled Growth of Pearlite in Ternary Steels", Proceedings of the Royal Society A, In press.

Ashwin Suresh Pandit
June 2011

Acknowledgements

I would like to express my sincere gratitude to my supervisor Professor Harshad Kumar Dharamshi Hansraj Bhadeshia for his invaluable guidance, inspiration and encouragement during the work and my stay here. Without his motivation and quest for excellence, this work would have never been fruitful.

I would like to thank Professor A. L. Greer for the provision of Laboratory facilities in the Department of Materials Science and Metallurgy at the University of Cambridge.

I earnestly acknowledge the financial support and study leave provided by Tata Steel Limited to pursue my research at the University of Cambridge. I would like to acknowledge the valuable support and guidance provided by Dr. Debashish Bhattacharjee, Director (Research, Development and Technology, Tata Steel Europe) as my industrial supervisor. I also express my gratitude to Robinson College Cambridge and Cambridge Philosophical Society for their valuable financial support during the course of completion of my research.

I would like to thank every member of the Department and staff for being helpful and supportive to me especially Kevin, Frank, Simon and Dave. I would like to thank Mathew, Arijit and Steve for the fruitful technical discussions on related matters. All the help and support provided by Amir, Stephane, Radu, Jaiven, Pei Yan, Hala, Aseel, James, Lucy, Ivan, Hector and other past and present group members is greatly acknowledged. I shall cherish for long the memory of being with the PT-group and the coffee time discussions. The association with friends in the college and the department has been very fruitful.

I wish to express the deepest sense of gratitude to my parents for instilling good values in me and for being a constant source of inspiration. I am greatly indebted to my wife, Nishita and daughter, Devanshi for their wholehearted support, understanding and for motivating me to pursue my goals. I really appreciate the perseverance

and self-sacrifice displayed by my wife through the course of this work and for standing firm by my side through the difficult situations. I am grateful to all my family members and friends for their continuous moral support.

Abstract

A new theory has been proposed for the growth of pearlite in a binary Fe-C alloy, which tackles simultaneously the diffusion flux in the austenite and through the transformation interface. This has been shown to better represent the experimental data reported on the growth of pearlite in spite of the fact that considerations of equilibrium at junctions between interfaces are abandoned for the sake of simplicity. The theory, for the first time, leads to a realistic value for the activation energy for the interfacial diffusion of carbon, less than that for volume diffusion in austenite and greater than for volume diffusion in ferrite. The maximum growth rate and maximum rate of entropy production criteria for determining the critical interlamellar spacing have been derived in the context of mixed flux model with the result that certain parameters which are normally assumed to be constant, become a function of the transformation temperature.

For the sake of completeness, a third diffusion flux through the ferrite has also been incorporated in the mixed diffusion–controlled growth theory. Although inclusion of flux through the ferrite leads to an increase in the growth rate as compared to that through the austenite alone, it is shown that the combination of fluxes through austenite and the interface represents the experimental data rather well. Furthermore, the evidence for cementite thickening behind the transformation front, which is a natural consequence of the flux through the ferrite, is weak. Hence it is suggested that this consideration may be excluded from the proposed theory.

The growth of pearlite in a more complex ternary system containing a mixture of interstitial and substitutional solutes has also been addressed. None of the experimental data for Mn and Cr containing steels are consistent with transformation involving no-partitioning or even the negligible–partitioning of the solute between the phases involved. The available data suggest that the growth of pearlite in ternary or multicomponent steels is accompanied by the partitioning of the substitutional solute between the product phases using the assumption of local equilibrium. The

growth rate is deduced using Hillert's approach based on the thermodynamic data available from the ternary phase boundaries and assuming that the interlamellar spacing adopted is consistent with maximum rate of entropy production. The importance of a reliable value of interfacial energy, $(\sigma^{\alpha\theta})$ of ferrite-cementite interfaces is emphasised, especially when the growth rates are to be calculated in the absence of interlamellar spacing data.

In order to be able to implement the theory developed so far to an industrial scenario, a "divorced"eutectoid transformation exploited during the spheroidising annealing of steels has been discussed quantitatively. It has been shown through a rigorous analysis that there exists a wider window for the processing of these steels, which should lead to a more efficient heat treatment process.

It is thought that the work presented in this thesis can be integrated into the simultaneous transformation model which includes various other transformation products typical in steels, that would lead to better algorithms for the calculation of microstructure.

Contents

Nomenclature

α	Ferrite
$\bar{c}$	Average concentration in austenite
ΔG	Free energy change
ΔG_{chem}	Chemical free energy change
ΔH	Enthalpy change during austenite-pearlite transformation
ΔH_{form}	Enthalpy change for vacancy formation
ΔH_{m}	Enthalpy change for vacancy migration
ΔS_{form}	Entropy change for vacancy formation
ΔS_{m}	Entropy change for vacancy migration
ΔT	Undercooling
δ	Thickness of the interface
$\dot{S}$	Entropy production rate
γ	Austenite
λ	Particle spacing

ν Jump frequency

ω_γ Nearest neighbour carbon-carbon interaction energy

$\overline{D}$ Weighted average diffusion coefficient of carbon in austenite

Ψ Factor representing difference in energy required for creation of an interface and the energy released due to removal of the grain boundary area

$\sigma^{\alpha\gamma}$ Interfacial free energy per unit area for ferrite-austenite interface

$\sigma^{\alpha\theta}$ Interfacial energy per unit area of ferrite-cementite interfaces

τ Incubation time for nucleation

θ Cementite

a^γ Activity of carbon in austenite

$c^{\alpha\theta}$ Concentration in ferrite which is in equilibrium with cementite

$c_e^{\alpha\gamma}$ Concentration in ferrite which is in equilibrium with austenite

$c_e^{\gamma\alpha}$ Concentration in austenite which is in equilibrium with ferrite

$c_e^{\gamma\theta}$ Concentration in austenite which is in equilibrium with cementite

$c_e^{\theta\gamma}$ Concentration in cementite which is in equilibrium with austenite

d Austenite grain size

D_α Diffusion coefficient of carbon in ferrite

D_B Boundary diffusion coefficient

D_C^γ Volume diffusion coefficient of carbon in austenite

D_{eff} Effective diffusion coefficient

$f(t)$	Fraction transformed at time t
G^*	Critical free energy for formation of nucleus
G_{strain}	Strain energy per unit volume
G_V^{α}	Free energy per unit volume of ferrite
G_V^{γ}	Free energy per unit volume of austenite
h	Planck's constant
J	Diffusion flux
J_{V}	Nucleation rate per unit volume
k	Boltzmann's constant
N_{b}	Number of nucleation sites at the grain boundaries
N_{c}	Number of nucleation sites at the grain corners
N_{e}	Number of nucleation sites at the grain edges
N_{V}	Number of nucleation sites per unit volume
N_j	Number of particles per unit volume of true diameter j
p_j^i	probability of finding a particle of apparent diameter range i on the plane of polish from a particle of true diameter range j
Q	Activation energy
R	Universal gas constant
r	Radius of spherical nucleus at any instance
r^*	Critical radius of the nucleus
S	Interlamellar spacing

s — Boundary segregation coefficient

S^{α} — Thickness of ferrite lamellae

S^{θ} — Thickness of cementite lamellae

S_{c} — Critical interlamellar spacing

T — Absolute temperature

v — Growth rate

V_{m} — Molar volume of austenite

W — Work done for the formation of critical nucleus

x_{C} — Mole fraction of carbon in steel

Y_{C} — Site fraction of carbon in interstitial sub-lattice

Z — Zeldovich non-equilibrium factor

z — Coordination number

Chapter 1

Introduction

Pearlite is a common constituent of steels and materially adds to its strength. Typical applications of pearlitic steels include rails, ropes for bridges and elevators, tyre cords *etc.* to list a few. It has been identified since more than a century and derives its name after Sorby, who first reported that the structure resembles the irridescence of a pearl [1]. The differential etching of ferrite with respect to cementite results in the latter acting as diffraction grating for the light of various wavelengths from the pearlite colony, thus giving it a "pearly" appearance. A colony of pearlite when viewed in three dimensions consists of an interpenetrating bicrystal of ferrite and cementite [2–4]. In planar sections the phases appear as lamellae which grow at a common front with the austenite.

It is well established that with the exception of cobalt, all other alloying elements retard the transformation of austenite to pearlite as these elements decrease the nucleation and the growth rate of pearlite by shifting the time-temperature-transformation curve to longer times. This has a great technological importance in the context of the ability to produce low temperature microstructures such as bainite and martensite.

It is well known that formation of pearlite is a reconstructive process and the growth is characterised by two distinct processes: (a) redistribution of carbon into

1

cementite and (b) change in crystallographic structure since the product phases have a structure different from the parent austenite and that the rate of growth is governed by the diffusion of carbon atoms especially in Fe-C steels [5]. The active nucleus for pearlite formation can be either ferrite or cementite depending on the temperature and composition. The nucleation sites can be grain boundaries or inclusions and once either the ferrite or cementite is nucleated, the conditions surrounding the new nucleus are ripe for nucleation of the other and pearlite grows in a co-operative manner. When the austenite is supercooled below the A_1 (eutectoid temperature), and isothermally transformed, the pearlite grows at a constant rate with a constant interlamellar spacing between the ferrite and cementite. The interlamellar spacing decreases at higher undercoolings and the pearlite formed under such conditions cannot be resolved using the optical microscope. When the interlamellar spacing is large, the diffusion distances for the transport of solute are larger and hence the growth of pearlite is slowed down. The growth rate increases at higher undercoolings since the free energy change accompanying the transformation increases. However since the reaction is diffusion-controlled, the diffusion distances must be reduced to compensate for the decrease in diffusivity. Consequently the interlamellar spacing is reduced as the transformation temperature decreases.

Under certain set of conditions, pearlite may exist as spheroidised cementite in the matrix of ferrite, also termed as "divorced eutectoid". The microstructure has been named so in recognition of the fact that there is no co-operation between the ferrite and cementite as in the case of lamellar pearlite. Such structures are produced by spheroidising annealing treatment where the primary objective is to reduce the hardness in order to achieve good machinability as in the case of bearings steels. The formation of divorced eutectoid relies on the presence of finely spaced pre-existing cementite particles in the austenite matrix. The key to achieve a completely spheroidised structure lies in the heat treatment process which should avoid the formation of lamellar structure when the steel is being cooled from the austenising temperature. This summary of a few aspects of the pearlite reaction conceals numerous difficulties in the quantitative expression of its growth kinetics. The de-

tails are described in a subsequent chapter but it is important to realise that the theoretical design of steels become difficult without a proper treatment of pearlite as an intervening phase mixture.

1.1 Scope of research

It has long been possible to estimate the growth rate of pearlite assuming volume diffusion–control [6, 7] and the work has been reviewed thoroughly in [8–11]. There have, on the other hand, been reports [12–14] that the rates calculated in this way significantly underestimate those measured, possibly because of mass transport within the transformation interface [15, 16]. Most of the comparisons with experimental data have been based either on the volume or interface diffusion–controlled approach in isolation, but none of them have proved to be convincing. The former assumes that the redistribution of carbon at the transformation front occurs as a result of diffusion through the volume of austenite while the latter relies on the migration of solute through the advancing pearlite-austenite growth front. There is in principle no reason why fluxes through both of these routes should not operate simultaneously. In the absence of a clear understanding of controlling mechanisms, the outcomes of calculations are ambiguous or rely on uncertain assumptions.

Most of the commercially produced steels contain either one or more alloying additions, principally in order to improve the hardenability. The ternary steels, Fe-C-X, containing a substitutional solute (X) have been studied in considerable detail during the growth of pre-eutectoid ferrite from austenite. With pearlite there is an additional complication because of the partitioning of the substitutional solute between the product phases. It has been reported that the growth of pearlite in such steels is accompanied by either long-range partitioning of X, termed as partitioning local equilibrium or by a limited partitioning resulting in a concentration spike ahead of the transformation front, or negligible partitioning local equilibrium. Earlier studies indicated a so-called no-partitioning temperature below which the substitutional solute does not partition and the growth of pearlite is limited by the diffusion of carbon

3

[17–19]. Above this characteristic temperature the diffusion of the substitutional solute through the boundary controls the growth rate of pearlite. However neither of these two scenarios could correctly predict the growth rate at low temperatures.

In view of the uncertainties surrounding the exact mechanism for the growth of pearlite in binary and ternary steels, the current research aims at providing a simplified theory without making any prior assumptions regarding the conditions under which one or the other diffusion flux is dominant.

Chapter 2

Literature Review

2.1   General Phase Transformations in Steel

Solid-state phase transformations in steel can be classified as reconstructive or displacive. A reconstructive transformation leads to an uncoordinated movement of atoms in which there is no atomic correspondence between the parent and product phase. There is a diffusion flux of atoms that leads to a new crystal structure. The flow of matter is sufficient to minimise the strain energy so that only the volume change contributes to the alteration of shape. Such a process requires long-range diffusion, which may be sluggish at low temperatures. Allotriomorphic ferrite, idiomorphic ferrite and pearlite are examples of reconstructive transformations.

Displacive transformation is characterised by a well-coordinated movement of atoms in which the atomic correspondence between the parent and product phases is preserved. This leads to a macroscopic change in shape of the sample when the latter is not constrained. In a polycrystalline material involving several grains adjacent to each other this product phase grows in the form of thin plates which is a morphology which reduces the strain energy associated with these transformations. Displacive transformations can occur at temperatures where diffusion becomes impossible over the time scales involved. Widmanstätten ferrite, bainite and martensite, all belong

to the class of displacive transformations.

2.1.1 Rate controlling factors

The rate at which the transformation interface moves depends on its intrinsic mobility (related to the transfer of atoms across the interface) and the ease of partitioning of solutes by diffusion ahead of the transformation front. These two processes are in series and the interface velocity as calculated from the mobility always equals that based on the diffusion of solute ahead of the interface. Both of these processes dissipate the free energy available for moving the interface. When most of this free energy is dissipated in the diffusion process, the interface motion is said to be controlled by diffusion. On the other hand, when the majority is consumed in transferring the atoms across the interface, the reaction is said to be interface controlled. The concentration profiles for both these modes are shown schematically in Fig. 2.1. The terms α and β represent the phases involved, where the former is growing from the latter. The average concentration of the solute far away from the interface is represented as $\bar{c}$ and the term $c^{\alpha\beta}$ refers to the concentration of solute in α which is in equilibrium with β and $c^{\beta\alpha}$ is similarly interpreted.
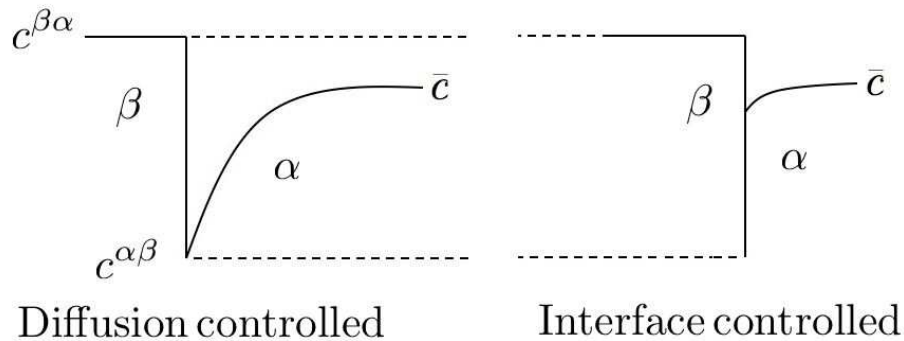

Figure 2.1: Schematic concentration profiles associated with modes of growth.

2.2 Theory of Pearlite Nucleation

2.2.1 Classical nucleation theory

One of the early contributions to classical nucleation theory was made by Volmer, and Becker and Döring, which led to intense activity on the subject. The theory states that atoms are in a state of random thermal fluctuations and only those clusters which lead to a reduction in free energy may survive and grow further. When small particles of a new phase form, there is initially an increase in the free energy because a significant proportion of atoms are situated in the transition region between the phases, where they do not have the characteristic pattern of the new phase. These small particles are thus enclosed by an interface which raises the free energy of the system. The contribution from the interfaces decreases eventually as the surface area to volume ratio of the particle decreases. In a metastable system this leads to a critical size of fluctuation beyond which the particle can grow with a reduction in free energy. Considering homogenous nucleation of a small spherical particle of radius r of a new phase α from the parent phase γ, the change in free energy is given by:

$$\Delta G = \frac{4}{3}\pi r^3 \Delta G_{\text{chem}} + \frac{4}{3}\pi r^3 G_{\text{strain}} + 4\pi r^2 \sigma^{\alpha\gamma} \qquad (2.1)$$

where $\Delta G_{\text{chem}} = G_V^{\alpha} - G_V^{\gamma}$, is the chemical free energy change and G_{strain} is the strain energy per unit volume associated with creation of α. G_V^{α} and G_V^{γ} represent the free energy per unit volume of ferrite and austenite respectively. $\sigma^{\alpha\gamma}$ is the interfacial free energy per unit area hindering the creation of the new phase. If the interfacial energy is zero then there is no barrier for nucleation and transformation starts as soon as the equilibrium temperature is exceeded. The free energy change, as a function of size of the spherical particle is shown in Fig. 2.2. Equation 2.1 can be differentiated with respect to radius, r and equating it to zero gives the maximum.

$$\frac{\delta(\Delta G)}{\delta r} = 4\pi r^2[\Delta G_{\text{chem}} + G_{\text{strain}}] + 8\pi r \sigma^{\alpha\gamma} \qquad (2.2)$$

7
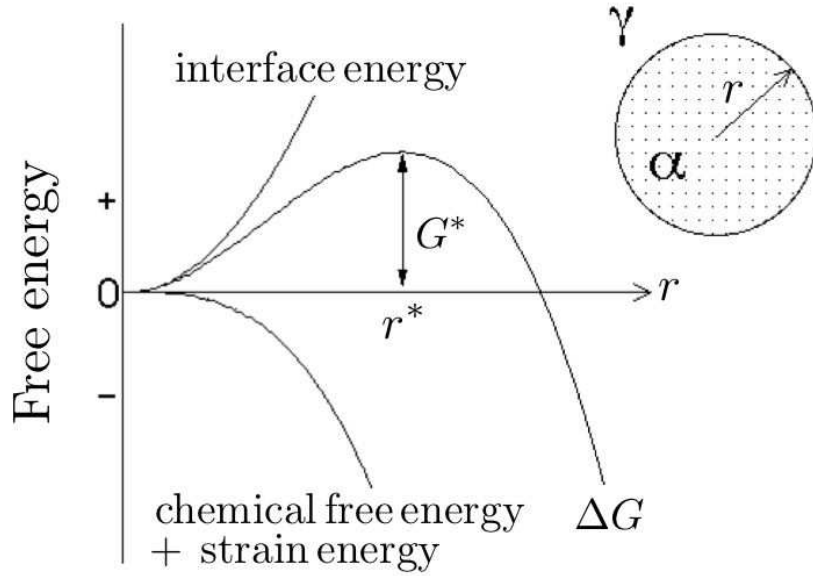
Figure 2.2: Activation energy barrier G^*.

The critical radius, r^*, can be obtained as

$$r^* = -\frac{2\sigma^{\alpha\gamma}}{\Delta G_{\text{chem}} + G_{\text{strain}}} \tag{2.3}$$

Substituting r^* in the equation 2.1 gives:

$$G^* = \frac{16\pi(\sigma^{\alpha\gamma})^3}{3(\Delta G_{\text{chem}} + G_{\text{strain}})^2} \tag{2.4}$$

The steady state nucleation rate per unit volume, J_V will depend on the attempt frequency, ν, the number of nucleation sites available per unit volume, N_V and the probability of a successful attempt:

$$J_V = Z N_V \nu \, \exp\left(\frac{-G^*}{kT}\right) \exp\left(\frac{-Q}{kT}\right) \tag{2.5}$$

where Q is the barrier for the transfer of atoms across the interface into the new phase. The above equation can also be written as:

$$J_{\mathrm{V}} = Z N_{\mathrm{V}} \frac{kT}{h} \, \exp\left(\frac{-G^*}{kT}\right) \, \exp\left(\frac{-Q}{kT}\right) \qquad (2.6)$$

The terms k and h represent the Boltzmann's constant and the Planck's constant respectively. The density of nucleation sites depends on the mode of nucleation *i.e.* from grain boundaries to edges to corners. N_{V} in the generic equation 2.6 can then be replaced by N_{b}, N_{e} and N_{c} depending on the site of nucleation. Cahn has derived the following expressions for the density of nucleation sites [20]

$N_{\mathrm{b}} = N_{\mathrm{V}}(\delta/d)$

$N_{\mathrm{e}} = N_{\mathrm{V}}(\delta/d)^2$

$N_{\mathrm{c}} = N_{\mathrm{V}}(\delta/d)^3$

where δ is the thickness of the grain boundary and d is the austenite grain size. The G^* can be written as: $G^* = \Psi/\Delta G_{\mathrm{V}}^2$ [21]. Ψ represents the difference in energy required for the creation of an interface and the energy released due to removal of the grain boundary area. The creation of a new nucleus requires energy for interface formation between the parent and product phase, which in turn is supplied by the removal of grain boundary area. The uncertainty in Ψ makes the nucleation rate difficult to estimate. A model by Lange gives $\Psi = 2.1 \times 10^{-6}$ J^3 m^{-6} for a nucleus where the shape is assumed as a pillbox [22]. Another by Clemm and Fisher predicts the Ψ as 3.3×10^{-3} J^3 m^{-6} for grain corner nucleation [23]. ΔG_{V}, which is the driving force for austenite to pearlite transformation can be calculated based on thermodynamics.

2.2.2 Theory of transient nucleation

According to classical nucleation theory, the time dependent nucleation rate can be expressed as [24]:

$$J_{\mathrm{V}} = Z \nu N_{\mathrm{V}} \, \exp\left(\frac{-G^*}{kT}\right) \exp\left(\frac{-\tau}{t}\right) \qquad (2.7)$$

where Z is the Zeldovich non-equilibrium factor which gives steady-state concentration of critical nuclei as opposed to the equilibrium concentration, τ is the incubation time and t is the time for nucleation. The time independent part of the above equation gives the steady state nucleation rate.

Offerman *et al.* studied a Fe-0.71C-0.61Mn-0.26Cr-0.34Si wt% steel to measure the nucleation and growth rate of pearlite using in-situ three-dimensional neutron dipolarisation technique [21]. They studied the steel at three different temperatures namely 953 K, 948 K and 943 K by holding each of them for different lengths of time. The nucleation rate was estimated based on the number of pearlite nuclei formed as a function of transformation time. It was observed that the number of pearlite colonies increased quadratically with time. The value of Ψ_θ was calculated as 2.2×10^{-3} J^3 m^{-6} for cementite nucleation during pearlite formation. From synchrotron measurements they determined Ψ_α as 5×10^{-8} J^3 m^{-6} for the nucleation of ferrite from austenite in a medium carbon steel [25]. The effect of interfacial energy on the activation energy of pearlite nucleation is about 5 orders of magnitude higher for cementite than for ferrite nucleation. It was suggested that the main difference between nucleation of pro-eutectoid ferrite and pearlitic cementite is that the former takes place on the high energy $\gamma - \gamma$ grain boundaries, whereas the latter takes place on the low energy $\gamma - \alpha$ interfaces. The lower value of Ψ_α suggested that the nucleation of proeutectoid ferrite was relatively easy as compared to that of pearlitic cementite.

2.3   Methods to Determine the Rate of Nucleation

The rate of nucleation is generally defined as the number of nuclei forming per unit time per unit volume of the untransformed matrix, designated as J_V and expressed as no. mm^{-3} s^{-1}. Mehl and co-workers have shown that the nucleation rate of pearlite increases with time and decreases with temperature before passing through a maximum and is slowed down by alloying additions which increases the hardenability

of the steel [26]. In the case of pearlite, where nucleation occurs on grain boundaries, N_V will be a function of the austenite grain size.

2.3.1 Measurements based on stereology

Stereological methods involve the estimation of the number of pearlite nodules per unit volume by measuring the particle size distribution [22]. The particle density, when divided by the unreacted grain boundary area per unit volume, gives the number of particles per unit unreacted grain boundary area. Such a procedure is repeatedly carried out for increasing times on specimens at a given temperature. The nucleation rate is thus obtained by taking the slope of plot of number of particles per unit unreacted grain boundary area as a function of reaction time. A further simplification of this analysis is done by assuming that particles are spherical, randomly distributed and are of the same size, which yields [22]:

$$N_V = N_A/2r_{max} \tag{2.8}$$

where N_V is the number of particles per unit volume, N_A is the number of particles of unit area on the plane of polish and r_{max} is the radius of the largest particle on the plane of polish. Another approach separates the particles into discrete diameter ranges measured on the polishing plane followed by a calculation of the distribution of true particle diameters. The equation can be described as:

$$N_j = \Sigma_{i=1}^{l} p_j^i n^i \tag{2.9}$$

where l is the number of size ranges, N_j is the number of particles per unit volume of true diameter j, p_j^i is the probability of finding a particle of apparent diameter range i on the plane of polish from a particle of true diameter range j, n^i is the number of measured (apparent) diameters in the ith category. Summing up the number of particles in all diameter ranges gives the particle number density N_V:

$$N_V = \Sigma N_j \tag{2.10}$$

The methods described above prove to be inaccurate when small particles cannot be resolved.

2.3.2 Based on transformed volume fractions

The simplest method for the calculation of nucleation rates using experimental data is based on the Johnson-Mehl approach. For specific assumptions outlined below it is expressed as:

$$f(t) = 1 - \exp(-\pi J_V v^3 t^4/3) \tag{2.11}$$

where $f(t)$ is the fraction transformed at time t, J_V is the nucleation rate per unit volume of the untransformed matrix and v is the growth rate. This method assumes that both the nucleation and growth rates are independent of time, the nuclei are randomly distributed spheres and the rate of transformation is proportional to the fraction of untransformed matrix. The average nucleation rate can be calculated by measuring $f(t)$ and v.

However, Cahn and Hagel have pointed out that for the pearlite reaction, nucleation and growth rates are usually not constant, the pearlite nodules are not normally spherical, nucleation sites are not random (preferably at grain boundaries) and all the sites are usually consumed at relatively low values of fraction transformed [27]. According to them, pearlite nucleation increases with time and in most steels it is fast enough to give site saturation at fairly high temperatures. While in the initial stages, pearlite reaction is sensitive to nucleation rate, J_V, drastic changes in J_V in the middle and later stages have little effect on the overall rate of transformation.

2.4 Influence of Grain Boundary Sites on Nucleation

Clemm and Fisher have derived the critical free energy for the formation of a nucleus at the two, three or four grain junctions, based on the knowledge of volume, surface

area and the matrix grain boundary area where the nucleus initiates [23]. Using the theory described earlier, the critical energy required for the formation of a nucleus of a new phase B in a homogeneous matrix of phase A can be rewritten as:

$$G^* = \frac{16\pi(\sigma^{\mathrm{AB}})^3}{3\Delta G_{\mathrm{V}}^2} \tag{2.12}$$

In a polycrystalline material, nucleation is more likely to take place at the grain boundaries or at junctions between several grains. This is because the energy required for the formation of a critical nucleus is provided partly by the grain boundary area which is destroyed by the formation of new nucleus, thereby reducing the activation barrier. Assuming that the grain boundary area of matrix A-A eliminated during the formation of a nucleus of B at a grain junction of A is $A_{AA} = ar^2$, where r is the radius of curvature of surface bounding the new phase, the new grain boundary area formed between A and B, be $A_{AB} = br^2$. Let the volume of the new phase formed be $V = cr^3$. The coefficients a, b and c are functions of grain boundary energies A-A and A-B. The work done in forming the nucleus is:

$$W = \sigma_{AB}br^2 - \sigma_{AA}ar^2 + \Delta G_{\mathrm{V}}cr^3 \tag{2.13}$$

The work done for the formation of critical nucleus corresponds to $dW/dr = 0$

$$G^* = 4\frac{(b\sigma_{AB} - a\sigma_{AA})^3}{27c^2\Delta G_V^2} \tag{2.14}$$

Nucleation at grain junctions can be evaluated by determining the values of a,b and c corresponding to 2, 3 or 4-grain junctions. The activation energies of nucleation of ferrite in austenite at the 2-grain, 3-grain and 4-grain junctions are shown in Fig. 2.3. It is concluded that G^* is the least for a 4-grain junction which means it is the most favoured site for ferrite nucleation, followed by 3-grain and 2-grain junctions. When the nucleus forms at the 4-grain junction, the energy supplied by the elimination of the boundary at these junctions is higher than in case of 2 or 3-grain junctions. Thus the requirement for net energy of critical nucleus formation is reduced in case

of 4-grain junctions.
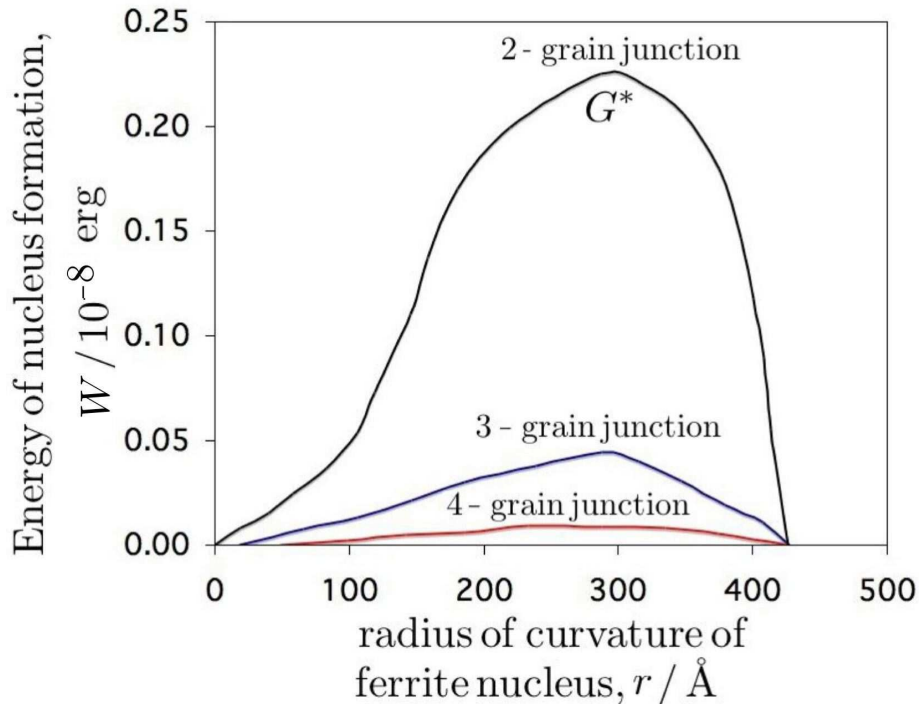
Figure 2.3: Energy for ferrite nucleus formation (adopted from Clemm and Fisher [23]). The calculations are based on $\sigma^{\gamma\gamma} = 0.85\,\mathrm{J\,m^{-2}}$ and $\sigma^{\gamma\alpha} = 0.6\,\mathrm{J\,m^{-2}}$.

2.5   Active Nucleus for Pearlite Formation

Mehl and Dubé suggested that the orientation relationship observed between the ferrite in pearlite and the parent austenite is not that observed when the ferrite forms directly from austenite [28]. Hence the active nucleus must be cementite. Subsequently Smith and Mehl reinforced this view by arguing that when the orientation of ferrite in bainite with respect to austenite was crystallographically identical to that of Widmanstätten ferrite, then ferrite was the active nucleus for bainite [29]. Conversely, the orientation of ferrite in pearlite was not the same as that for Wid-

manstätten ferrite, cementite must be the active nucleus for pearlite formation. The authors did not recognise the fact that pearlitic ferrite could be unrelated to the austenite grain in which it was growing.

Smith suggested that the crystal of proeutectoid ferrite, formed at the boundary between the two austenite grains would have a definite orientation relationship to one of them, resulting in a partially coherent interface. As a consequence of this, it will form an incoherent interface with the adjacent austenite grain. At lower undercoolings, the ferrite with an incoherent interface will grow into the grain with which it has no orientation relationship. In a similar way, the ferrite component of a pearlite colony formed at the austenite grain boundary should also be related to one of the austenite grains, irrespective of whether it is nucleated before or after the cementite. Consequently, the pearlite colony will be able to grow by the movement of an incoherent ferrite-austenite interface *i.e.* into the austenite grain to which the ferrite is unrelated. The pearlitic ferrite should then bear a specific orientation relationship to the neighbouring austenite grain. This hypothesis was thus able to refute the observations made by Mehl and Dubé regarding different orientation relationships for pearlitic and Widmanstätten ferrite with respect to the austenite grain [30]. Thus ferrite may also serve as an active nucleus for pearlite formation. Hillert suggested that the misinterpretation of X-ray results of Mehl *et al.* may be attributed to the fact that they had used a single crystal of austenite in their study of pearlite and observed that the pearlitic ferrite did not have an orientation relationship with the parent austenite [31]. Such a conclusion had no bearing on a polycrystalline specimen.

Nicholson used the phase diagram to show that both ferrite and cementite can be active nuclei depending on composition and temperature, which affect the nucleation rates of these two phases [32]. Below the eutectoid temperature, the austenite is supersaturated with both ferrite and cementite and for whichever phase it is greatest, that phase will nucleate first. These considerations are based entirely on the concentration and hence not strictly valid.

However, Russell, using free energy diagrams, put forward the following theory [33]. Below the eutectoid temperature ferrite and cementite are the stable phases and the equilibrium concentrations are given by drawing a common tangent, AB to the pairs of free energy curves shown in Fig. 2.4. For an alloy of composition c_1, the driving force for nucleation is given by drawing a tangent to the austenite curve at c_1 and the intersection of these tangents with the iso-concentration lines of ferrite and cementite at the equilibrium concentrations of these two phases, c^α and c^θ. For austenite of composition c_1, the chemical free energy change for nucleation of cementite is ΔG_{Va} which is negative and for ferrite it is ΔG_{Vb} which is positive. As a result, the nucleation of cementite is thermodynamically feasible, whereas that of ferrite is not. When the composition of austenite is c_2, the situation is reversed and ferrite nucleation becomes feasible with the driving force as ΔG_{Vd} and the cementite nucleation is not possible ($\Delta G_{Vc} > 0$). In this case, ferrite will nucleate first and the cementite will not nucleate until the local composition of austenite near the ferrite is readjusted such that cementite nucleation becomes thermodynamically feasible. At composition c_0, the free energy change for ferrite and cementite becomes equal ($\Delta G_V < 0$) and hence there is an equal probability of ferrite and cementite nucleation. Based on this discussion, Russell concluded that ferrite would be the active nucleus in case of hypoeutectoid steels and cementite for hypereutectoid steels.

2.6   Orientation Gradients in Pearlite

The strength of a ferrite-pearlite steel is generally attributed to the interlamellar spacing of ferrite and cementite in the pearlite colonies and it follows a Hall-Petch type relationship [35]. Apart from the contribution of interlamellar spacing, the strength is often attributed to the prior austenite grain size, size of the pearlite colony, amount of elements in solid solution and dislocation density in ferrite, *etc.* Ray and Mondal have shown that the strength of steel may not be dictated by a Hall-Petch type relationship and there is a considerable variation in the strength levels even with constant interlamellar spacing in pearlite colonies in case of hypoeutectoid steels [36]. They attributed the strength variation to the hydrostatic stresses exerted by the
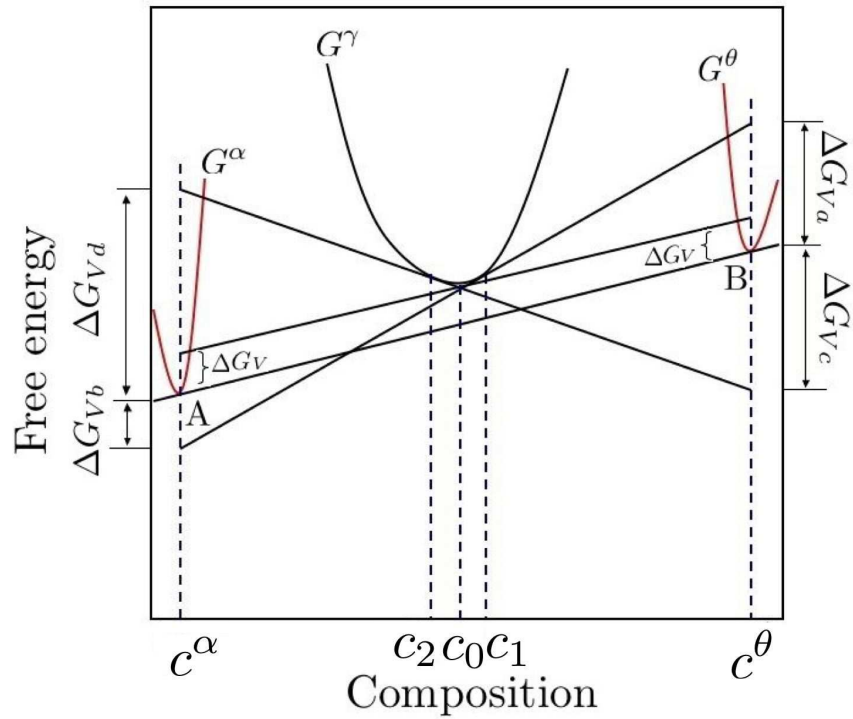
Figure 2.4: Free energy composition diagram for pearlite nucleation (adapted from P. R. Engel [34]).

presence of proeutectoid ferrite in the microstructure. It is a common observation that the lamellar structure of pearlite is not always homogeneous and consists of various substructures even in the annealed condition.

Bramfit and Marder have shown that these substructural faults may be due to higher dislocation densities and extended dislocation substructures in the pearlitic ferrite and were associated with the discontinuities in the growth of that pearlite colony [37]. They also cited other substructural features such as dislocations at the cementite-ferrite interface and discontinuities in cementite lamellae containing a high density of dislocations. The substructural faults may originate as a combination of factors such as stresses due to phase transformation, due to inherent difference in crystallographic structures of ferrite and cementite and stresses resulting from external factors such as cooling from the transformation temperature. Reviewing these observations, Bramfit and Marder suggested that the effect of these factors on the strength of pearlite has been grossly underestimated. The contribution of these influencing factors have only been restricted to explain the deviations in the strength of pearlite during statistical analyses.

Takahashi *et al.* have dealt with the influence of substructure and the crystallographic texture of pearlite in their review [38]. They used a high resolution electron backscattered diffraction technique for the analysis of pearlitic ferrite and found that large misorientation gradients were observed, in contrast to the proeutectoid ferrite surrounding the pearlite colony, where no such gradients were observed. They also observed the orientation relationship between the ferrite and cementite in the pearlitic colonies was closer to Pitsch-Petch. The pearlite colonies showed a large number of geometrically necessary dislocations and it was suggested that these were formed during the course of pearlite growth. They attributed the large scatter observed in the strength of pearlite to the density of these dislocations.

2.7   Mechanism of Diffusion in Metals

Substitutional diffusion in metals is controlled by a vacancy mechanism. The diffusion coefficient can be expressed in classical form as:

$$D = ga^2\nu \exp\left(\frac{\Delta S_{\text{form}} + \Delta S_{\text{m}}}{k}\right) \exp\left(-\frac{\Delta H_{\text{form}} + \Delta H_{\text{m}}}{kT}\right) \qquad (2.15)$$

where g is a geometric factor, a is the lattice constant, ν is an attempt frequency and T is the absolute temperature. ΔS_{form} and ΔS_{m} are the changes in vibrational entropy of the crystal associated with the formation and migration of the vacancy respectively and ΔH_{form} and ΔH_{m} are the corresponding changes in enthalpy of vibration.

The term $ga^2\nu \exp\left(\frac{\Delta S_{\text{form}} + \Delta S_{\text{m}}}{k}\right)$ is often summed up as the pre-exponential factor D_0 and the activation energy is the sum of ΔH_{form} and ΔH_{m}. Bokshtein stated that the evaluation of pre-exponential factor using the theory of transition state projects the values of D_0 in the range of 10^{-2} and $1\,\text{cm}^2\,\text{s}^{-1}$ and that values lower than these are incompatible [39]. He further included a factor f which accounts for the fact that the atomic jumps in case of self and impurity diffusion are not random. For cubic crystals, in case of self-diffusion by vacancy mechanism $f = 1 - \frac{2}{z}$, where z is the coordination number; hence for a face-centred cubic (FCC) lattice, f would be 0.78.

The vacancy concentration in the material increases exponentially with temperature, although its absolute value is not large. Even at temperatures close to melting point it does not exceed 0.01-0.1 vol.%.

2.7.1 Volume diffusion coefficient of carbon in austenite

Ågren formulated an equation for the volume diffusion coefficient of carbon in austenite, D_C^γ, based on the temperature and average carbon concentration [40]:

$$D_C^\gamma = 4.53 \times 10^{-7} \left(1 + Y_C(1 - Y_C)\frac{8339.9}{T}\right) \exp\left\{-\left(\frac{1}{T} - 2.221 \times 10^{-4}(17767 - 26436Y_C)\right)\right\} \tag{2.16}$$

where D_C^γ is in m^2 s^{-1} and temperature, T in K. The site fraction Y_C of carbon in the interstitial sub-lattice is given by :

$$Y_C = \frac{x_C}{1 - x_C} \tag{2.17}$$

where x_C is the mole fraction of carbon in the steel. Since the diffusivity of carbon is strongly dependent on concentration, it becomes imperative to account for this in the diffusion controlled growth reactions where there are gradients in concentration. Trivedi and Pound have demonstrated that a weighted average diffusion coefficient can adequately represent the effective diffusivity of carbon in austenite [41]:

$$\bar{D} = \int_{c_e^{\gamma\theta}}^{c_e^{\gamma\alpha}} \frac{D_{11}\{c^\gamma, T\}}{c_e^{\gamma\alpha} - c_e^{\gamma\theta}} dc^\gamma \tag{2.18}$$

where $c_e^{\gamma\alpha}$ is the concentration expressed as mole fractions of carbon in austenite which is in equilibrium with ferrite. c^γ is the concentration of carbon in austenite and is expressed as a mole fraction. A theoretical expression for $D_{11}\{c^\gamma, T\}$ given by Siller and McLellan considers both the thermodynamic and kinetic behaviour of carbon in austenite [42]. This model takes into account the concentration dependence of the activity of carbon in austenite and the existence of a finite repulsive interaction between nearest neighbouring carbon atoms situated in octahedral sites. The diffusivity is represented by:

$$D_{11}\{c^\gamma, T\} = \frac{kT}{h} \exp\left(\frac{-\Delta G^a}{kT}\right) \left(\frac{\lambda_d^2}{3\Gamma_m}\right) \eta(\theta) \tag{2.19}$$

$$\eta(\theta) = a^\gamma \left[\left(1 + \frac{z(1+\theta)}{1 - (0.5z+1)\theta + [0.25z^2 + 0.5z][1-\phi]\theta^2} + (1+\theta)\frac{\partial a_1{}^\gamma}{\partial \theta} \right] \quad (2.20)$$

where z is the number of octahedral interstices around a single interstice (z=12 for austenite), ΔG^a is the activation free energy, Γ_m is the activity coefficient of the activated complex, λ_d is the distance between two austenite planes, and a^γ is the activity of carbon in austenite. The term ϕ is given by:

$$\phi = 1 - \exp\left(\frac{-\omega_\gamma}{kT}\right) \quad (2.21)$$

where ω_γ is the nearest neighbour carbon-carbon interaction energy. Bhadeshia found $\Delta G^a / k = 21230$ K and $\ln(\Gamma_m/\lambda_d^2)$=31.84 [43].

2.7.2 Grain boundary diffusivity

Grain boundary diffusion plays a vital role in many processes such as discontinuous precipitation, recrystallisation, grain growth etc. It is also a well-established fact that a grain boundary provides an easy diffusion path for solutes due to its more open structure than the otherwise perfect lattice. In the case of self diffusion, the grain boundary diffusivity is usually expressed in terms of two parameters namely the thickness δ and the diffusion coefficient D_B due to the difficulty in measuring the thickness of the grain boundary. In case of impurities, however the coefficient is expressed as $sD_B\delta$, where s is the boundary segregation coefficient (ratio of solute in the interface to that in the bulk). In spite of the importance of grain boundary diffusion, not many experimental data exist and one has to rely on approximations. Fridberg *et al.* compared the diffusion coefficients of alloy elements with the self-diffusion of iron in the same phase. They measured the grain boundary diffusivities of some substitutional elements like Cr, Mn, Ni and Mo in austenite and found them to be nearly the same as grain boundary diffusivity of iron in austenite. This may not be surprising since these are some of the nearest neighbours of iron in the periodic

table [44]. Thus the term $D_{\mathrm{B}}\,\delta$ was taken as :

$$D_{\mathrm{B}}\,\delta = 5.4 \times 10^{-14} \exp\left(\frac{-155000\,\mathrm{J\,mol}^{-1}}{RT}\right) \quad \mathrm{m}^3\mathrm{s}^{-1} \qquad (2.22)$$

where D_{B} is the boundary diffusion coefficient of the solute.

2.7.3 Diffusion along phase boundaries

A phase boundary has lots of similarities to that between grains of identical structure with respect to the crystallographic discontinuity, accumulation of dislocations and chemical segregation etc. The diffusivity at these boundaries may differ considerably from that in the lattice. Most commercial alloys exist as heterogeneous structures and have two or more phases. In the case of the pearlite transformation in steels, diffusion along the transformation front becomes significant for substitutional solutes. The diffusivity depends on the state of coherency of the interface, with diffusivities becoming faster as the structure becomes less coherent. In this context Bokshtein *et al.* [39] reported a fundamental difference between a grain boundary and a phase boundary. The second phase serves as an inclusion in the matrix and hence the phase boundary may not exist as a branched network as opposed to a grain boundary network, in which case the material transport through the phase boundary is slower than the network of grain boundaries (During isothermal holding at high temperature, the state of the grain boundary does not change appreciably) but there is a significant alteration in the case of a phase boundary. Such changes are observed during ageing treatments, wherein there is a transition in the second phase from coherence to the state of separation leading to changes in structure, surface energy and other properties. In a quantitative evaluation of diffusion of Ni in cast iron using autoradiography and sectioning technique, the activation energy of Ni diffusion along the ferrite-graphite interphase boundary was reported as 121 kJ mol^{-1} [45]. This value is close to the activation energy of self diffusion in iron, 128 kJ mol^{-1}. The high diffusivity here is attributed to the weak interaction between the ferrite graphite-phases at the boundary. The kinetics of diffusion are also believed to be

a function of shape of the second phase particles apart from the size reflecting the differences in the structure and energy of the phase boundary. It has been shown that for diffusion of Ni in steel for a structure containing globular cementite, the activation energy energy ($163.8 \, \mathrm{kJ \, mol^{-1}}$) is higher than for a lamellar cementite ($134.4 \, \mathrm{kJ \, mol^{-1}}$) in a temperature range 500°C to 650°C [45]. This may be attributed to the larger defect density at the lamellar interface as compared to the globular interface.

2.8 Mechanisms of Pearlite Growth

There are two principal mechanisms cited in the literature to explain the kinetics of pearlite growth, one involves the volume diffusion of carbon ahead of the transformation front, while the other relies on interfacial diffusion as the rate-controlling step.

2.8.1 Volume diffusion

Zener-Hillert theory: During the growth of pearlite, carbon must be transported from the edges of the ferrite lamellae to neighbouring cementite lamellae [7]. Here the diffusion is assumed to occur through the parent austenite phase. If the interfaces of ferrite-austenite and cementite-austenite are assumed to be planar, the concentration difference which drives the diffusion would be ($c_e^{\gamma\alpha}$-$c_e^{\gamma\theta}$), where $c_e^{\gamma\alpha}$ and $c_e^{\gamma\theta}$ are the concentrations in austenite which is in equilibrium with ferrite and cementite respectively. These terms can be obtained from the extrapolated phase boundaries of the $Fe - Fe_3C$ phase diagram. However, because of curvature, the ($\gamma/\alpha+\gamma$) phase boundaries cannot simply be extrapolated linearly but should be extended based on thermodynamic considerations. It was suggested by Zener that the real concentration difference would be represented approximately by (1-S_c/S)($c_e^{\gamma\alpha}$-$c_e^{\gamma\theta}$) because of the α/θ interfaces. S_c is the critical spacing at which the pearlite growth rate becomes zero and S is the interlamellar spacing. The term $(1 - S_c/S)$ in equation, accounts for the decrease in free energy available for diffusion and can be derived using Hillert's theory [16]. Out of the total free energy available for pearlite transformation, a

part of it goes into the creation of interfaces between ferrite and cementite and is given by

$$\Delta G_{\mathrm{m}}^{surface} = \frac{2\sigma^{\alpha\theta}V_{\mathrm{m}}}{S} \tag{2.23}$$

where $\sigma^{\alpha\theta}$ is the interfacial energy per unit area and V_{m} is the molar volume of austenite. As the interlamellar spacing decreases, more and more of the available free energy is converted into interfacial energy until a critical spacing S_{c}, is reached where all the available free energy is consumed in the creation of interfaces. Thus,

$$\Delta G_{\mathrm{m}}^{total} = \frac{2\sigma^{\alpha\theta}V_{\mathrm{m}}}{S_{\mathrm{c}}} \tag{2.24}$$

The free energy is thus reduced by a factor of $\left(\Delta G_{\mathrm{m}}^{total} - \Delta G_{\mathrm{m}}^{surface}\right)/\Delta G_{\mathrm{m}}^{total} = \left(1 - \frac{S_{\mathrm{c}}}{S}\right)$. The diffusion of carbon from the tip of ferrite up to a cementite lamella can be represented as [16]:

$$J = \frac{-A^{\alpha}}{V_{\mathrm{m}}}D_C^{\gamma}\frac{dc}{dx} = \frac{D_C^{\gamma}\,b\,S^{\alpha}}{V_{\mathrm{m}}}\frac{(c^{\gamma\alpha} - c^{\gamma\theta})}{S^{\alpha}/2} \tag{2.25}$$

V_{m} is the molar volume and is considered same for all the phases involved, and A^{α} is the cross sectional area of the the interface, which is equal to $S^{\alpha}\,b$, where b is an arbitrary distance perpendicular to the growth direction. The diffusion distance can be approximated to $S^{\alpha}/2$ for the growth of ferrite lamellae. This diffusion causes the edgewise growth of α lamellae in γ with a velocity v and can be written as:

$$J = \frac{vbS^{\alpha}}{V_{\mathrm{m}}}(\bar{c} - c^{\alpha\gamma}) \tag{2.26}$$

where $\bar{c}$ is the initial composition of austenite. The ratio between the thickness of two kinds of lamellae is determined by the original composition of austenite, $\bar{c}$, which exists far away from the reaction front and the transformation temperature. Neglecting the volume change which accompanies the reaction, the material balance at the tip of each lamellae is given by:

$$\frac{v\,b\,S^{\alpha}}{V_{\mathrm{m}}}(\bar{c} - c^{\alpha\gamma}) = \frac{v\,b\,S^{\theta}}{V_{\mathrm{m}}}(c^{\theta\gamma} - \bar{c}) = \frac{v\,b\,S^{\alpha}S^{\theta}}{S\,V_{\mathrm{m}}}(c^{\theta\gamma} - c^{\alpha\gamma}) \tag{2.27}$$

where S^α and S^θ represent the thickness of ferrite and cementite lamellae. Equating equation 2.26 and equation 2.27 and combining it with equation 2.25 leads to:

$$v = \frac{2D_C^\gamma S}{S^\alpha S^\theta} \left(\frac{c^{\gamma\alpha} - c^{\gamma\theta}}{c^{\theta\gamma} - c^{\alpha\gamma}} \right) \tag{2.28}$$

The maximum growth rate v_{max}, as suggested by Zener was found at $S = 2S_{\mathrm{c}}$, the details of which have been described in chapter 3 [6].

Ridley suggested that the equation for pearlite growth gives a relation between velocity, spacings, concentration gradient and diffusivity [46]. The concentration difference is proportional to the undercooling, which in turn is proportional to the reciprocal spacing, hence the equation for volume diffusion-controlled growth can be written as:

$$v\,S^2 = k_1\,D \tag{2.29}$$

The Zener-Hillert theory has often been used to determine the rate controlling process for pearlite growth. The usual method is to incorporate the measured values of interlamellar spacings, calculated interfacial compositions and the diffusion coefficient into the growth equation and then compare the calculated growth rates with those determined experimentally. This approach led many of the researchers to believe that the data are reasonably consistent with the volume diffusion of carbon in austenite as the rate controlling step, though there was a discrepancy of up to 50 times or more. Puls and Kirkaldy [47] and Cheetham and Ridley [48] evaluated the diffusion coefficient of carbon in austenite based on an average carbon content and calculated growth rates bringing down the discrepancy with measurements to 2-3 times.

Forced velocity growth provides another way of studying the pearlite formation. In this technique, a specimen, usually a rod, is translated at a constant velocity relative to the temperature gradient which establishes a single transformation interface which is sufficiently steep to prevent nucleation ahead of the growing front. This technique is essentially different from the isothermal growth rate measurements with

respect to the fact that here the growth rate is fixed as imposed by the translation velocity and the transformation temperature is a free variable. This was first applied to Fe-C alloys by Bramfitt and Marder [49]. This technique was alternately used by Bolling and Richman [50] who examined the relationship of interlamellar spacing and velocity and obtained the relation $vS^n = $ constant, where $n = 2.3 \pm 0.1$. For a forced velocity growth 100 to 1 $\mu\mathrm{m\,s}^{-1}$, Verhoeven and Pearson [51] obtained an exponent of S equal to 2.07. Over the range of forced velocities studied all the spacing and velocity data showed a good agreement and gave the relationship vS^2=constant and hence provided a strong support for volume diffusion being the rate controlling process.

In spite of these attempts to justify the volume diffusion of carbon as the rate-controlling mechanism in Fe-C steels, there still exist discrepancies with the experimentally observed pearlite growth rates. These discrepancies are sufficiently large to render the microstructural calculations associated with steel development to be doubtful.

2.8.2   Interface diffusion

The principal reason behind the attempt to introduce boundary diffusion is the inability of the volume diffusion to account for experimentally observed growth rates in Fe-C and other non-ferrous alloys, rates which are usually higher than expected. This led many researchers to believe that there must be an alternate mechanism for the transport of solute and the interface diffusion theory seemed to be the most plausible explanation [27, 52]. Sundquist assumed the interface diffusion of carbon to be a dominant mechanism driving the edgewise growth of pearlite [15]. The growth rate was calculated using the assumption of local equilibrium and included the effect of capillarity. Using the experimental data for pearlite growth velocity for Fe-C steels, the activation energy for interface diffusion was calculated as 191 kJ mol^{-1} which was far too high. Although, it was attributed to the presence of impurity atoms present in the steel, the justification seems to be unrealistic.

As an approximate treatment, Hillert modified Zener's volume diffusion theory for the interface diffusion controlled growth [16]. He suggested that the cross section of the grain boundary through which the diffusion takes place is equal to $2b\delta$, where δ is the thickness of the boundary layer. The factor of 2 accounts for the diffusion on both sides of α lamellae. The effective diffusion distance was taken proportional to S to make the result independent of ferrite and cementite and was approximated by $S/4$ for the case of symmetric eutectoid.

The diffusion flux through the boundary can be written as:

$$J = \frac{-A^\alpha}{V_m} D_B \frac{dc}{dx} = \frac{2sD_B\, b\delta\, (c_e^{\gamma\alpha} - c_e^{\gamma\theta})}{V_m\, S/4}\left(1 - \frac{S_c}{S}\right) \qquad (2.30)$$

where s is the boundary segregation coefficient between the boundary and the austenite phase. The mass flow causes both the phases to grow and their growth rates must be equal. Neglecting the volume change that accompanies the reaction and considering the material balance at the edges of α and θ lamellae, the Lever rule can be used to relate the lamellar thickness with the growth rate as in equation 2.27.

Combining the equation 2.27 and 2.30 results in:

$$v_B = \frac{8sD_B\delta}{S^\alpha S^\theta}\left(\frac{c_e^{\gamma\alpha} - c_e^{\gamma\theta}}{c^\theta - c^\alpha}\right)\left(1 - \frac{S_c}{S}\right) \qquad (2.31)$$

Turnbull in his theory of cellular precipitation described interface diffusion as the rate controlling step for precipitate growth [53]. He suggested that the cell boundary (or the interface) provides a diffusion short circuit for the solute elements. This cell boundary is incoherent and sweeps the solutes as the cell grows. For the precipitation of tin from lead, the observed rates were many orders of magnitude greater than those calculated from the diffusion data of Seith and Laird [54] assuming volume diffusion mechanism. Assuming that the solute is drained only by diffusion along the cell

boundary, the growth rate given by Zener can be modified as

$$v_B = \left(\frac{c_e^{\gamma\alpha} - c_\infty^{\gamma}}{c_e^{\gamma\alpha}} \right) \left(\frac{\delta}{\tau_1} \right) \tag{2.32}$$

where τ_1 is the time required to drain the solute from the grain boundary region and is given by

$$\tau_1 = \frac{S^2}{D_{\mathrm{B}}}. \tag{2.33}$$

Therefore,

$$v_B = \left(\frac{c_e^{\gamma\alpha} - c_\infty^{\gamma}}{c_e^{\gamma\alpha}} \right) \left(\frac{\delta D_{\mathrm{B}}}{S^2} \right) \tag{2.34}$$

Accounting for the observed growth rates, the D_{B} would have to be 10^{-6} to 10^{-7} cm^2 s^{-1}. This magnitude of D_{B} corresponds to an activation energy, Q_B, for boundary diffusion equal to 37.68 kJ mol^{-1}, compared with the activation energy of volume diffusion, Q_V which is 108.7 kJ mol^{-1}. The ratio Q_B/Q_V is 0.35 and agrees fairly well with $Q_B/Q_V = 0.44$ for self diffusion in silver. This was thought to be reasonably sound evidence to justify that the diffusion of tin atoms along the cell boundary was the rate controlling step since it was entirely consistent with experimental evidence.

For many alloy systems, when the partitioning of the substitutional element, X, is significant during the growth of pearlite, it is likely that interfacial diffusion of alloying elements may control the growth of pearlite. The bulk diffusivity of substitutional alloying element is much smaller than that of carbon. As a result, the substitutional elements diffuse through the boundary which provides a faster diffusion path and partition into the product phases [7]. The interface diffusion-controlled growth rate, v_B would be

$$v_B = \frac{12 s D_{\mathrm{B}} \delta S^2}{S^\alpha S^\theta} \left(\frac{c_X^{\gamma\alpha} - c_X^{\gamma\theta}}{\bar{c}_X} \right) \frac{1}{S^2} \left(1 - \frac{S_{\mathrm{c}}}{S} \right) \tag{2.35}$$

where s, the boundary segregation coefficient, is the ratio between alloying element concentration in austenite near the boundary and at the boundary, $c_X^{\gamma\alpha}$ and $c_X^{\gamma\theta}$ are the concentrations of X in austenite which is equilibrium with ferrite and cementite and $\bar{c}_X$ is the bulk concentration of the alloying element in steel.

2.8.3   Other proposed mechanisms for pearlite

Cahn's theory: Cahn and Hagel considered the diffusion process by which interstitial and substitutional elements get redistributed and how growth is affected during their diffusion in austenite, ferrite and along the austenite-pearlite interface [27]. Since there is a considerable difference of opinion about the exact growth mechanism, rather than calculating the growth rates based on any of these mechanisms, they took a different approach and tried to check the consistency between the measured growth rate, interlamellar spacing and the diffusivities.

A kinetic parameter β_i was considered, which gave a measure of resistance to segregation. It was suggested that there exists one such parameter for each element and each phase [27].

$$\beta_i = \frac{vS}{2\pi D_i} \tag{2.36}$$

Another term β_i' can be written in terms of a thermodynamic parameter as:

$$\beta_i' = \frac{1}{2}\frac{c_i^{\gamma\alpha} - c_i^{\gamma\theta}}{c_i^{\theta\gamma} - c_i^{\alpha\gamma}} \tag{2.37}$$

where $c_i^{\gamma\alpha}, c_i^{\gamma\theta}, c_i^{\theta\gamma}, c_i^{\alpha\gamma}$ are the concentrations which can be obtained from the phase diagram and i represents the solute. If β_i is large (*i.e.* low D_i and high v and S) and since there is an upper limit to $(c_i^{\gamma\alpha} - c_i^{\gamma\theta})$, $(c_i^{\theta\gamma} - c_i^{\alpha\gamma})$ will be small and hence little partitioning of the solute element, i will occur. When β_i is small (*i.e.* high D_i or low v and S), because there in an upper limit to $(c_i^{\theta\gamma} - c_i^{\alpha\gamma})$; $(c_i^{\gamma\alpha} - c_i^{\gamma\theta})$ will be small and hence the concentration gradient driving the diffusion at the pearlite-austenite interface would be small. β_i can be established from the observed values of v, S and D_i based on the equation 2.36 and β_i' can be estimated from the phase diagram. For a 2-component system, thermodynamic reasons necessitate an upper limit on $(c_i^{\gamma\alpha} - c_i^{\gamma\theta})$ and a lower limit on $(c_i^{\theta\gamma} - c_i^{\alpha\gamma})$, since the carbon segregation to cementite cannot be zero, and hence an upper limit on β_i' which as per equation 2.37 is half their ratio and this is termed as β_0. In order to compare β_i with β_0, the authors

calculated β_0 and based on the experimental values of v and S. They argued what value of D_i will make $\beta_i = \beta_0$ or what apparent diffusivity D_{app} would be necessary to give the required segregation of solute elements.

If the value of β_i is equal to β_0, this can be considered as an evidence that the growth rate of pearlite is controlled by the volume diffusion of solute through the austenite. If the observed value of β_i is less than β_0, then some process other than the diffusion in austenite is controlling the rate. If β_i exceeds β_0, this can point to the existence of a faster diffusion path.

In the case of non ferrous pearlite, Cahn and Hagel showed that the apparent diffusivities D_{app} are higher than the D_i (or the experimental diffusivity) by orders of magnitude. Hence β_i exceeds β_0 and that was taken as strong indication that an alternate diffusion path or a diffusion short circuit exists. Regarding pearlite in steel, there was a reasonable agreement between D_{app} and the D_C^γ in plain carbon steels for which the v, S and β_0 are known and hence led to the conclusion that carbon diffusion in austenite controls the pearlite growth in these steels. However, the v and S that they used in their calculations were not measured for the same steel. Moreover, pearlite growth in plain carbon steels is as fast as permitted by carbon diffusion in austenite, but in high purity steels it grows almost 50 times faster. This could well be attributed to the spacings in high purity steels, but the measurements showed that the spacings were almost comparable to those in plain carbon steels. This further strengthens the fact that another mechanism is operative for carbon diffusion.

Diffusion through ferrite: Nakajima *et al.* considered the effect of diffusion in ferrite along with that in austenite using a phase field approach [55]. They reported that since the diffusion in ferrite is much faster than in austenite and when this was coupled with the latter, the difference in calculated and the experimental growth rate of pearlite was narrowed down. It was argued that the higher velocity (compared to that in austenite alone) resulting from their model, apart from faster diffusivity in ferrite, was due to a large ratio of ferrite-cementite interfacial area as compared

to that in case of cementite-austenite interfaces. The phase field calculations show the thickening of cementite behind the transformation front when the diffusion occurs in ferrite. Cahn and Hagel considered the effect of diffusion in ferrite but did not observe any tapering of cementite at the transformation front [27]. Since the calculated velocities were still not able to explain the observed growth rates, they attributed the same to the influence of transformation strain or diffusion through the boundary. Steinbach and Apel [56] modelled the pearlite using the phase field calculations and studied the influence of transformation strains present due to the concentration gradients in austenite whilst considering the diffusion in ferrite. According to their theory, the transformation strains inhibit the co-operative growth of ferrite and cementite resulting in solitary growth of wedge-shaped cementite ahead of the ferrite which they termed as 'staggered growth'. Again the effect of interface diffusion control was ignored apparently due to the lack of interface diffusivity data. But in the Fe-C alloys studied to date, wedge shaped cementite has never been observed experimentally. Although this theory could further bridge the gap between the calculated and the observed growth rate in Fe-C system compared with those of Nakajima *et al.*, this was fundamentally weak due to the fact that in a reconstructive transformation, the transformation strains are mitigated during the course of the reaction.

Combined volume and phase boundary diffusion: Hashiguchi and Kirkaldy, for the first time made an elegant attempt to simultaneously deal with interface and volume diffusion in Fe-C alloys [57]. They assumed a parallel mass flow through the volume of austenite and the advancing pearlite-austenite interface, with a mechanical equilibrium at the interface junctions and the effects of capillarity. The distribution coefficient describing the ratio of composition in austenite in contact with ferrite and cementite and in the transformation front was assumed to be constant even though the interfacial energies $\sigma^{\gamma\alpha}$ and $\sigma^{\gamma\theta}$ are not expected to be the same. They used the growth and spacing data of Brown and Ridley [58] in their model in order to arrive at the activation energy for the boundary diffusion of carbon, which was in the range of 159-169 kJ mol^{-1}. This clearly did not make sense as the value obtained

was greater than activation energy for volume diffusion of both ferrite and austenite. The interfacial energy values $\sigma_{\alpha\theta}$ obtained were also rather too large. The theory thus developed was too complex to be implemented, requiring approximations which rendered the details unimportant.

2.9 Pearlite in Multicomponent Steels

Most of the commercially produced steels contain either one or many alloying additions. The presence of the substitutional elements and their interaction with carbon makes the calculation of diffusion controlled growth in such systems quite complicated. The growth of proeutectoid ferrite from austenite in Fe-C-X system, where X is the substitutional alloying element has been studied in considerable details owing to the relative simplicity of the influence of a ternary addition on the growth rate [59–62]. However in case of pearlite growth, the situation is more complex owing to the partitioning of the substitutional element between the two product phases namely ferrite and cementite. For a ternary system involving carbon and a substitutional element, different diffusion paths can exist. The pearlite growth rate can be controlled by diffusion of carbon or substitutional solute through the volume of austenite or the pearlite-austenite interface, or simultaneous diffusion of both these species.

2.9.1 Thermodynamics of ternary systems

In a binary alloy system, the common tangent construction using a free energy-composition diagram can easily give the composition of the growing phase (or phases) in equilibrium with the parent phase. However in a ternary steel (Fe-C-X) containing a substitutional alloying element, X, the situation is more complex. The free energy curves for the parent and product phases become three dimensional surfaces and an infinite set of tangent planes can be constructed. In order to choose a unique set of $\gamma+\alpha/\alpha$ and $\gamma+\theta/\theta$ tie-lines, the two fluxes of carbon and X must be simultaneously

satisfied.

$$(c_C^{\gamma\alpha} - c_C^{\gamma\theta})\, v = -\, D_C \bigtriangledown c_C \tag{2.38}$$

$$(c_X^{\gamma\alpha} - c_X^{\gamma\theta})\, v = -\, D_X \bigtriangledown c_X \tag{2.39}$$

where the $\bigtriangledown c_C$ and $\bigtriangledown c_X$ are the concentration gradients for carbon and X respectively at the interface. Since $D_C >> D_X$ (by an order of 6), the two equations cannot in general be simultaneously satisfied using the tie-line passing through the alloy composition. In order to deal with this problem, Kirkaldy [63] and Purdy *et al.* [61] suggested that either the fast diffuser (C) has to slow down and keep pace with the slow diffusing species (X) in which case the driving force for C has to be negligible or the slow diffusing species has to have a large driving force. This is termed as partitioning local equilibrium (PLE) in which the alloying element partitions between the austenite and the product phases and hence slows down the reaction owing to the slow diffusivity of the substitutional element. The second reaction, termed as negligible partitioning local equilibrium (NP-LE) involves only a short range diffusion of the substitutional element (a sharp spike at the interface) and the reaction proceeds by diffusion of carbon through a combination of austenite and the interface as has been shown recently for the pearlite growth in a binary Fe-C system [64]. In this case the alloying element affects the reaction kinetics only through its thermodynamic influence on the driving force for carbon diffusion. It is generally believed that the partitioning reaction takes place at low supersaturation whereas the no-partitioning reaction happens at high supersaturations [65]. A schematic profile of both these scenerios is shown in Fig. 2.5

2.9.2   Partitioning during the growth of pearlite

Partitioning of solutes from parent to the product phase and between the product phases in case of pearlite is likely for a diffusional transformation. In case of steels containing alloying additions, partitioning of these elements may occur at or behind the transformation front. Carbide forming elements such as Mn, Cr, Mo would
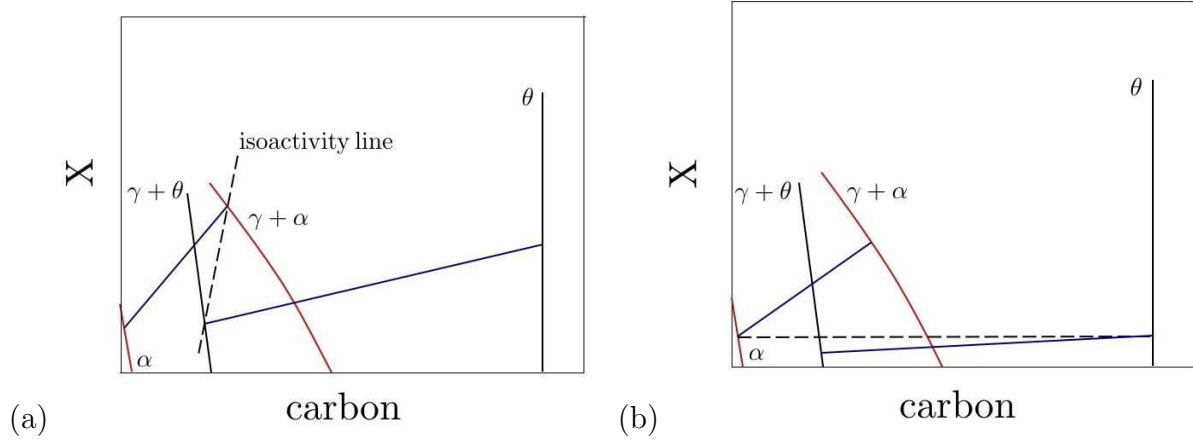
Figure 2.5: Schematic representations of (a) PLE and (b) NP-LE conditions.

partition to the pearlitic cementite whereas Si, Ni and Co would tend to segregate to the ferrite. Most of the partitioning studies have been carried out using analytical electron microscopy of thin foils or carbide extraction replicas and the results are expressed as partition coefficient, which is defined as the ratio of concentration of alloying element in cementite to that in ferrite. Atom probe microanalysis is another technique which is used routinely for partitioning studies where the spatial resolution is of the order of 2-5 nm. Most of these alloying additions retard the growth rate of pearlite through their effect on the carbon concentration gradient, which in turn is proportional to the driving force at the transformation front.

Picklesimer *et al.* measured the growth rate of pearlite based on the modified absolute rate theory of the form:

$$r = b \, \Delta T \, \Delta G \exp\left(\frac{-Q}{RT}\right) \tag{2.40}$$

where r is the growth rate in mm s^{-1}, b is a constant, ΔG is the free energy difference of austenite to pearlite transformation and Q is the activation energy. They argued that the rate of pearlite growth is neither controlled by diffusion of Mn and probably not by carbon. According to them the presence of Mn decreases the growth rate

of pearlite by increasing the activation energy for those atomic movements at the moving interface which are required because of the differences in crystal structure of austenite and ferrite and cementite in contact with it. They observed partitioning of Mn to cementite based on the chemical analysis of the extracted carbides for a 1.0Mn wt% eutectoid steel above 640°C. These data involved a contribution of Mn partitioning from ferrite to cementite behind the growth front (the steel was held at the transformation temperature for 24 h) and hence it was difficult to exactly determine the no-partitioning temperature.

Razik *et al.* suggested that the electron probe micro-analyser was not an effective tool for partitioning studies owing to its poor resolution (2 μm) as it could not measure the composition of cementite lamella only, the thickness of which was far less than 2 μm. They used analytical electron microscopy to study the partitioning behaviour of manganese between cementite and ferrite during austenite to pearlite transformation in 1.08 and 1.8Mn wt% steel [17]. It was observed that the manganese partitions preferentially to cementite at the transformation interface above a certain temperature which was described as the no-partition temperature, which depends on the composition. Partitioning of Mn to cementite was not observed at temperatures below 683°C and 645°C for 1.08 and 1.8Mn wt% respectively. The values obtained were in good agreement with those determined from thermodynamic data for the two steels. It is worth noting that the compositions used in plotting the $\gamma/\gamma + \alpha$ and $\gamma/\gamma + \theta$ phase boundaries for these two steels were based on a binary phase diagram. This was clearly an incorrect procedure since the effect of ternary addition, *i.e.* Mn should have been considered using isothermal sections of a ternary phase diagram for calculating the interfacial compositions by choosing a correct tie-line. Further they assumed that below this characteristic no-partition temperature, the growth of pearlite is controlled by either the volume or interface diffusion of carbon and that the both the mechanisms are equally probable. The pearlite growth rate calculated using this assumption deviated from those observed experimentally by a factor of 1-3 for both these mechanisms.

In a separate study, Razik *et al.* used Fe-1.29Cr-0.8C wt% and reported the no-partitioning temperature as 703°C, below which there was no chromium partitioning observed at the transformation front [18]. The pearlite growth rate below the no-partition temperature calculated using the assumption of volume diffusion of carbon was lower than the experimentally observed rate by a factor of 2 to 4. The same when calculated using the assumption of interfacial diffusion of carbon was found to be higher than the experimentally determined rate by a factor of 12-17.

Sharma *et al.* studied the pearlite growth kinetics of Fe-Cr-C alloys by experimentally measuring the growth rate and interlamellar spacing for 0.4, 0.9 and 1.8Cr wt% and then compared the same with those calculated using the thermodynamic and kinetic models. According to them at high temperature, the reaction is controlled by phase boundary (interface) diffusion of Cr and that the volume diffusion of the same is too small. They calculated the driving force for Cr boundary diffusion controlled growth by assuming a uniform carbon activity in austenite ahead of the pearlite-austenite interface. The growth rate was calculated based on the equation given by Hillert and by taking $S^\theta/S = 1/8$ and $S^\alpha/S = 7/8$ and assuming maximum rate of entropy production criterion:

$$v = 54 s D_\text{B} \delta \left[\frac{c_\text{Cr}^{\gamma\alpha} - c_\text{Cr}^{\gamma\theta}}{\bar{c}_\text{Cr}} \right] \tag{2.41}$$

The experimental data for the growth velocity of pearlite along with spacing was used to determine the activation energy for the boundary diffusion of Cr. The value of 168.6 kJ mol^{-1} obtained was close to that suggested by Fridberg [44] for the boundary diffusion of substitutional solutes. Similar to their predecessors, they believed that at lower temperatures (high supersaturation), the growth rate of pearlite is controlled by carbon volume diffusion. The diffusion coefficient of carbon in austenite was obtained by extrapolating the data of Wells *et al.* to the weighted average carbon concentration at the interface using the relation:

$$c_\text{C} = \left(\frac{S^\alpha}{S} c_\text{C}^{\gamma\alpha} + \frac{S^\theta}{S} c_\text{C}^{\gamma\theta} \right) \tag{2.42}$$

36

A comparison of experimental and calculated growth rates by Sharma *et al.* for various Cr contents is shown in Fig. 2.6.

Al-Salman *et al.* studied the partitioning behaviour in a Fe-1.0Mn-1.0Cr-0.8C wt% eutectoid steel and observed simultaneous segregation of Cr and Mn to the cementite at the transformation front down to 600°C, but they were unable to identify a no-partition temperature [66]. It was argued that the resolution of the analytical technique used by Razik *et al.* was insufficient causing the overlap of the beam on the adjacent ferrite lamella. Another reason might be the extrapolation technique used by these researchers might have led to an overestimation of the partitioning temperature. Ricks studied the partitioning behaviour of 13Mn wt.% eutectoid steel and a Fe-10Cr-0.2C wt.% steel and observed full partitioning of Mn and Cr to the cementite and suggested that the diffusion path of these solutes was the interface, since there was no gradient of these solutes observed in austenite [67].

Tiwari and Sharma [68] calculated the pearlite growth rate in alloys containing a range of elements (Mn, Cr, Ni, Si) using a model developed by Sharma [69] and Sharma *et al.* [70]. They considered the thermodynamic effect of the ternary solute in determining the phase boundaries of the austenite in equilibrium with ferrite and cementite. The calculations were based on the fact that at low supersaturations, the pearlite growth rate is governed by the interface diffusion of the substitutional solute and at high supersaturations, carbon volume diffusion controls the growth rate. It was suggested that the partitioning-no partitioning temperature was a function of the alloy composition and it decreases with the increase in substitutional solute content. They also calculated the growth rates based on para-equilibrium conditions, but such a condition clearly cannot be justified given the reconstructive nature of the pearlite transformation.

Hutchinson *et al.* measured the composition profile of Mn across the austenite-pearlite interface as a function of time in steel containing manganese using the analytical transmission electron microscopy [71]. The results were compared with those cal-
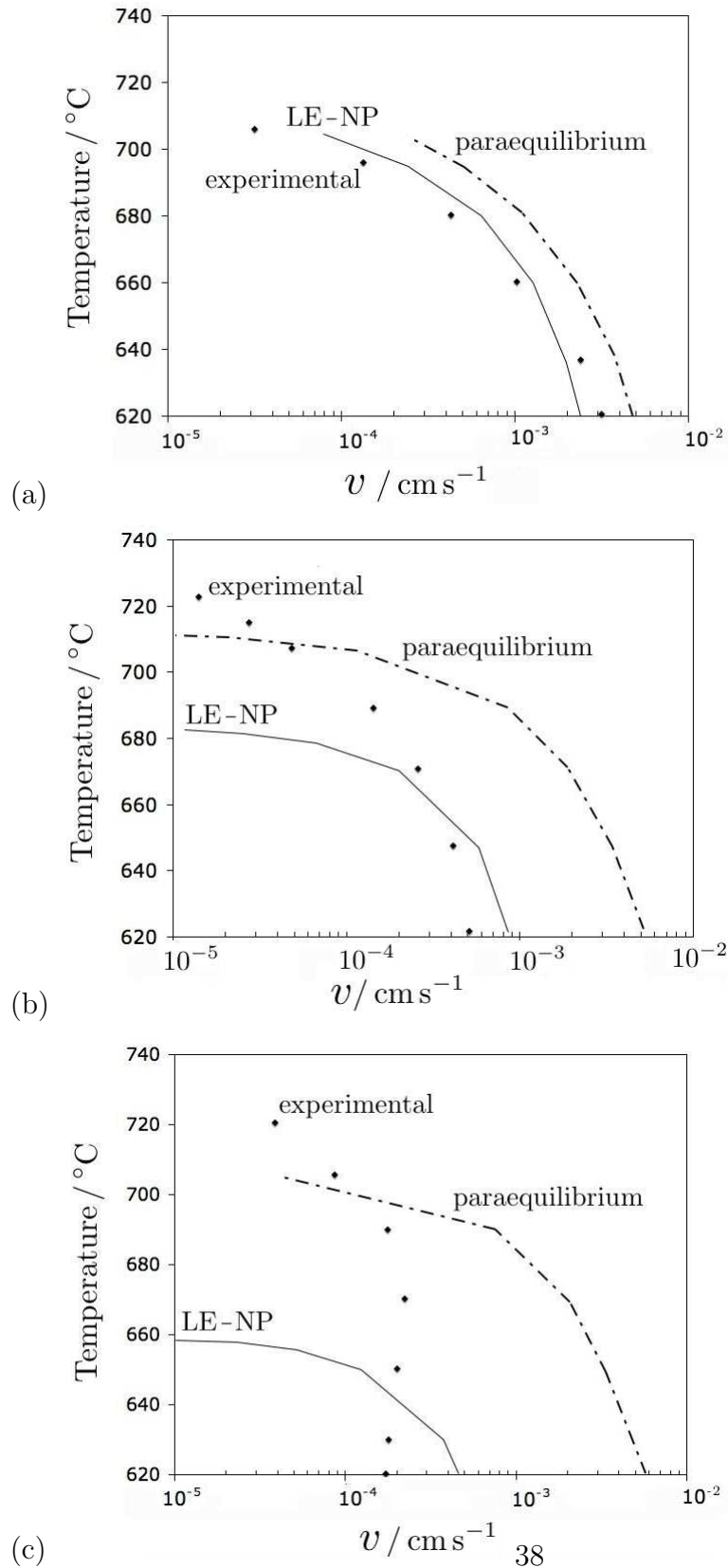
(a)

(b)

(c)

38

Figure 2.6: Pearlite growth rates calculated by Sharma *et al.* for (a) 0.4, (b) 0.9 and (c) 1.8Cr wt%.

culated using local equilibrium (LE) assumption. The alloy (Fe-3.51Mn-0.54C wt%) treated at 625°C for 2.5, 5 and 10 h in the two phase $(\alpha + \theta)$ region revealed that the composition of Mn in both the ferrite and cementite remained constant during the steady state growth and can be well approximated by the LE condition.

2.10 Divergent Pearlite

In certain alloys, pearlite can form above the lower A_{e1} temperature when the steel is isothermally held in the 3 phase region (austenite+ferrite+cementite) for a prolonged length of time. This phenomenon was first observed in pearlite by Cahn and Hagel in Fe-5.2Mn-0.6C wt% steel in the temperature range of 500-650°C wherein at a given reaction temperature, the growth rate decreased as a function of time and the interlamellar spacing increased [72]. This results from the continuously changing carbon concentration in the austenite, until it reaches a composition in equilibrium with ferrite and cementite and the reaction stops at this point. Hillert explained the divergency of pearlite based on the thermodynamics of the ternary Fe-Mn-C phase diagram [73]. In an alloy steel containing Mn, it is reasonable to assume that the growth rate of pearlite is so slow that there is sufficient time for carbon to establish a uniform carbon activity along the pearlite-austenite interface. He suggested that the conditions at the interface can be examined by choosing a carbon activity corresponding to the average alloy composition and by plotting an iso-activity line. In Fig. 2.7, the point of intersection of this iso-activity line with the $\gamma + \alpha$ and $\gamma + \theta$ phase boundaries (marked with an open circle) represent the composition of austenite at the ferrite and cementite interfaces. The end of these tie lines would give the corresponding composition of the growing ferrite and cementite (solid circles). Since the average alloy content cannot change, the growing pearlite must lie on the line joining the compositions of growing ferrite and cementite (represented as a solid diamond). The growing pearlite has a carbon content which is much higher than the alloy and hence it draws carbon from the parent austenite leaving a zone depleted with carbon. This leads to a reduction in the activity of carbon in austenite in the vicinity of the interface over a period of time. As the transformation progresses, the

conditions prevailing at the interface can be described by the carbon isoactivity line corresponding to lower carbon activities moving to the left (in the direction of arrow). This would mean that the Δc^{γ}_{Mn}, (2.7), which is the driving force for partitioning of Mn decreases continuously, thereby slowing the growth rate and leading to a concomitant increase in the interlamellar spacing. As the carbon activity in austenite falls to a value where the isoactivity line approaches the one passing through the stable austenite corner (marked E), the growth rate will cease before the transformation is complete. Hutchinson *et al.* analysed a Fe-0.55C-5.42Mn wt% steel and observed a similar divergency in the pearlitic structure when held at 625°C for 168 and 384h [71]. Using analyical transmission electron microscopy technique, it was observed that during the course of formation of such pearlite, the Mn composition of ferrite and cementite increased continuously with time.
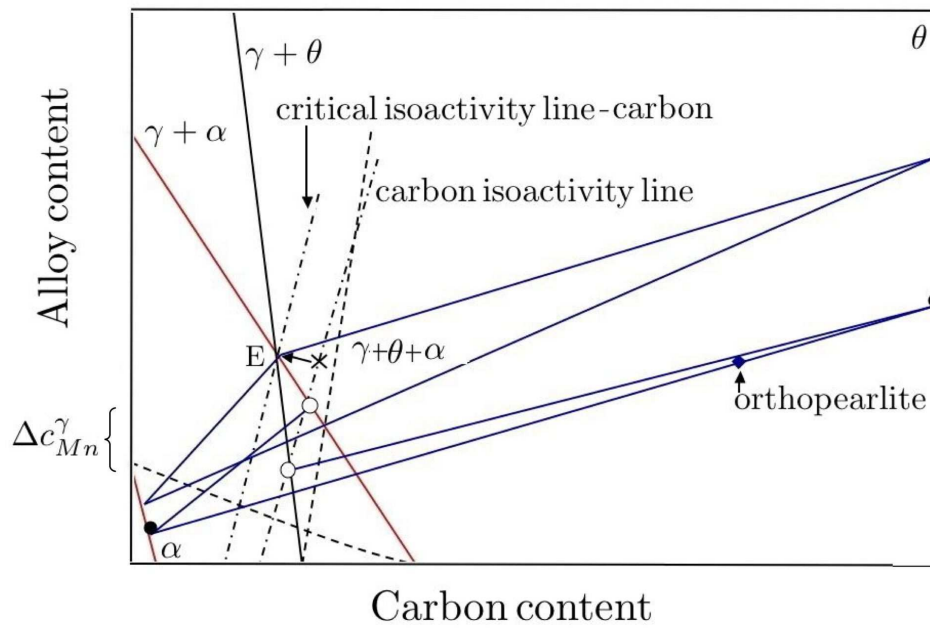
Figure 2.7: Schematic isothermal section of the Fe-C-X phase diagram showing the formation of divergent pearlite. The cross represents the average alloy composition in the 3-phase region.

Chapter 3

Pearlite Growth in Fe-C alloys

3.1 Introduction

Cementite is rich in carbon whereas ferrite accommodates very little when it is in equilibrium with either cementite or austenite. It is therefore necessary for carbon to be redistributed at the transformation front. This can happen either by diffusion in the austenite in a direction parallel to the transformation front, or by the migration of solute atoms within the α/γ and θ/γ interfaces. When the mobility of the interface is large, both of these mechanisms are said to be diffusion–controlled, *i.e.,* most of the available free energy is dissipated in driving diffusion [74]. This chapter discusses the conventional pearlite growth theories in Fe-C alloys and a new theory is formulated for simultaneous diffusion through the austenite and the pearlite-austenite transformation front. It is pertinent to begin the discussion with a brief account of the interlamellar spacing criteria.

3.2 Interlamellar Spacing Criteria

The equation for the velocity of pearlite for volume or boundary diffusion-controlled growth described in chapter 2 does not give a unique solution for the growth rate, but rather a range of velocities and spacings which would satisfy the equation. Hence in

order to obtain a unique solution, there is a need to impose a further condition by using an optimisation principle. There are 3 different solutions reported for optimising the interlamellar spacing.

3.2.1 Maximum growth rate

Zener suggested that during the growth of pearlite, the ferrite-austenite and the cementite-austenite interfaces are not flat, but are actually convex and bulging towards the parent austenite phase. This curvature effectively reduces the concentration difference driving the diffusion, owing to the effect of capillarity. Zener proposed that the concentration difference would be reduced by a factor of $(1 - S_c/S)$ where S is the interlamellar spacing and S_c is the critical spacing at which the growth rate becomes zero. A generic form of equation formulated by Zener can be written as :

$$v = \frac{c_e^{\gamma\alpha} - c_e^{\gamma\theta}}{(c_e^{\theta\gamma} - c_e^{\alpha\gamma})} \frac{D}{L} \left(1 - \frac{S_c}{S}\right) \tag{3.1}$$

where L is the effective diffusion distance which can be related to the interlamellar spacing. In order to maximise the growth rate, differentiation with respect to S, and equating to zero gives the relation $S = 2\,S_c$.

3.2.2 Maximum rate of entropy production

This criterion has its origin in the thermodynamics of irreversible processes which deals with systems which are not in equilibrium but at steady state. An irreversible process dissipates energy and entropy is created continuously. One of the examples of dissipation of free energy is diffusion ahead of the moving interface. The rate at which energy is dissipated is the product of temperature and the rate of entropy production $(\dot{S})$, *i.e.* $T\,\dot{S}$ which is given as:

$$T\,\dot{S} = J\,X \tag{3.2}$$

where J and X are the generalised flux and force respectively, the flux always being a function of the force. For an isothermal, isobaric and a unidirectional system,

$$\dot{S} = v \frac{\Delta G_V}{T} \tag{3.3}$$

where v is the transformation velocity and ΔG_V is the average Gibb's free energy per unit volume dissipated in the reaction. ΔG_V can be described as the difference between the maximum chemical free energy available and the surface energy accumulated.

$$\Delta G_V = \Delta G_V^0 - \frac{2\sigma}{S} \tag{3.4}$$

ΔG_V^0 can be estimated as:

$$\Delta G_V^0 = \frac{\Delta H \Delta T}{T} \tag{3.5}$$

where ΔH is the latent heat evolved per unit volume and ΔT is the undercooling.

$$\Delta G_V = \frac{\Delta H \Delta T}{T_e} \left(1 - \frac{2\sigma T_e}{\Delta H \Delta T} \frac{1}{S} \right) = \frac{\Delta H \Delta T}{T_e} \left(1 - \frac{S_c}{S} \right) \tag{3.6}$$

Incorporating the velocity of pearlite growth from equation 2.28 into equation 3.3, the rate of entropy production for the case of volume diffusion is given as:

$$\dot{S} = \beta \left(\frac{2 \overline{D}_V}{S} \right) \frac{\Delta H \Delta T}{T_E} \frac{1}{T} \left(1 - \frac{S_c}{S} \right)^2 \tag{3.7}$$

where β contains the concentration terms. The maximum in $\dot{S}$ is obtained on differentiating equation 3.7 with respect to spacing and equating it to zero, which gives $S = 3 S_c$ and $S = 2 S_c$ for volume and boundary diffusion–controlled growth respectively.

3.2.3 Interface instability

The velocity of edgewise growth of pearlite can be calculated once the diffusivity, interfacial compositions and interlamellar spacing are known. Based on the available

data, a curve of velocity versus spacing can be plotted. But it is important to understand which point on this plot would correspond to the actual velocity and spacing observed experimentally. Sundquist in his theory of optimal spacing has considered two mechanisms which can lead to the changes in interlamellar spacings [15].

In the first mechanism, U, (which is the velocity of pearlite growth normalised by the boundary diffusivity of carbon and the thickness of the interface) as a function of pearlite interlamellar spacing for a particular set of conditions is shown Fig. 3.1. It was suggested that the interface may be unstable with respect to some infinitesimal perturbation under certain conditions. For a situation where the spacing is very small, the driving free energy is less than that required to maintain ferrite-cementite interface and hence the velocity is negative. Consider a range of spacings where the $\partial U/\partial S$ is positive, and those less than the spacing pertaining to maximum velocity. Jackson and Hunt [75] suggested that the interface with such spacings is unstable with respect to a small perturbation. As a result, those with smaller interlamellar spacings will have a growth velocity less than its immediate neighbour and hence the bigger lamella will begin to outgrow the smaller one leading to its elimination. This leads to a situation where any spacing with a velocity smaller than that corresponding to the maximum is inherently unstable and will change quickly to that of the maximum velocity. This was referred to as the lower catastrophic limit.

Using an argument similar to the one above, it has been shown that any spacing with a negative $\partial U/\partial S$ will be stable with respect to a small perturbation and the perturbations in spacing will die out leading to a perfectly uniform spacing throughout the growing pearlite colony. Thus, this treatment based on the stability of interface could theoretically predict the transition zone beyond which the spacings would be stable.

In the second mechanism consider a case where the interlamellar spacing is large. From calculations by Sundquist, it is clear that the interface shapes are dependent largely on the interlamellar spacings. At smaller spacings, the interfaces are convex
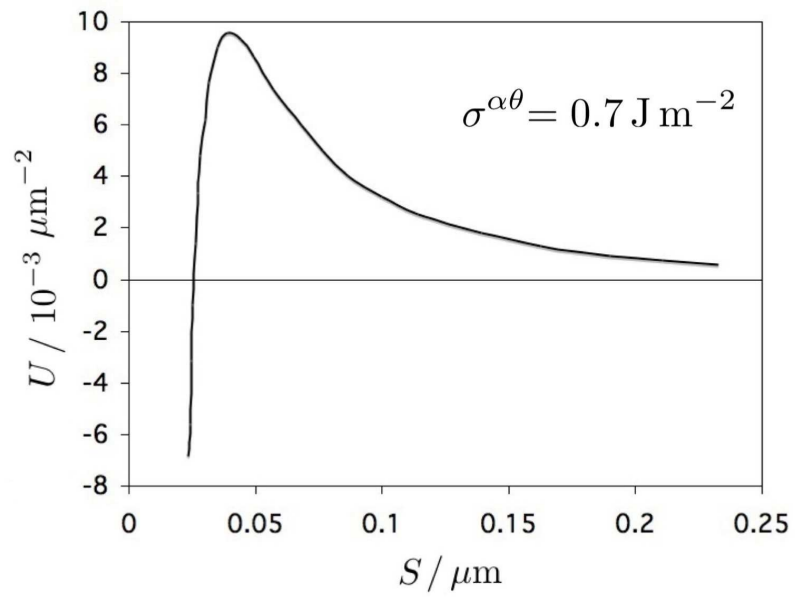
Figure 3.1: Velocity of pearlite as a function of interlamellar spacing, adopted from Sundquist [15]

towards austenite and at the intermediate spacings they are more or less flat, being slightly convex or concave depending on the exact value of the spacing. At large spacing, there is no real steady-state shape. The interface may double back to expose a new cementite-austenite interface. This may lead to the branching of a new cementite lamella and a concurrent decrease in the interlamellar spacing. This imposes an upper limit on the spacing that pearlite can maintain under a steady-state. Pearlite growing with a larger spacing than this would be subjected to a sudden introduction of a new cementite lamella. This in effect would lead to a reduction in spacing and hence the upper catastrophic limit.

3.3 Pearlite Growth Based on Conventional Theories

The existing theories of pearlite growth are based on either the volume diffusion-control [6–11] or the interface diffusion-control [15, 16]. There have been reports that the rates calculated using the volume diffusion mechanism significantly underestimate those measured [12, 14, 58] and that the latter is a dominant mode of solute transport. The interface diffusion mechanism has also been considered in the context of cellular precipitation where the cell boundary provides an easy diffusion path, with an activation energy for the boundary diffusion coefficient which was less than half that for volume diffusion [53].

Both these approaches to determine the growth rate of pearlite in a Fe-0.8C wt% steel are now examined. The first one is based on the volume diffusion–control using the Zener-Hillert theory. This theory assumes that pearlite grows by the redistribution of carbon through the volume of austenite and the transformation rate is given by:

$$v = \frac{2\,D_{\mathrm{C}}^{\gamma}\,S}{S^{\alpha}S^{\theta}} \left(\frac{c_{\mathrm{e}}^{\gamma\alpha} - c_{\mathrm{e}}^{\gamma\theta}}{c_{\mathrm{e}}^{\theta\gamma} - c_{\mathrm{e}}^{\alpha\gamma}} \right) \left(1 - \frac{S_{\mathrm{c}}}{S} \right) \tag{3.8}$$

where $c_e^{\gamma\alpha}$ is the concentration of carbon in austenite in equilibrium with ferrite and the other concentration terms are interpreted in the same way. These terms were determined using MTDATA (TCFE database) [76]. D_C^γ has been determined using Ågren's equation [40]. The critical spacing, S_c was calculated from the experimental interlamellar spacing using both the maximum growth rate and maximum entropy production rate criteria discussed in section 3.2:

$$S_c = \frac{2\,\sigma^{\alpha\theta}\,T_e}{\Delta T\,\Delta H} \tag{3.9}$$

The $\sigma^{\alpha\theta}$, T_e and ΔH corresponds to the energy per unit area of ferrite-cementite interfaces, eutectoid temperature and the enthalpy change respectively. The interfacial energy, $\sigma^{\alpha\theta}$ was assumed to be $0.7\ \mathrm{J\,m^{-2}}$ based on the data due to Kramer [77]. The growth rates determined using the volume diffusion theory are shown in Fig. 3.2 and is clearly much slower than those experimentally measured by Brown and Ridley [13].

In order to overcome the discrepancies observed in the growth rate calculated using the volume diffusion approach and those measured experimentally, the growth rate of pearlite was calculated wherein the mass transfer occurs through the phase boundary which provides a much faster path for the diffusion of the solute. The growth rate for diffusion through the pearlite-austenite interface was calculated as proposed by Hillert [16] :

$$v = \frac{12\,s\,D_B\,\delta S^2}{S^\alpha S^\theta}\left(\frac{c_e^{\gamma\alpha} - c_e^{\gamma\theta}}{c_e^{\theta\gamma} - c_e^{\alpha\gamma}}\right)\left(\frac{1}{S^2}\right)\left(1 - \frac{S_c}{S}\right) \tag{3.10}$$

where s is the boundary segregation coefficient and is defined as the ratio of solute in the phase boundary to that in the parent austenite. In case of pearlite, there should be two such coefficients, one for the γ/α and γ/θ boundary. D_B is the boundary diffusion coefficient. Since there exists no measured value of the boundary diffusion coefficient of carbon, an approximate value for the activation energy is chosen which is half of that for volume diffusion [78]. The growth rates obtained using boundary diffusion as the rate controlling step was calculated and compared with
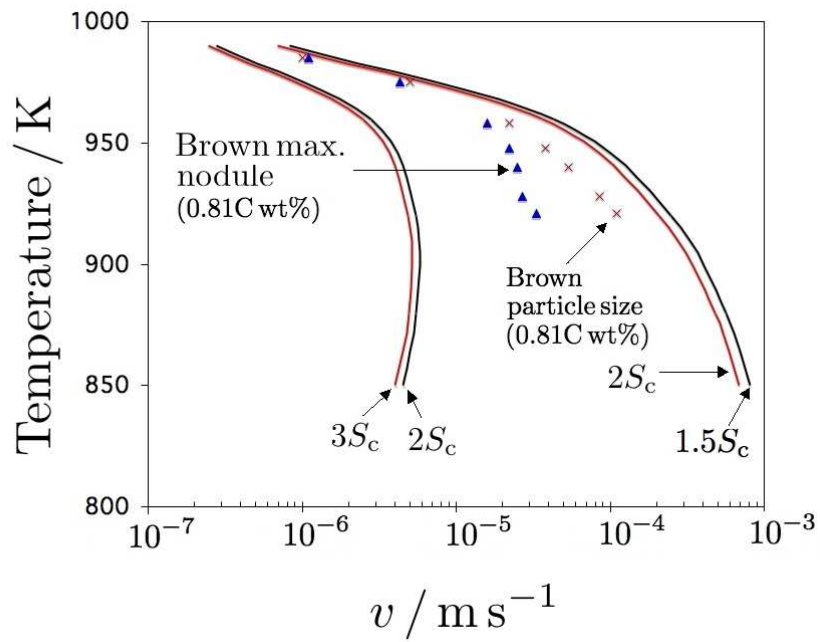
Figure 3.2: Comparison of pearlite growth rate calculated assuming volume diffusion in austenite and boundary diffusion (solid lines) with those determined by Brown and Ridley (points).

the available experimental data (Fig. 3.2). It is observed that the calculated growth rate overestimates observations by a factor of 2 at low temperatures. However, there seems to be no sound justification for ignoring the flux through the volume of austenite. The assumption regarding the magnitude of the activation energy for boundary diffusion of carbon may also be crude.

Apart from the theories discussed above, Pearson and Verhoeven [14] proposed that transformation strain enhances diffusion, but this neglects the fact that pearlite forms by reconstructive transformation in which case transformation strains should not be significant; furthermore, it has not been necessary to invoke such an argument in the case of other reconstructive transformations where the closure between experiment and theory is satisfactory [74].

Most of the comparisons between experiment and theory have been based on assumptions of either volume or interface–diffusion control; in other words, mechanisms in isolation. Fluxes through both of these processes must in practice contribute to diffusion and the relative contributions from each of these mechanisms will vary with circumstances.

3.3.1   Collector plate model

Aaron and Aaronson devised a way to combine the effect of volume and boundary diffusion using a collector plate model [79]. They analysed the lengthening and thickening of θ precipitates in Al-4Cu wt% which nucleate on the grain boundaries and preferentially grow along them as allotriomorphs. The experimentally determined lengthening and thickening rates were far too rapid to be described by the volume diffusion of Cu towards the growing allotriomorphs. The mechanism suggests that for lengthening of θ precipitates, Cu diffuses to the α/α grain boundaries by volume diffusion, followed by grain boundary diffusion to the tip of growing allotriomorph. The analysis led to the relation of the form $R = k_2 t^{1/4}$ where k_2 is a constant. The thickening of precipitates is controlled by the rate of diffusion of Cu along the α/θ boundary through the broad faces of the allotriomorphs and the rate is given as

$R = k_2 t^{1/2}$. This mechanism assumes that the ratio of α/α grain boundary diffusivity to that of volume diffusivity is almost infinitely higher and is restricted to low temperatures. Subsequently this model was refined by Goldman *et al.* to account for the growth mechanism of Al-4Cu wt% at higher temperature, $T/T_{\text{solidus}} \approx 0.91$ where volume diffusion becomes significant [80].

In the case of pearlite growth in steels, there is no long-range transport of solute since that of carbon is from the tips of adjacent ferrite lamellae. This model also assumes that volume and boundary diffusion occur in series, which may not be a valid argument for pearlite, where they are simultaneous. Hence it was assumed that the collector plate model may not be applicable to pearlite growth in steels, thus necessitating an alternative approach to consider combined fluxes.

3.3.2 Combined volume and phase boundary diffusion

Hashiguchi and Kirkaldy [57] made a first attempt by assuming parallel mass transfer in the volume ahead of the interface and through the interface, allowing for the Gibbs–Thomson effect at both the γ/θ and γ/α boundaries, and for mechanical equilibrium at the various interfacial junctions. The result was a rather complex theory which could not be implemented without making important approximations:

- in spite of the requirement of mechanical equilibrium, the interfaces with austenite were approximated as being flat except in the close proximity of the three–phase junctions;

- the segregation coefficient describing the ratio of the composition in the austenite in contact with ferrite or cementite, and in the transformation front was assumed to be constant, even though the interfacial energies $\sigma^{\gamma\alpha}$ and $\sigma^{\gamma\theta}$ are not expected to be identical;

- a simplification was made that $\sigma^{\gamma\alpha} \propto \sigma^{\alpha\theta}$ and $\sigma^{\gamma\theta} \propto \sigma^{\alpha\theta}$.

Whilst these approximations are entirely understandable, some clearly are inconsistent with the detailed theory and the whole problem might be simplified by abandon-

ing the need for mechanical equilibrium. Indeed, it is not strictly necessary during growth when the rate of free energy dissipation is large, for equilibrium configurations to be respected as long as the process leads to a net reduction in free energy. This can be seen during two–dimensional grain growth simulations assuming orientation–independent boundary energies, where the triple junctions do not maintain 120° angles during the process of growth, as might be required by mechanical equilibrium [81]. Another analogy is phase transformation where the chemical potential of a particular solute can increase with the passage of the interface as long as the overall free energy is reduced.

The goal of the present work was to derive a simplified theory which still deals with diffusion simultaneously through the boundary and volume and to compare the data against experiments.

3.4 Model Formulation: Mixed Diffusion-Controlled Growth

3.4.1 Assumptions

(i) To be consistent with diffusion–controlled growth, local equilibrium is assumed to exist at the interfaces so that the chemical potentials μ of all elements are uniform there:

$$\mu_{\mathrm{Fe}}^{\gamma} = \mu_{\mathrm{Fe}}^{\alpha} \qquad \text{and } \mu_{\mathrm{C}}^{\gamma} = \mu_{\mathrm{C}}^{\alpha}$$

It follows that the compositions where the different phases are in contact are given by tie–lines of the equilibrium Fe–C phase diagram, which were calculated using MTDATA [76] and the TCFE database, Fig. 3.3.

(ii) Since the kinetic theory gives the growth rate as a function of interlamellar spacing rather than a unique velocity, it is assumed that the actual spacing adopted is that which leads to a maximum in the rate of entropy production [57] although the maximum growth rate criterion [6] is also considered for the sake of completeness.

(iii) The model is created for conditions in which fluxes from diffusion within the austenite ahead of the transformation front, and that via transport through the transformation front both contribute to growth.
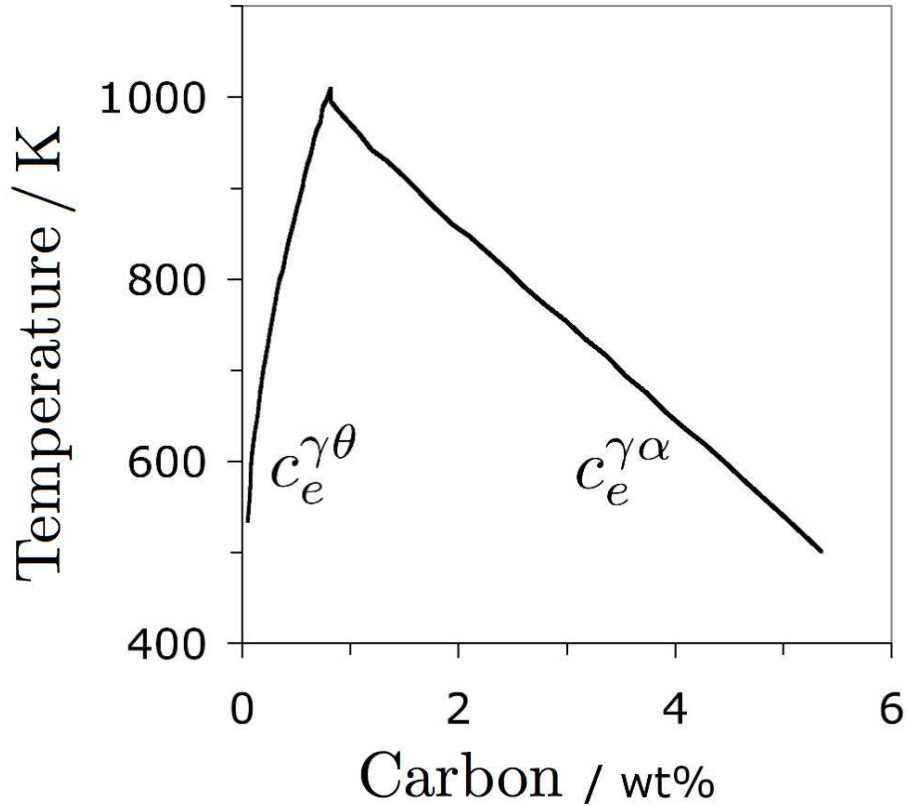
Figure 3.3: The extrapolated phase boundaries for equilibrium between austenite and cementite, and austenite and ferrite, in the Fe–C system.

3.4.2   Weighted average diffusion coefficient

The diffusion coefficient D_C^γ of carbon in austenite is strongly dependent on concentration [82, 83]. A model which takes into account the thermodynamics of carbon–carbon interactions [42, 43] has been used in determining the diffusion coefficient,

Table 3.1: Parameters used in the calculation of $\overline{D}$

Temperature	a^γ	$\frac{\partial a_1{}^\gamma}{\partial \theta}$	η	θ	$\overline{D}$
K					$\mathrm{m^2\,s^{-1}}$
840	14.87	329.22	871.85	$8.49{\times}10^{-2}$	$2.52{\times}10^{-13}$
880	7.56	176.66	399.29	$7.15{\times}10^{-2}$	$4.13{\times}10^{-13}$
920	3.88	99.75	195.80	$5.85{\times}10^{-2}$	$6.42{\times}10^{-13}$
940	2.78	76.41	140.25	$5.23{\times}10^{-2}$	$7.86{\times}10^{-13}$
960	1.98	59.33	101.97	$4.64{\times}10^{-2}$	$9.53{\times}10^{-13}$
970	1.67	52.56	87.45	$4.35{\times}10^{-2}$	$1.04{\times}10^{-12}$
980	1.41	46.73	75.31	$4.07{\times}10^{-2}$	$1.14{\times}10^{-12}$

D_{C}^γ, the details of which were discussed in the previous chapter. The weighted average diffusion coefficient accounting for the variation of carbon in austenite upto the pearlite-austenite interface has been calculated based on the equation 3.11 derived by Trivedi [41].

$$\overline{D} = \int_{c_{\mathrm{e}}^{\gamma\theta}}^{c_{\mathrm{e}}^{\gamma\alpha}} \frac{D\{c^\gamma, T\}}{c_{\mathrm{e}}^{\gamma\alpha} - c_{\mathrm{e}}^{\gamma\theta}} dc^\gamma \tag{3.11}$$

This equation is solved numerically using the trapezoidal rule and the composition limits have been determined using MTDATA and TCFE database [76]. All the parameters used in the calculation of weighted average diffusivity of carbon in austenite are listed in Table 3.1, the details of which were discussed in chapter 2.

3.4.3   Combined fluxes during pearlite growth

A model is developed here which accounts for fluxes through both the austenite and within the transformation front, on average parallel to the front [64]. For reasons stated earlier, the notion of interfacial tensions being balanced at three–phase junctions is abandoned. As in previous work, it is assumed that diffusion within the interface can be described by a single distribution coefficient, rather than two sep-

arate values corresponding to the α/γ and θ/γ interfaces. Fig. 3.4 illustrates the geometry of the pearlite colony.
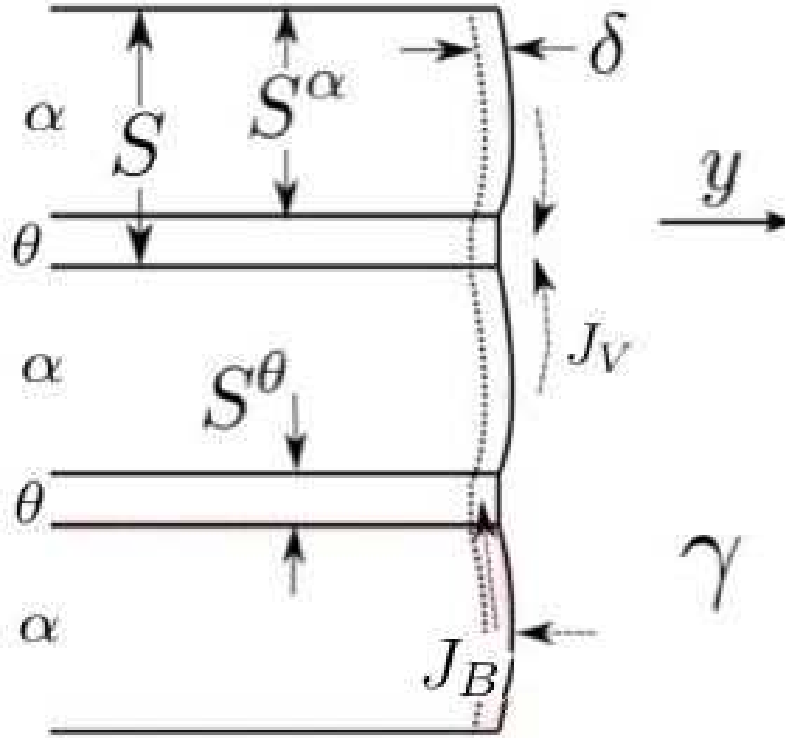
Figure 3.4: Geometry of pearlite colony. The dashed arrows indicate the volume and boundary diffusion processes. The thickness of the boundary is written δ.

The flux J_V away from the ferrite (equal to that towards the cementite), through the volume of the austenite is given by:

$$J_V = -\frac{A^\alpha}{V_m}\overline{D}\frac{dc}{dx} = \frac{\overline{D}\,b\,S^\alpha}{V_m}\frac{(c^{\gamma\alpha} - c^{\gamma\theta})}{S^\alpha/2} \tag{3.12}$$

where V_m is the molar volume of austenite (7.1×10^{-6} m^3 mol^{-1}) and to a good approximation assumed to be the same for all the phases involved, and A^α is the

cross sectional area of the interface, which for a unit depth into the diagram (Fig. 3.4) is equal to S^α, and the diffusion distance parallel to the interface, from the ferrite to the cementite is on average $S^\alpha/2$. An equation similar to the one above can be written for the boundary–diffusion flux J_B of carbon through the interface between austenite and ferrite towards the cementite [8]:

$$J_{\mathrm{B}} = -\frac{A^\alpha}{V_{\mathrm{m}}} D_{\mathrm{B}} \frac{dc}{dx} = \frac{12 D_{\mathrm{B}} \delta (c^{\gamma\alpha} - c^{\gamma\theta})}{V_{\mathrm{m}} S} \tag{3.13}$$

Interfaces are created between cementite and ferrite during the growth of pearlite, thus consuming some of the free energy ΔG of transformation. All of the available free energy is consumed in this way when the spacing between lamellae reaches a critical value $S_{\mathrm{c}} = 2\,\sigma^{\alpha\theta} V_{\mathrm{m}}/\Delta G$, where $\sigma^{\alpha\theta}$ is the α/θ interfacial energy per unit area. The growth rate then becomes zero but for $S > S_{\mathrm{c}}$ the free energy change is reduced by a factor $(1 - S_{\mathrm{c}}/S)$ and the concentration difference driving diffusion becomes $(c_{\mathrm{e}}^{\gamma\alpha} - c_{\mathrm{e}}^{\gamma\theta})\,(1 - S_{\mathrm{c}}/S)$ [6].

The total flux arriving at the θ/γ interface is a combination from transport through the volume of austenite and via the boundary. It follows that for a growth velocity v, the material balance at the transformation front is given by equation 2.27. Combining equations 3.12, 3.13 and 2.27 yields:

$$\frac{v\,S^\alpha S^\theta}{S}(c^{\theta\gamma} - c^{\alpha\gamma}) = 2\,\overline{D}\,(c^{\gamma\alpha} - c^{\gamma\theta}) + \frac{12\,D_{\mathrm{B}}\,\delta(c^{\gamma\alpha} - c^{\gamma\theta})}{S} \tag{3.14}$$

where $\bar{c}$ is the average concentration in the austenite. The growth velocity is now isolated as follows:

$$v = \left(\frac{c_{\mathrm{e}}^{\gamma\alpha} - c_{\mathrm{e}}^{\gamma\theta}}{c^{\theta\gamma} - c^{\alpha\gamma}}\right)\left(2\,\overline{D} + \frac{12 D_{\mathrm{B}}\,\delta}{S}\right)\frac{S}{S^\alpha S^\theta}\left(1 - \frac{S_{\mathrm{c}}}{S}\right) \tag{3.15}$$

The problems associated with using a correct boundary diffusion coefficient have already been emphasised. It was decided therefore to deduce this using measured data on growth rate and interlamellar spacing, due to Brown and Ridley [13], based on the more reliable method of size distributions rather than the observation of what

might be the largest colony. Given that $\overline{D}$ is well established, the only unknown then becomes D_B (Fig. 3.5), from which an activation energy for boundary diffusion during the pearlite reaction was derived to be $Q_B \approx 97\,\mathrm{kJ\,mol^{-1}}$, with

$$D_B = 8.51 \times 10^{-5} \exp\left(-\frac{96851\,\mathrm{J\,mol^{-1}}}{RT}\right)\,\mathrm{m^2\,s^{-1}} \tag{3.16}$$

It is interesting that unlike previous work [21, 57] where the activation energy for boundary diffusion was found to be greater than for volume diffusion in both austenite and ferrite, here Q_B is bracketed between $Q_V^\alpha = 70\,\mathrm{kJ\,mol^{-1}}$ and $Q_V^\gamma = 135\,\mathrm{kJ\,mol^{-1}}$ [84].
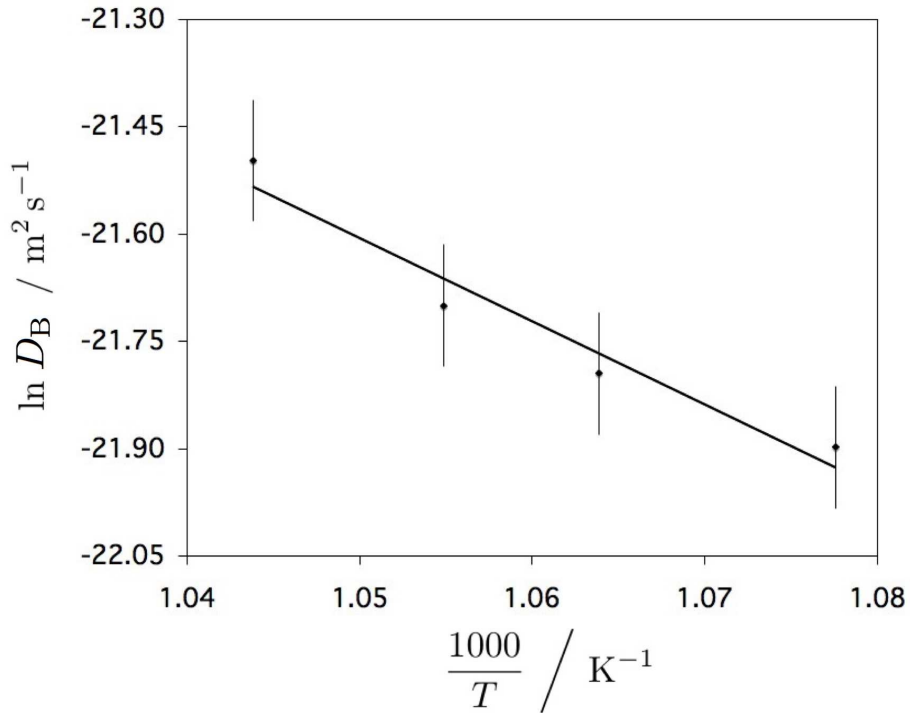
Figure 3.5: Arrhenius plot of D_B versus inverse of temperature in Fe-0.8C wt% steel for mixed mode diffusion–controlled pearlite growth.

The ratio of boundary to volume diffusion flux is shown as a function of temper-

ature in Fig. 3.6; as might be expected, boundary diffusion dominates except at the highest of transformation temperatures.
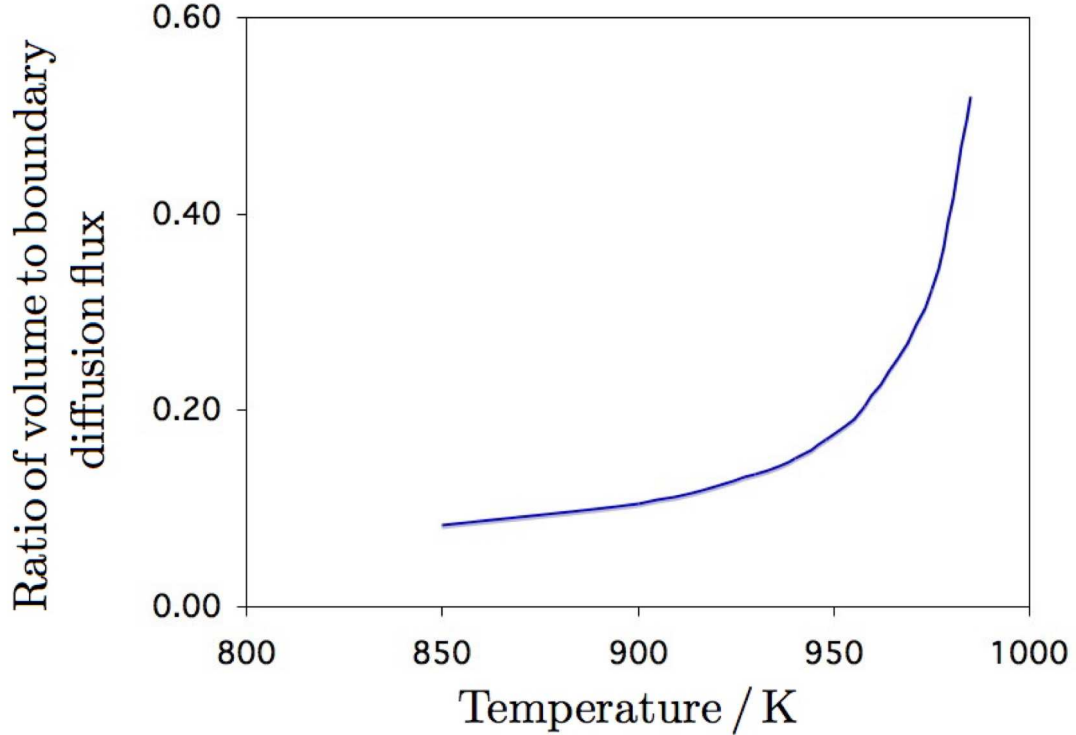
Figure 3.6: Relative contributions of volume and boundary diffusion fluxes during the formation of pearlite in Fe-0.8C wt% steel.

3.4.4   Evaluation of spacing criteria

In order to determine the growth rate of pearlite for the new mixed–diffusion theory, it is imperative to determine the relation between S and S_c. How these numbers are modified for the mixed volume and boundary–diffusion modes is discussed here.

Maximum growth rate: The velocity can be plotted as a function of S/S_c over a range of temperatures. The concentration gradient is constant for a particular

temperature and hence would not affect the relative position of the curve with respect to S/S_c. Approximate value of interlamellar spacing is assumed and the critical spacing is evaluated assuming $\sigma^{\alpha\theta} = 0.7 \, \mathrm{J\,m^{-2}}$, since the S/S_c is independent of the interfacial energy:

$$S_c = \frac{2 \, \sigma^{\alpha\theta}}{\Delta G} \tag{3.17}$$

The term, ΔG is the total free energy available during the transformation and is calculated using MTDATA and TCFE database [76]. The interlamellar spacing is then gradually increased to generate a set of S/S_c data. From the plot of velocity versus spacing, the S/S_c at which the velocity is maximum is determined. Fig. 3.7 shows the pearlite growth velocity versus spacing plots for a range of temperatures. The values of S/S_c vary from 1.36 to 1.53 over the range of temperatures studied.

Maximum rate of entropy production: The rate of entropy production $\dot{S}$ based on the equation 3.7 has been calculated using an approach similar to the one discussed for the maximum growth rate. The maximum in $\dot{S}$ is obtained when S/S_c is between 2.01 to 2.17 depending on the temperature of transformation, but independent of the interfacial energy $\sigma^{\alpha\theta}$. The variation of $\dot{S}$ as a function of spacing is shown in Fig. 3.8 for the range of temperatures under consideration.

3.4.5   Interfacial energy

The interfacial energy per unit area of the ferrite-cementite interfaces, $(\sigma^{\alpha\theta})$ plays a vital role during the pearlite transformation. In the absence of experimental data for interlamellar spacing, it becomes imperative to know the interfacial energy in order to predict the growth rate of pearlite. Zener [6] has shown that the pearlite growth is maximum when the interfacial energy of ferrite-cementite interfaces is half of the total free energy available for transformation assuming diffusion–controlled growth. Kramer *et al.* deduced the $\sigma^{\alpha\theta}$ using Zener's free energy and spacing data to be 2.8 $\mathrm{J\,m^{-2}}$. They calculated the energy of ferrite-cementite interfaces using a calorimetric method [77]. Interfacial enthalpy of pearlite-austenite was measured as
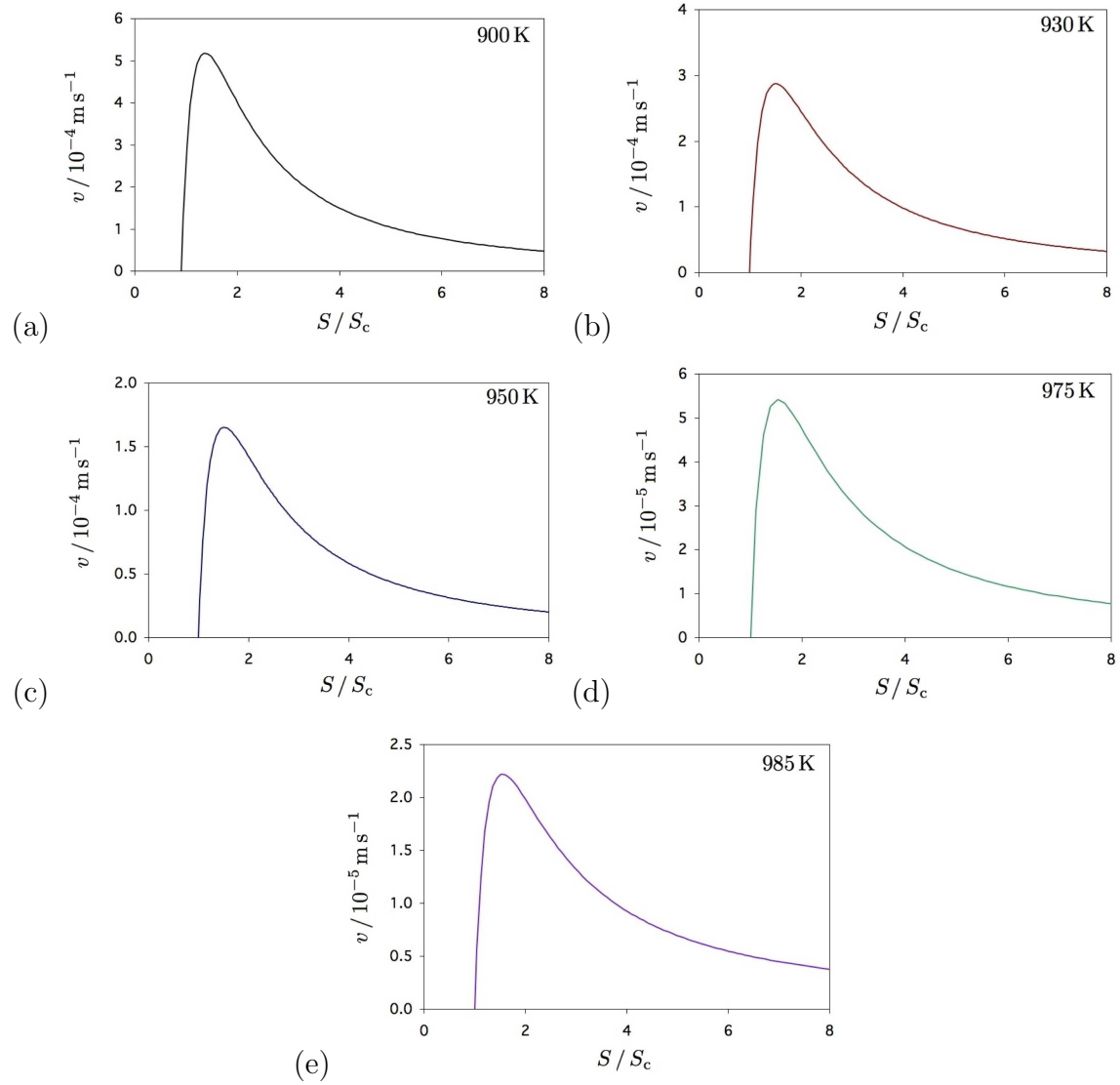
Figure 3.7: (a) Variation in the growth rate as a function of the normalised inter-lamellar spacing.
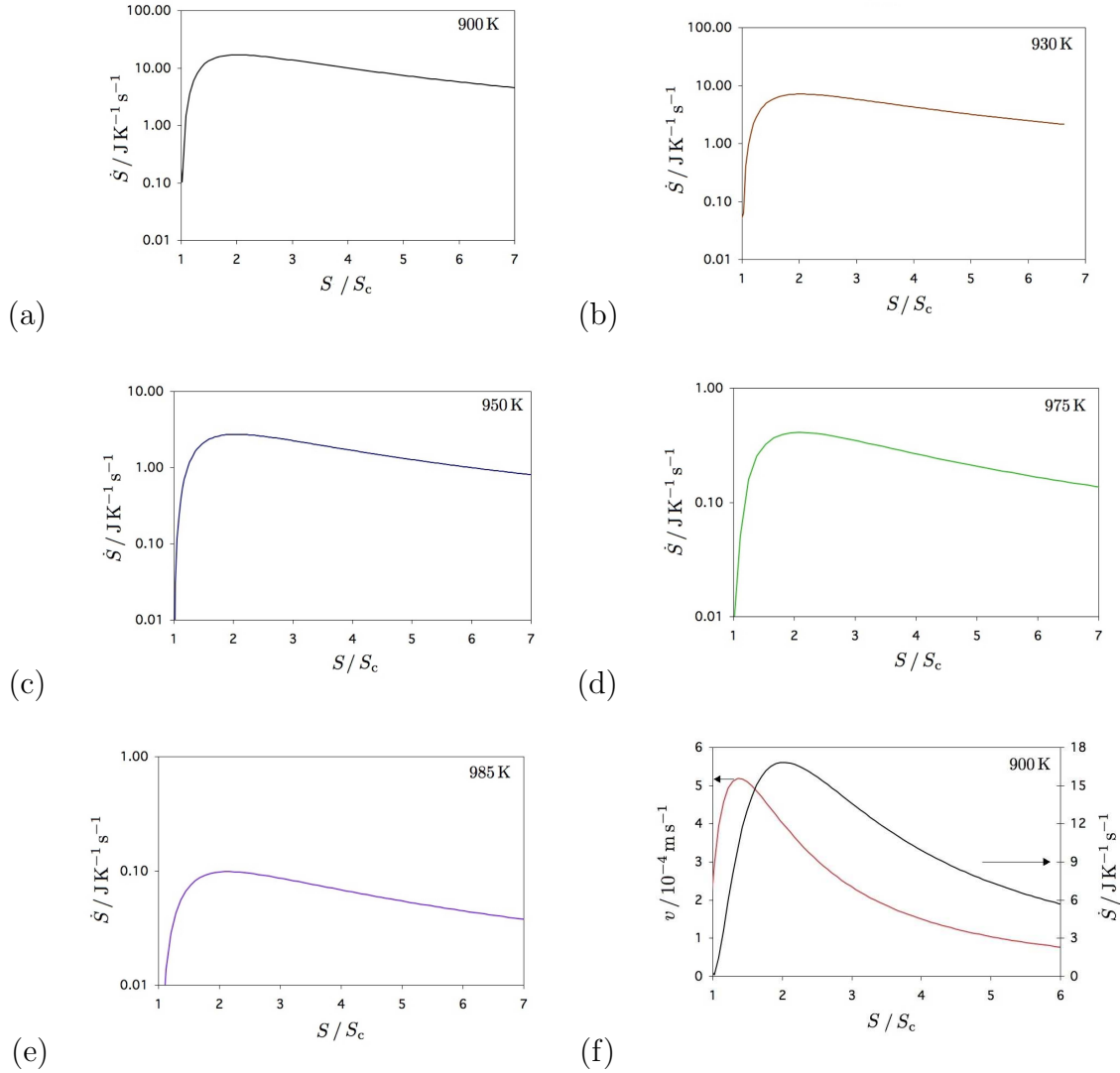
Figure 3.8: (a) Variation in the entropy production rate as a function of the normalised interlamellar spacing. Comparison of maximum growth rate and entropy production rate at 900 K is shown in Fig. 3.8 (f).

Table 3.2: Published values of the ferrite–cementite interfacial energy per unit area.

Reference	Temperature K	Method	σ $\mathrm{J\,m^{-2}}$
[87]	861	coarsening rate and data fitting	0.56
[88]	903-963	coarsening rate and data fitting	0.248-0.417
[77]	1000	interfacial enthalpy measurement	0.7±0.3
[89]	973	dihedral angle	0.52 ±0.13
[90]	-	atomistic simulation	0.615
[91]	-	interfacial enthalpy measurement	0.5 ± 0.36

a function of spacings and the entropy value for the interface was assumed as $(6.6 \times 10^{-4}\,\mathrm{J\,m^{-2}\,K^{-1}})$ in order to compute the interfacial energy. The value of interfacial entropy for ferrite-cementite interfaces was assumed based on those measured for gold $(0.5 \times 10^{-3}\,\mathrm{J\,m^{-2}\,K^{-1}})$ [85] and silver $1 \times 10^{-3}\,\mathrm{J\,m^{-2}\,K^{-1}}$ [86] determined from surface tension measurements. The corresponding interfacial free energy was estimated to be $0.7 \pm 0.3\,\mathrm{J\,m^{-2}}$ at 727 °C.

Das *et al.* [87] and Deb *et al.* [88] calculated the ferrite-cementite interfacial energy for coarsening of cementite particles in ferrite matrix in steel. The $\sigma^{\alpha\theta}$ is obtained from the coarsening rate constant, which is determined by fitting experimental growth rate data. It is worth noting here that these data are for a different morphology (spherical) of ferrite-cementite interface which is lesser than in case of lamellar pearlite. Martin and Sellars calculated the interfacial energy for lenticular cementite precipitates on the ferrite grain boundaries based on dihedral angle measurements and reported a value of 0.52 ± 0.13 Jm^{-2}. Ruda *et al.* computed the ferrite-cementite interfacial energy in Fe-C alloy using atomistic simulations and reported the same to be 0.615 Jm^{-2}. Although there was no mention about the temperature at which this value was reported, it can be assumed to be the same at 0 K as is normally the case in all the first principle calculations. Independent, published measurements of $\sigma^{\alpha\theta}$ are listed in Table 3.2.

In the absence of any reliable data on the interfacial energy, it is possible to derive from the kinetic data on pearlite growth, the interfacial energy relating cementite and ferrite [57].

$$\sigma^{\alpha\theta} = \frac{1}{2}\, S_{\mathrm{c}}\, \Delta G \approx \frac{S_{\mathrm{c}}\, \Delta T\, \Delta H}{2\, T_{\mathrm{e}}} \qquad (3.18)$$

where the approximation on the right hand side is based on the assumption that the entropy of transformation in independent of temperature [25, 46, 78]. This approximation has been avoided by calculating both the enthalpy and entropy changes (Table 3.3) using MTDATA [76], Fig. 3.9. Values of S_{c} can be calculated using measured spacings from Brown [13] and the entropy production calculations illustrated in Fig. 3.8. The interfacial energy derived in this way is illustrated as a function of temperature in Fig. 3.10. The interfacial energy values calculated here vary from those of Hashiguchi and Kirkaldy [57], though the spacing and velocity data are in both cases from the same experimental measurements [58]. This difference may be attributed to two factors:

(i) The σ calculated [57] is based on the assumption that the entropy change during the pearlite transformation is independent of temperature, whereas it is shown to be a function of temperature in the present work.

(ii) The computation of S/S_{c} based on the maximum entropy production rate was the range 2.18–2.4 [57], whereas in the present work it has been shown graphically that this ratio lies in the range of 2.03–2.17 for the temperatures studied. This is attributed to the different growth equations used in the two studies.

Fig. 3.10 compares the values of interfacial energy derived from pearlite growth rate measurements with the independently measured values. The discrepancies are large for the lower transformation temperatures, relative to the data based on coarsening reactions and dihedral angle measurements. These are both techniques which are kinetically slow; it is possible therefore that the measured values are influenced by the segregation of solutes to the interface, which would lead to a reduction in energy. In contrast, the cementite–ferrite interfaces in pearlite are created fresh as
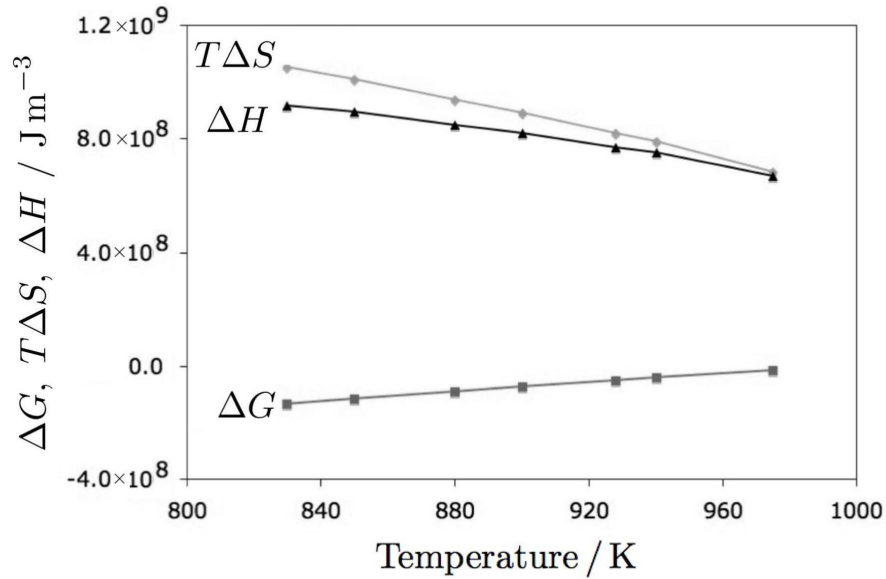
Figure 3.9: Free energy, enthalpy and entropy change as a function of temperature for a Fe-0.8C wt% steel.

a consequence of transformation. Entropy requires that the extent of segregation should be reduced at high temperatures. One further difficulty is that the diffusivity D_B is likely to increase with interfacial energy since a high value of the latter implies a less coherent interface. We are not able to account for this effect given the absence of relevant grain boundary diffusion data.

The growth rate determined using the mixed–diffusion controlled growth of pearlite described here gives a reasonable match with those predicted experimentally. Although the growth rate is calculated based on fitting the experimental data, the value of activation energy obtained is realistic, since it lies between the activation energy for volume diffusion in both ferrite and austenite. This approach proves to be a useful one, especially due to the lack of boundary diffusion data of carbon and also the segregation coefficient of the solute at the γ/α and γ/θ phase boundary. The match with experimental data is better when compared with prior work, (Fig. 3.11) of Puls and Kirkaldy [47] who had assumed the flux only through the austenite alone. Their predicted growth rates were lower than those measured experimentally by a
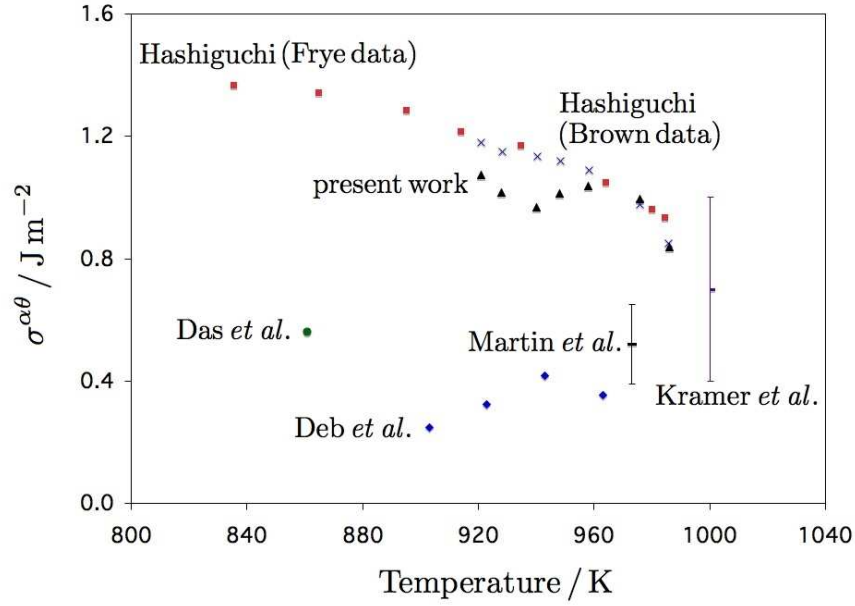
Figure 3.10: Comparison of calculated ferrite-cementite interfacial energy values and those reported in previous work by Hashiguchi and Kirkaldy [57].

Table 3.3: Calculated values of the ferrite–cementite interfacial energy per unit area based on MTDATA (TCFE database)

Temperature	G^γ	$G^{\alpha+\theta}$	ΔG	S	S_{c}	$\sigma^{\alpha\theta}$
K	J	J	$\mathrm{J\,m^{-3}}$	m	m	$\mathrm{J\,m^{-2}}$
920	$-6.56{\times}10^7$	$-6.64{\times}10^7$	$-5.61{\times}10^7$	$7.8{\times}10^{-8}$	$3.83{\times}10^{-8}$	1.07
928	$-6.66{\times}10^7$	$-6.73{\times}10^7$	$-4.98{\times}10^7$	$8.3{\times}10^{-8}$	$4.07{\times}10^{-8}$	1.01
940	$-6.81{\times}10^7$	$-6.87{\times}10^7$	$-4.07{\times}10^7$	$9.7{\times}10^{-8}$	$4.75{\times}10^{-8}$	0.97
948	$-6.91{\times}10^7$	$-6.96{\times}10^7$	$-3.48{\times}10^7$	$1.19{\times}10^{-7}$	$5.83{\times}10^{-8}$	1.01
958	$-7.04{\times}10^7$	$-7.08{\times}10^7$	$-2.76{\times}10^7$	$1.54{\times}10^{-7}$	$7.52{\times}10^{-8}$	1.04
976	$-7.26{\times}10^7$	$-7.28{\times}10^7$	$-1.59{\times}10^7$	$2.61{\times}10^{-7}$	$1.25{\times}10^{-7}$	0.99
985	$-7.39{\times}10^7$	$-7.40{\times}10^7$	$-9.30{\times}10^6$	$3.84{\times}10^{-7}$	$1.80{\times}10^{-7}$	0.84

factor of 2-4. It was suggested that the effective volume diffusion coefficient (which is the weighted average diffusion coefficient) of carbon in austenite is independent of temperature and hence trying to extract the activation energy from Fe-C pearlite data would be fruitless. However, our calculation shows that the weighted average diffusion coefficient, $\overline{D}$ does vary quite substantially with temperature and the same has been shown in Table 3.1.

The results were compared with those of Hashiguchi and Kirkaldy [57] who also assumed mass transport through the volume and pearlite-austenite phase boundary. It appears that they used the experimental data of Brown and Ridley [58] and Frye *et al.* [12] which were determined using a maximum nodule radius method, which has a limitation that it measures the maximum rather than an average growth rate. Hence it is difficult to apply it to rapidly transforming specimens and cannot be used once there is a significant impingement of the pearlite colonies. When the approximated model [57] was fitted to experimental data, rather large $\sigma^{\alpha\theta}$ interfacial energies were obtained, and the activation energy for the boundary diffusion of carbon was deduced to be in the range of 159920–169925 J mol^{-1}, which surprisingly was greater than for volume diffusion in both ferrite and austenite. It is noteworthy that Sundquist [15] reported an even larger activation energy for the boundary diffusion of carbon, commenting that the expected value should be much smaller; he attributed the discrepancy to a possible role of substitutional solute impurities.

Fig. 3.12 compares the experimental growth rates of pearlite obtained by various researchers for nearly eutectoid Fe-C alloys. However there is an important distinction with respect to the methods used by them. Frye *et al.* [12], Hull [92] and Brown and Ridley [58] measured the growth rates of pearlite using the maximum size of the pearlite colony. However Brown and Ridley also measured the same using two other methods namely, the Cahn-Hagel method [27] and another based on the size distribution of pearlite nodules. The latter seems to be a more comprehensive method since it is based on the size distribution rather than on the size of the largest colony.

In order to calculate the pearlite growth rate for Fe-C alloy in the absence of interlamellar spacing data, one must have a knowledge of the interfacial energy per
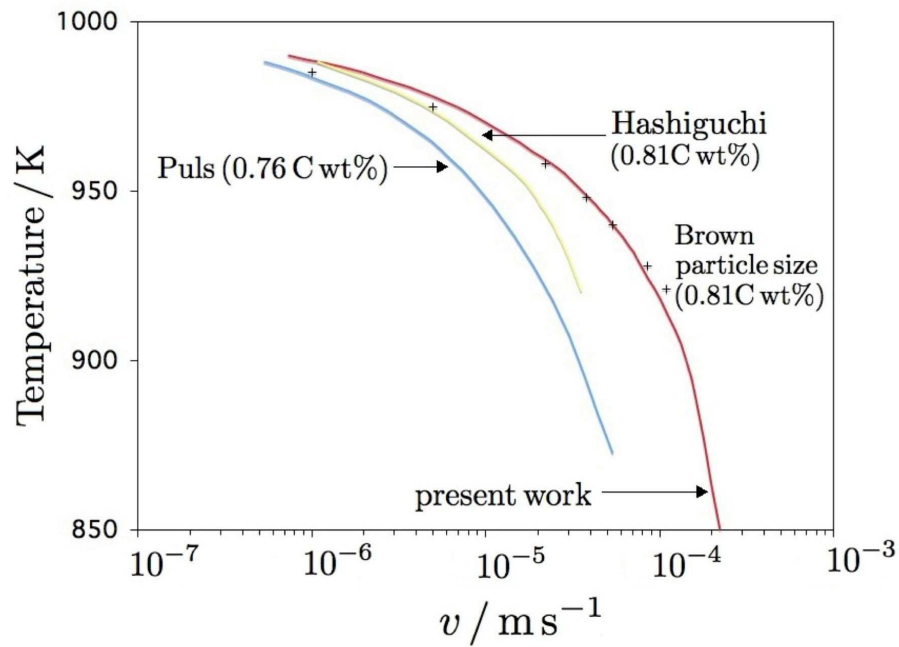
Figure 3.11: Temperature versus pearlite growth rate plot for Fe-0.8C wt% steel. Solid lines are calculated. The data from [58] based on particle size analysis are regarded as the most reliable for reasons discussed in the text.
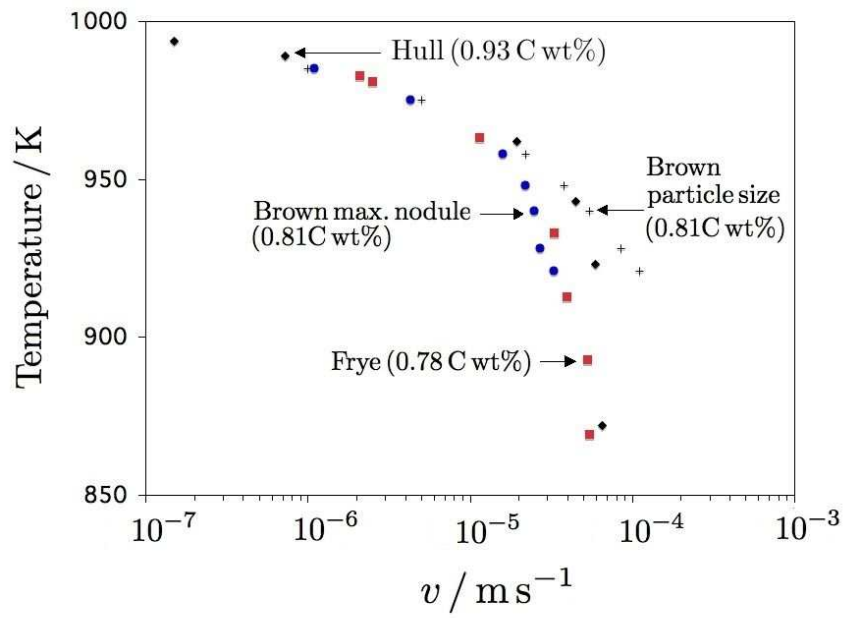
Figure 3.12: Comparison of experimental pearlite growth rate measured by various researchers [12, 58, 92].

unit area between ferrite and cementite, $\sigma^{\alpha\theta}$. Since this is shown to be a variable quantity with respect to temperature (Fig. 3.10), it is appropriate to calculate the growth rate for the minimum (0.84 J m^{-2}), maximum (1.07 J m^{-2}) and average value (0.99 J m^{-2}) of $\sigma^{\alpha\theta}$ and determine the sensitivity of growth rate to these changes. Fig. 3.13 shows the effect of $\sigma^{\alpha\theta}$ on the growth rate for Fe-0.8C wt% steel. The average value of $\sigma^{\alpha\theta}$ gives a good match with the experimental data of Brown and Ridley based on the particle size method. The difference between the growth rates calculated using the maximum $\sigma^{\alpha\theta}$ do not vary significantly as compared to the average value, however it tends to give a better match with the experimental data at higher temperatures.
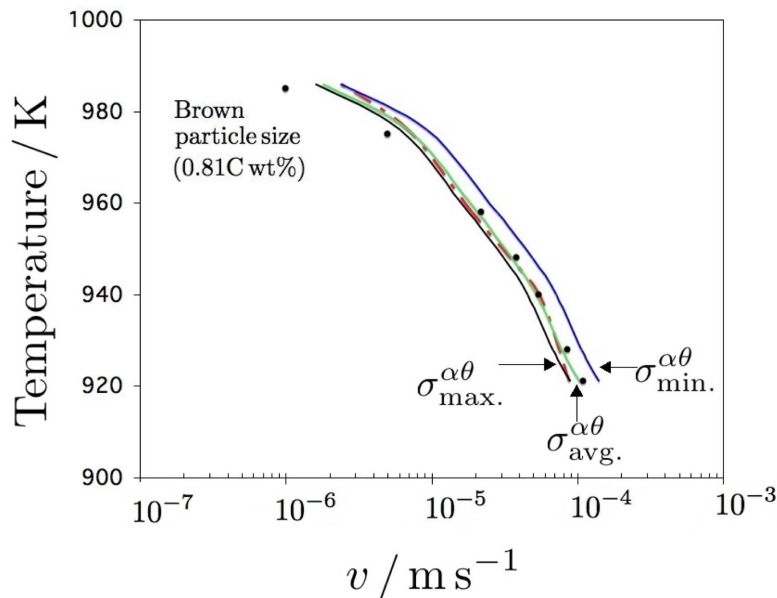
Figure 3.13: Sensitivity of the growth rate calculations to the α/θ interfacial energy. The points represent the experimental data and the red dash-dot line represents the change in growth rate as a function of temperature dependant interfacial energy.

3.5   Conclusions

A simplified theory has been proposed which combines the contributions from volume and boundary diffusivities, to represent the pearlite growth mechanism in Fe–C steels. The match with experimental data is better when compared with prior work, in spite of the fact that considerations of equilibrium at junctions between interfaces are abandoned. As might be expected, the flux through the boundary between pearlite and austenite dominates the transport of carbon at all but the highest of transformation temperatures. The theory for the first time leads to a realistic value for the activation energy for the grain boundary diffusion of carbon, less than that for volume diffusion in austenite and greater than for volume diffusion in ferrite.

The maximum entropy and growth rate criteria have been derived in the context of this mixed-mode diffusion theory, with the result that S/S_c is not constant but becomes a function of the transformation temperature. The ferrite–cementite interfacial energy has been deduced assuming that the pearlite interlamellar spacing is determined by the need to maximise the entropy production rate. The energy is lower than determined in previous work, but still much higher than reported in independent experiments, possibly because the interfaces created during pearlite transformation are fresh. It has been shown that in the absence of interlamellar spacing data, it is possible to calculate the critical and the nominal spacing based on the average energy of ferrite-cementite interfaces over a range of temperatures, although at higher temperatures, the maximum energy value would give a better prediction of the pearlite growth rate.

In is argued that this simplified theory avoids many of the approximations required to implement a more complex model in which the shape of the transformation front is determined by equilibrium at interfacial junctions.

Chapter 4

Influence of Diffusion in Ferrite on Pearlite Growth

4.1   Introduction

The theories discussed in the previous chapter for the mechanism of growth of pearlite, deal with either the diffusion of the solute through the austenite or the pearlite–austenite phase boundary in isolation or simultaneously through both of these. The mixed diffusion–controlled growth of pearlite has been shown to be a reliable theory to explain the experimentally measured growth rates [64]. Nakajima *et al.* [55] used a phase field model to treat the possibility that a flux in the ferrite, behind the pearlite–austenite transformation front, also contributes to the growth rate of pearlite. However they neglected the flux within the transformation front itself. This chapter describes the analytical treatment of growth of pearlite which considers the contribution of all three of the fluxes, that through the austenite, the transformation front and within the ferrite.

4.2   Diffusion in Ferrite

The diffusivity of carbon in ferrite is about two orders of magnitude higher than that in the austenite and hence one may be tempted to consider it to be a dominant factor to explain the growth rates observed experimentally. Cahn and Hagel examined the diffusion in ferrite alongside that in austenite, but they showed that the flux through the ferrite would still be lower on account of the smaller concentration gradient in ferrite despite the higher diffusivity [27]. It was suggested that the evidence of carbon diffusion through the ferrite can be verified experimentally depending on whether or not the carbide lamellae taper behind the transformation front. But they did not observe such behaviour and hence rejected the idea.

Nakajima *et al.* assumed that the flux through ferrite plays a key role in determining the pearlite transformation along with that in the austenite [55]. They developed a multi-phase field model which accounted for simultaneous diffusion through the ferrite and austenite. Since the diffusivity of carbon in ferrite is higher than that in austenite, it was argued that this would lead to a better agreement with the experimental growth rates. The interfacial energy of all the interfaces involved was assumed to be 1.0 $\mathrm{J\,m^{-2}}$, but the basis for selection was not clearly stated. The mobility of α/θ interface was assumed to be three orders of magnitude lower than the two other interfaces due to the instabilites arising out of the large composition differences involved; this is an artefact of the phase field model. The diffusion coefficients of carbon in austenite and ferrite were taken from the handbook [93]. The results of the phase field calculations show that the pearlite growth velocities for diffusion simultaneously through ferrite and austenite are higher than that through the austenite alone by about 4 times. It was suggested that the coupled diffusion through the ferrite and austenite gave a better agreement with the experimental data, although it did not fully explain them. Their model also showed a tapered profile of cementite with gradual increase in the thickness behind the transformation front, Fig. 4.1, an outcome of the diffusion in ferrite. The figure also shows the difference in concentration profile of carbon at the transformation front in both the cases. For

the case of diffusion through austenite and ferrite, the concentration of carbon at the transformation interface is lower than in case of its diffusion in austenite, attributed to some of the carbon being lost via diffusion in ferrite.
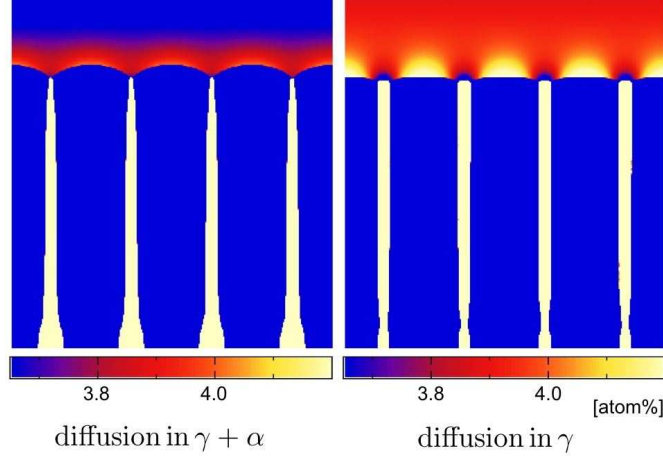
Figure 4.1: Comparison of carbon concentration profile during pearlite growth for different diffusion paths. $\Delta T = 30\,\mathrm{K}$ and $S = 0.3\,\mu\mathrm{m}$. Reproduced from Nakajima *et al.* [55] with permission from the journal.

4.3 Model Formulation

In order to account for the simultaneous diffusion in ferrite, austenite and the transformation front, an analytical treatment is presented here which combines the fluxes through all of these. For the growth velocity, v, the material balance at the transformation front is given by:

$$\frac{v\,S^{\alpha}}{V_{\mathrm{m}}}(\bar{c} - c^{\alpha\gamma}) = \frac{v\,S^{\theta}}{V_{\mathrm{m}}}(c^{\theta\gamma} - \bar{c}) = \frac{v\,S^{\alpha}S^{\theta}}{S\,V_{\mathrm{m}}}(c^{\theta\gamma} - c^{\alpha\gamma}) \tag{4.1}$$

where $\bar{c}$ is the average concentration of carbon in austenite. The flux through the volume of austenite as described in the chapter 3 can be written as:

$$J_V = -\frac{A^\alpha}{V_m} \overline{D} \frac{dc}{dx} = \frac{\overline{D} \, b \, S^\alpha}{V_m} \frac{(c^{\gamma\alpha} - c^{\gamma\theta})}{S^\alpha/2} \tag{4.2}$$

where V_m is the molar volume of austenite $(7.1{\times}10^{-6}~\mathrm{m^3\,mol^{-1}})$ and to a good approximation assumed to be the same for all the phases involved. A^α is the cross sectional area of the interface, which for a unit depth into the diagram (Fig. 4.2) is equal to S^α, and the diffusion distance parallel to the interface, from the ferrite to the cementite is on average $S^\alpha/2$. Similar equations can be written for the flux through the boundary and the ferrite. Hence the total flux of solute arriving at the transformation front is a combination of all of these. Combining equation 4.1 along with other diffusion fluxes leads to:
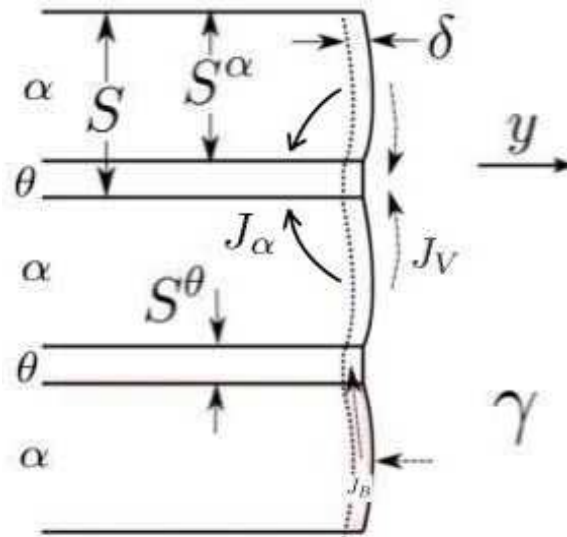
Figure 4.2: Geometry of pearlite colony. The arrows indicate the diffusion flux through austenite, ferrite and the phase boundary.

$$\frac{v\,S^\alpha S^\theta}{S}(c^{\theta\gamma} - c^{\alpha\gamma}) = 2\,\overline{D}\,(c^{\gamma\alpha} - c^{\gamma\theta}) + \frac{12\,D_{\mathrm{B}}\,\delta(c^{\gamma\alpha} - c^{\gamma\theta})}{S} - \frac{2\,D_\alpha(c^{\alpha\gamma} - c^{\alpha\theta})}{x} \quad (4.3)$$

where the term on the extreme right represents the flux within the ferrite, towards the cementite, behind the transformation front. $c^{\alpha\gamma}$ and $c^{\alpha\theta}$ represent the concentrations at the respective interfaces, which may not be necessarily given by equilibrium, since as will be discussed latter, the thickening of cementite is interface–controlled and not controlled by diffusion. D_α is the diffusivity of carbon in ferrite. The average diffusion distance from the ferrite–austenite, to its interface with the cementite is written $0.5\,x\,S^\alpha$, where x is some factor, the calculation of which will be discussed at a latter stage. S^α and S^θ have been determined by applying Lever rule and the interlamellar spacings, S are calculated using regression equation obtained from the measured data of Brown and Ridley [13].

The sign of this flux is different from the other two terms because it occurs in the product phase leading to a net reduction in the other two fluxes. As a result of flux through the ferrite, the effective concentration of carbon at the transformation front is reduced and hence the thickness of cementite at or near the transformation front will be lower than that far away from it. In order to work out the modified thicknesses of cementite and hence the ferrite lamellae as a result of diffusion flux in ferrite, a new factor f ($f = \Delta c \times D$) is evaluated for ferrite as well as austenite. The Δc and D represents the concentration difference and diffusivity in ferrite and austenite. Since f^α is greater than f^γ, the thickness of cementite is reduced by a proportionate amount.

For the diffusion–controlled growth of cementite, the rate at which carbon is incorporated in the growing cementite must equal the diffusion flux in ferrite:

$$v_{\mathrm{D}}^\theta(c_{\mathrm{e}}^{\theta\alpha} - c_{\mathrm{e}}^{\alpha\theta}) = D_\alpha \nabla C^\alpha \qquad (4.4)$$

v_{D}^θ is the growth rate of cementite for diffusion–controlled transformation and ∇C^α is the concentration gradient in ferrite. D_α is determined based on a model by McLellan *et al.* [94] and calculated using the MAP subroutine [95]. Fig. 4.3 represents a

schematic Fe-C phase diagram and depicts the various concentration terms under discussion.
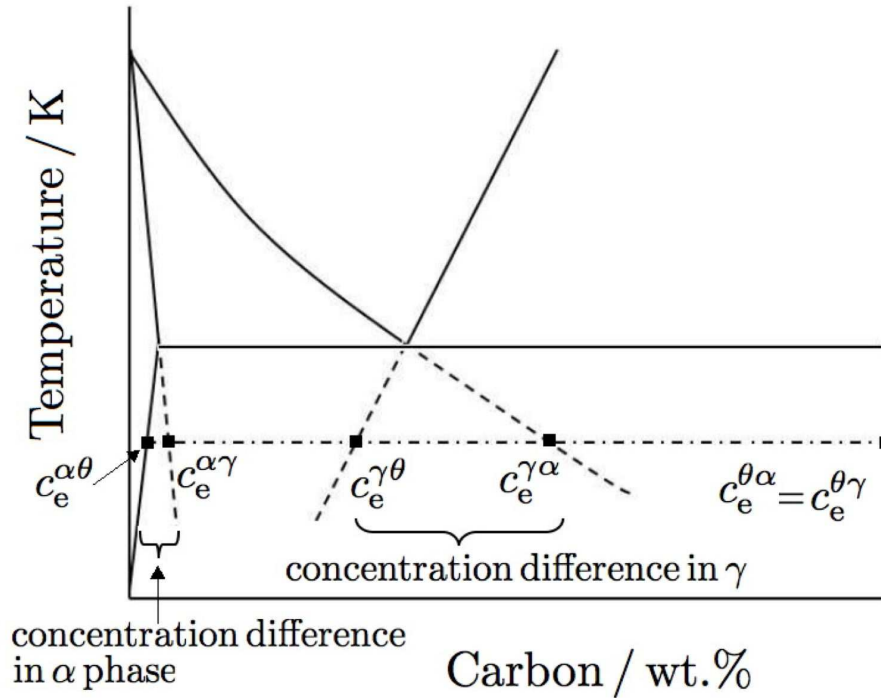
Figure 4.3: Schematic of Fe-C phase diagram.

It is possible that the carbon flux in ferrite calculated in this manner may or may not be commensurate to what the growing cementite can absorb. In order to evaluate the thickening rate of cementite, we calculate the migration rate of ferrite-cementite interface using the interface–controlled theory. The amount of free energy dissipated at the interface is proportional to the velocity of the interface and is given by:

$$\frac{\Delta G_I^{\alpha\theta}}{V_m} = \frac{v_I^{\theta}}{M^{\alpha\theta}} \qquad (4.5)$$

where $G_I^{\alpha\theta}$ is driving force for cementite growth and is calculated using the MTDATA

and TCFE database. $M^{\alpha\theta}$ is the mobility of the ferrite-cementite interface, and is taken from the work of Nakajima *et al.* and although the mobility should change with temperature, in the present calculation, due to absence of an accurate data, it is taken as constant (5×10^{-15} m^4 J s^{-1}). The velocity of the ferrite-cementite interface is shown in Fig. 4.4 and it appears to be about three orders of magnitude lower than if it were to be calculated based on diffusion–controlled growth. This leads to the conclusion that the rate of thickening of cementite is an interface and not a diffusion–controlled process. Using the mobility equation 4.5, the actual gradient
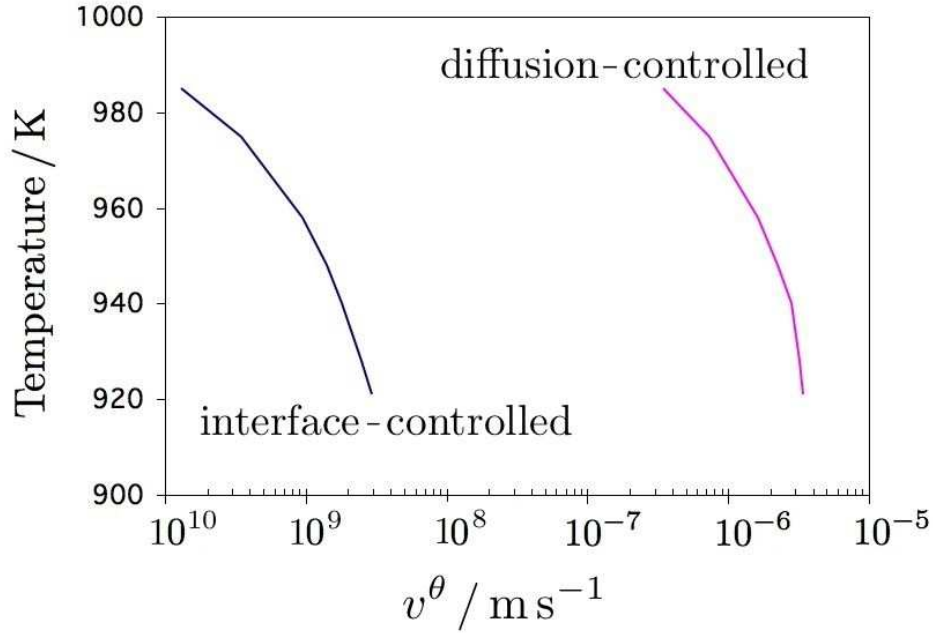
Figure 4.4: Comparison of thickening rates of cementite using interface and diffusion–controlled growth mechanisms.

within the ferrite is given by a mass balance, that the flux must equal the rate at which the cementite absorbs carbon as it grows:

$$\frac{D_\alpha \left(c^{\alpha\gamma} - c^{\alpha\theta} \right)}{0.5 x S^\alpha} = v_{\mathrm{D}}^\theta (c_{\mathrm{e}}^{\theta\alpha} - c_{\mathrm{e}}^{\alpha\theta}) \tag{4.6}$$

The concentration gradient in ferrite obtained here seems to be lower than that based on the equilibrium concentrations used in diffusion–controlled growth of cementite. From the knowledge of respective carbon diffusion fluxes, the growth rate of pearlite can be determined for the transport of solute through the ferrite, austenite and the phase boundary using the equation :

$$
v = S \left(\frac{\left[2\,\overline{D}\,(c_e^{\gamma\alpha} - c_e^{\gamma\theta}) + 12\,D_B\,\delta(c_e^{\gamma\alpha} - c_e^{\gamma\theta})/S \right]\left(1 - S_c/S \right) - 2D_\alpha(c^{\alpha\gamma} - c^{\alpha\theta})/x}{S^\alpha S^\theta (c_e^{\theta\gamma} - c_e^{\alpha\gamma})} \right)
$$

(4.7)

The term x in the average diffusion distance in ferrite, mentioned previously is given by the ratio of v/v_I^θ, where v is the experimental growth rate of pearlite [13]. This is because a relatively large pearlite growth rate would lead to greater diffusion distances within the ferrite. The maximum rate of entropy production criterion has been used to determine the critical spacing, S_c.

Fig. 4.5 shows the pearlite growth velocity determined by Nakajima *et al*. for the diffusion flux in γ and $\gamma + \alpha$ using multi–phase field calculations along with the analytical solution using diffusion only in the austenite phase. Although, the flux through $\gamma + \alpha$ gave a better match as compared to the diffusion in austenite, it still did not fully explain the measured growth rates [13]. This may be attributed to the following two factors: (i) the flux through the pearlite-austenite interface was neglected and (ii) the underlying uncertainty in the choice of interface mobilities. Their results for simultaneous flux through austenite and ferrite are lower than those calculated by us for a similar situation and the difference may be attributed to the diffusivities used by them for both ferrite and austenite which were lower than those in our calculations by 2-5 times.

Although it was shown in the previous chapter that the diffusion through austenite and the phase boundary adequately explains the measured rates of pearlite growth in Fe-C alloys, the same was calculated analytically using the equation 4.7 incorporat-

ing the fluxes through ferrite, austenite and the phase boundary. Fig. 4.6 compares the growth rates of the three flux model against that involving only boundary and volume diffusion in the austenite. The results indicate that inclusion of the flux through the ferrite would indeed lead to an increase in the growth rate, but the model (including the austenite and phase boundary) without the flux within the ferrite actually represents the experimental data rather well.
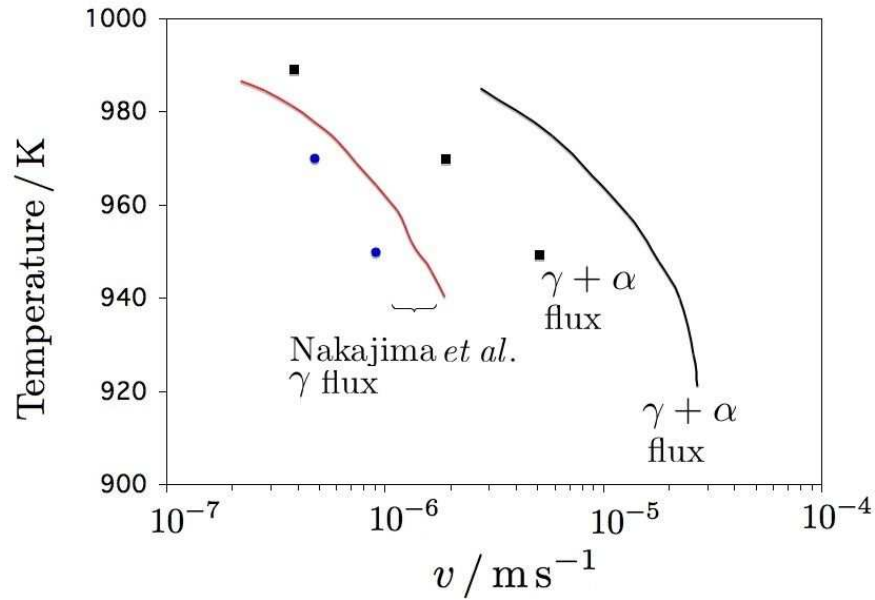
Figure 4.5: Comparison of pearlite growth rates. The points represent the phase field calculations (Nakajima $et\,al.$) and the lines are calculated. Red line indicates the growth rate based on analytical model [55] and black line indicates those calculated in the present work.

4.4 Conclusions

The pearlite growth rates have been calculated in a Fe-0.8C wt% steel assuming the diffusion flux through the austenite, ferrite and the phase boundary. Inclusion of flux through the ferrite does lead to an increase in the growth rate as compared to
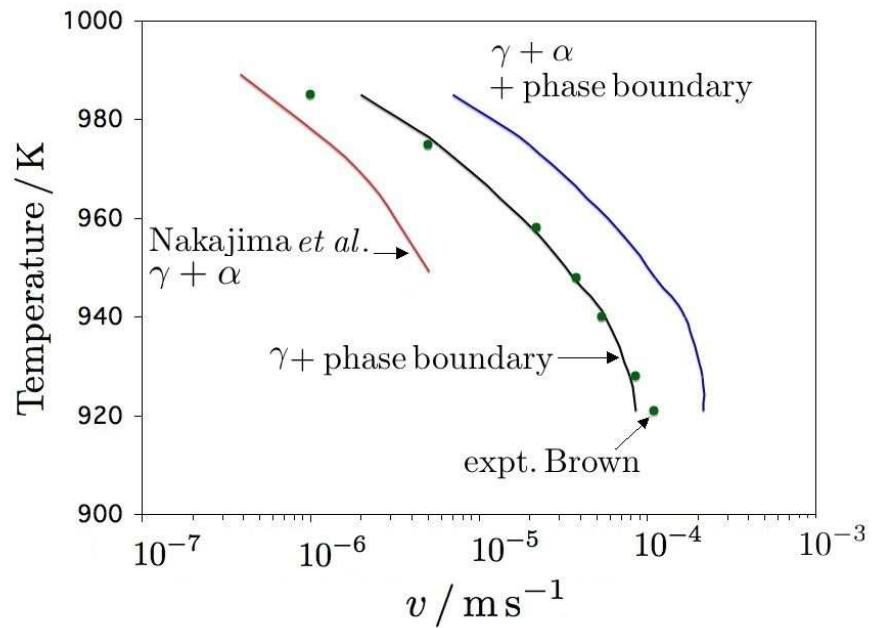
Figure 4.6: Calculated growth rates of pearlite based on phase field calculations with those in the present work assuming the 2 (boundary and austenite) and 3 (austenite, boundary and ferrite) fluxes. The points represent the experimental data.

that through austenite alone, although the agreement with the experimental data is still not good. Rather the match between the model based on the diffusion through the austenite and the phase boundary is much better when compared with the measured growth rates. The greatest uncertainty in the three–flux model arises in the mobility of the cementite–ferrite interface for which there are no experimental data. It was also pointed out earlier that evidence for the thickening of cementite behind the transformation front is weak. To summarise, it does not at the moment seem necessary or justified to include any flux within the ferrite to explain pearlite growth data.

Chapter 5

Pearlite Growth in Ternary alloys

5.1 Introduction

In the previous chapters, a method for calculating the growth rate of pearlite in a binary Fe–C system was established [64], without making *a priori* assumptions about whether the process should be controlled by the diffusion of carbon in the bulk of the parent phase, or short–circuited by diffusion in the transformation front, or whether diffusion through the ferrite behind the transformation front plays a role. The method permits all processes to occur simultaneously within an analytical framework with the extent of contribution from a particular mechanism depending naturally on circumstances such as the supercooling below the equilibrium temperature and the pertinent diffusion coefficients.

The purpose of this chapter is to extend this treatment to ternary steels designated Fe–C–X, where 'X' stands for a substitutional solute such as manganese. The complication here is that the diffusivity of a substitutional solute is far smaller than that of interstitial carbon. It then becomes difficult to discover conditions in which all solutes can maintain local equilibrium at the transformation front. The problem was elegantly solved some time ago in the case of the growth of allotriomorphic ferrite from austenite [59–62]. In essence, there is an additional degree of freedom afforded by the presence of the second solute which permits equilibrium between two phases

to exist for a range of compositions, rather than being defined uniquely for a binary alloy. This means that it is possible to pick interface compositions which maintain local equilibrium and yet allow the fluxes of the fast and slow diffusing species to keep pace.

The situation for pearlite is further complicated by the fact that two phases, ferrite and cementite, grow in a coupled manner at a common front with the austenite. It is even possible that local equilibrium, although a comforting and well–defined concept, is not in fact maintained during growth. It is relevant therefore to begin with a short assessment of the experimental data that exist on the partitioning of solutes as growth occurs.

5.2   Partitioning of Substitutional Solutes

Partitioning describes the redistribution of solute between the phases participating in the transformation process. Early studies in the context of pearlite in Fe–C–Mn and Fe–C–Cr indicated a so–called no–partition temperature below which the substitutional solute does not redistribute and pearlite growth is limited by the diffusion of carbon [17, 18]. It was argued that above this temperature, it is the diffusion of X through the transformation interface that determined the growth rate. Fig. 5.1 shows the partitioning data obtained by Razik and co-workers for Mn and Cr containing steels which depicts a transition from partitioning to zero–partitioning of these elements. Sharma *et al.* [70] calculated the pearlite growth rates for Cr containing steels using a similar argument, but they too could not justify the experimentally observed growth rates. However, neither of these scenarios was able to correctly estimate the growth rate at low temperatures. The equilibrium partition coefficients were calculated for steels containing Mn and Cr using MTDATA and TCFE database and compared with those obtained by Razik *et al.* for steel containing Mn (Fig. 5.2). The coefficient for Cr was much larger than that for Mn owing to its higher tendency to segregate to cementite.

Picklesimer [19] observed partitioning of Mn to cementite based on the chemical analysis of the extracted carbides for a 1.0Mn wt% eutectoid steel above 640°C.

(a)

(b)
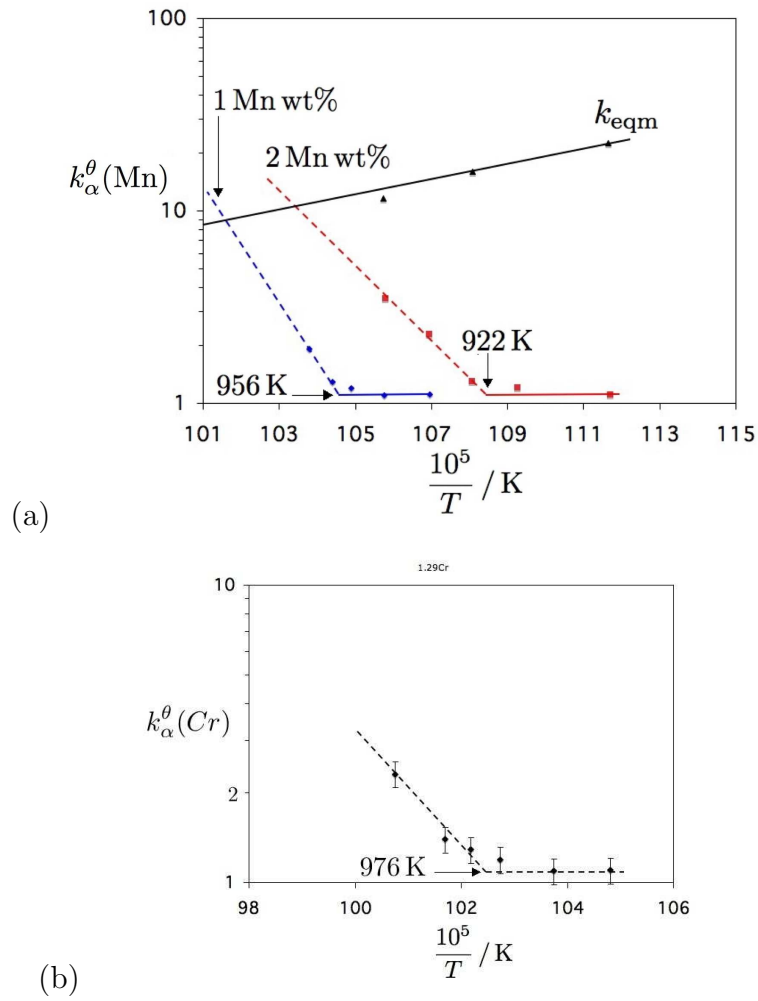
Figure 5.1: Partition coefficient of Mn and Cr in (a) Fe-C-Mn [17] and (b) Fe-C-1.29Cr wt% [18] steels as a function of reciprocal temperature.
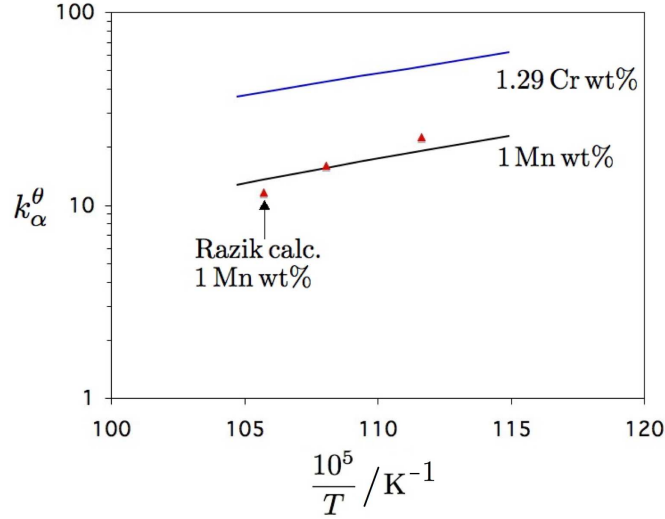
Figure 5.2: Equilibrium partition coefficient calculated using MTDATA as a function of inverse of temperature.

These data involved a contribution of Mn partitioning from ferrite to cementite behind the growth front (the steel was held at the transformation temperature for 24 hours) and hence it was difficult to exactly determine the no-partitioning temperature.

Al-Salman *et al.* [66] found that both chromium and manganese partitioned into cementite at the growth front in a Fe–Cr–Mn–C alloy down to a transformation temperature of 600°C, but were unable to identify a no–partition temperature. Experiments conducted with better resolution on Fe–C–Cr revealed that chromium in fact continues to partition in this manner to temperatures as low as 550°C [96], with the extent of partitioning increasing with temperature; once again, a no–partitioning temperature could not be identified. It was demonstrated that the rate of growth at low temperatures could be explained equally well by carbon volume diffusion or interfacial diffusion of chromium; there is of course, no logical reason to assume that the flux of carbon should be confined to the volume without a contribution through the interface. Hutchinson *et al.* studied the partitioning behaviour of steels containing 3.5Mn wt% and observed that it partitioned significantly during transformation

at 625°C, but the measurements were on samples heat treated for 2.5 h in which case it is not established whether the redistribution of solute occurred during growth or as a consequence of the extended heat treatment following the cessation of growth [71].

The experimental observations to date can lead to one firm conclusion, that substitutional solutes do partition at all temperatures where pearlite is known to grow; this might be expected since the transformation is reconstructive. It may reasonably be assumed that when a temperature is reached where the mobilities of the substitutional atoms are sufficiently small, pearlite simply ceases to form and austenite transforms instead by a displacive mechanism. The development of a model for the growth process for pearlite in ternary steels is discussed and assessed in the following sections.

5.3 Local Equilibrium in Ternary Systems

One well–known difficulty in dealing with ternary steels is that the interstitial carbon typically diffuses many orders of magnitude faster than substitutional solutes. To maintain local equilibrium at the interface, the rate at which solute is absorbed (or rejected) by the growing phase must equal that at which it arrives by diffusion (or diffuses away) from the interface. This requires the following two equations, one for each solute, to be satisfied simultaneously:

$$(c_C^{\gamma\alpha} - c_C^{\gamma\theta})v = -D_C \nabla c_C \tag{5.1}$$

$$(c_{Mn}^{\gamma\alpha} - c_{Mn}^{\gamma\theta})v = -D_{Mn} \nabla c_{Mn} \tag{5.2}$$

where v is the velocity of the transformation front and D represents the diffusivity of the solute identified by the subscript. Any interactions between the solutes, associated with cross-diffusion coefficients are neglected here. Given that $D_C \gg D_{Mn}$, there are two ways of choosing a tie–line which can satisfy these equations [62, 97], involving either the maximisation of ∇c_{Mn} or the minimisation of ∇c_C; in the former

case the sluggish diffusion of Mn is compensated for by selecting a tie–line which maximises its gradient, and in the latter case the tie–line is such that the gradient of carbon is minimised, thus allowing the two solutes to keep pace with the single moving interface.

For simplicity, the scenarios for the growth of a single phase, ferrite, from austenite is illustrated and as will be seen later, even this simple presentation can clarify the mechanism of pearlite growth. The case where the gradient of carbon is diminished is illustrated in Fig. 5.3a, where the austenite is supercooled into the two–phase field near the $\alpha + \gamma/\gamma$ boundary. This necessitates the partitioning and hence long range diffusion of manganese, so the mode is designated as 'partitioning local equilibrium' (P–LE). In contrast, a large supersaturation, whence the austenite is supercooled to a location in the two–phase field close to the $\alpha + \gamma/\alpha$ boundary leads to the case where the Mn concentration in α is similar to that in the alloy, or the 'negligible partitioning local equilibrium' (NP–LE) mode (Fig. 5.3b). Note that both cases involve local equilibrium at the interface and are exclusive; Fig. 5.3c shows the domains of the two–phase field within which each of the mode operates. A simple examination of the location of the alloy within the $\alpha + \gamma$ phase field therefore can establish whether or not Mn will partition during ferrite growth or whether growth will occur with negligible partitioning of the substitutional solute. The important point to recognise is that if partitioning must occur during ferrite growth then it necessarily means that pearlite growth must also involve partitioning since the ferrite is one of the components of pearlite.

This discussion of the growth of ferrite is well–established [62, 97] but it can be applied immediately to reach conclusions about pearlite, where two phases grow from austenite. It is necessary then to consider both the $\alpha + \gamma$ and $\theta + \gamma$ phase fields, and two separate tie–lines must be chosen to fix the compositions at the α/γ and θ/γ interfaces, as illustrated in Fig. 5.3d. The case illustrated is for NP–LE and it is only possible for the alloy marked 'A' to transform in this manner because the situation illustrated corresponds to a high–supersaturation. It has been observed that growth with NP–LE is thermodynamically not possible for any of the experimental data [17, 18] reported for the growth of pearlite.
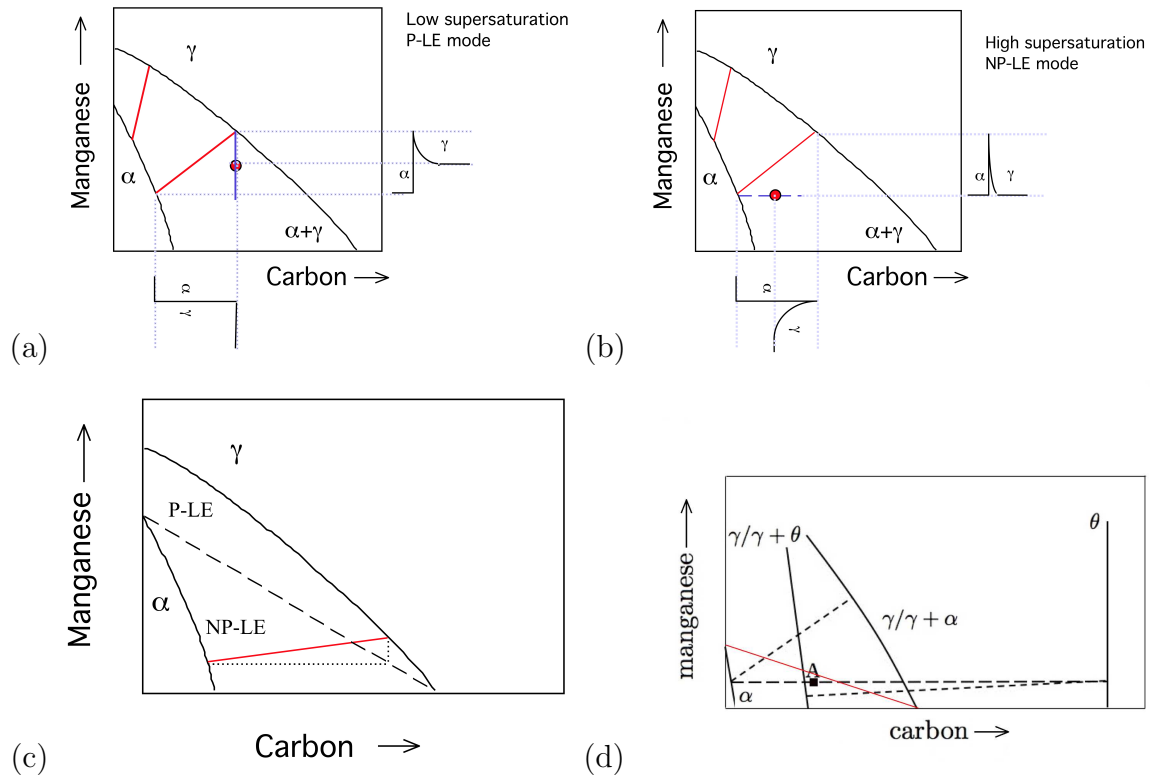
Figure 5.3: (a–c) Growth of ferrite with local equilibrium at the interface. The tie–lines are illustrated in red. When the alloy (indicated by dot) in its austenitic state is quenched into the $\alpha+\gamma$ phase field, the supersaturation is small if the alloy falls close to the $\alpha + \gamma/\gamma$ phase boundary. (a) P–LE mode involving the long–range diffusion of manganese. (b) NP–LE mode with negligible partitioning of Mn. (c) Division of the two–phase $\alpha + \gamma$ phase field into NP–LE and P–LE domains. For more details see [74]. (d) Schematic ternary isothermal section for the NP–LE condition satisfied for both cementite and ferrite during the growth of pearlite, because the point 'A' falls under the red line which separates the NP–LE and P–LE domains for ferrite.

5.3.1 Partitioning local–equilibrium in Fe-C-Mn

The partitioning local–equilibrium case corresponds to one in which the activity of carbon in the austenite ahead of the interface is almost uniform, thus allowing the flux of the slow diffusing manganese to keep pace. The activity of carbon in austenite for the alloy composition was calculated using MTDATA. The point of intersection of carbon iso-activity line with the phase boundaries of $\gamma/\gamma+\theta$ and $\gamma/\gamma+\alpha$ gives the interfacial compositions of Mn in austenite in equilibrium with ferrite and cementite. The tie-line corresponding to these points should then give the quantities $c_{\mathrm{Mn}}^{\alpha\gamma}$, $c_{\mathrm{Mn}}^{\gamma\alpha}$, $c_{\mathrm{Mn}}^{\theta\gamma}$ and $c_{\mathrm{Mn}}^{\gamma\theta}$.

It is found that the iso-activity line passing through the point Fe-0.8C-1.0Mn wt % never intersects the $\gamma/\gamma+\theta$ phase boundary, as has been observed in previous work (Fig. 5.4) for Fe–C–Mn hypo–eutectoid steels [71]. The strict P–LE condition is therefore impossible to achieve. The best that can be done in order to set $c_{\mathrm{Mn}}^{\gamma\theta}$ whilst at the same time ensuring that $c_{\mathrm{Mn}}^{\gamma\theta} < \bar{c}_{\mathrm{Mn}} < c_{\mathrm{Mn}}^{\theta\gamma}$, where $\bar{c}$ is the average composition of the alloy, is to assume that the tie-line connecting cementite and austenite passes through the alloy composition as illustrated for a range of temperatures Fig. 5.5(a-d). Fig. 5.5(e) depicts the P-LE condition at 945 K with schematic concentration profiles at the interfaces under consideration.

5.4 Grain Boundary Diffusion

Grain boundary diffusion plays a vital role in many processes such as discontinuous precipitation, recrystallisation, grain growth etc. It is also a well established fact that grain boundary provides easy diffusion path to solutes due to its more open structure than the otherwise perfect lattice structure. The influence of grain boundary diffusivity on the growth rates of pearlite in Fe-C alloys has already been discussed in the previous chapter. In case of a ternary system, Fe-C-X, this assumes greater significance as the substitutional solute partitions into the product phase/s preferably through the advancing phase boundary since the volume diffusivity associated with these is much lower. However there is a difficulty in dealing with the grain boundary
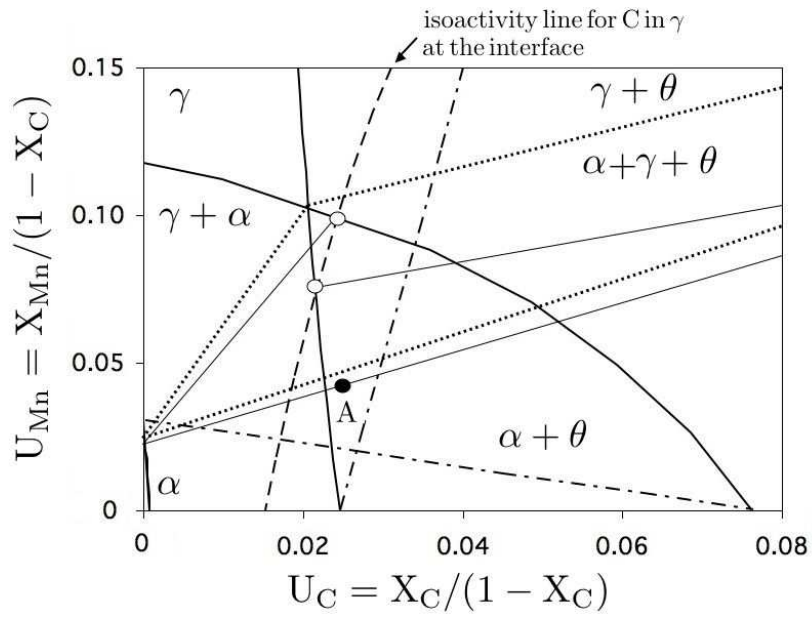
Figure 5.4: Fe-C-Mn phase diagram at 625 °C with the alloy 'A 'lying in the two phase region. Adapted from Huchinson *et al.* [71]
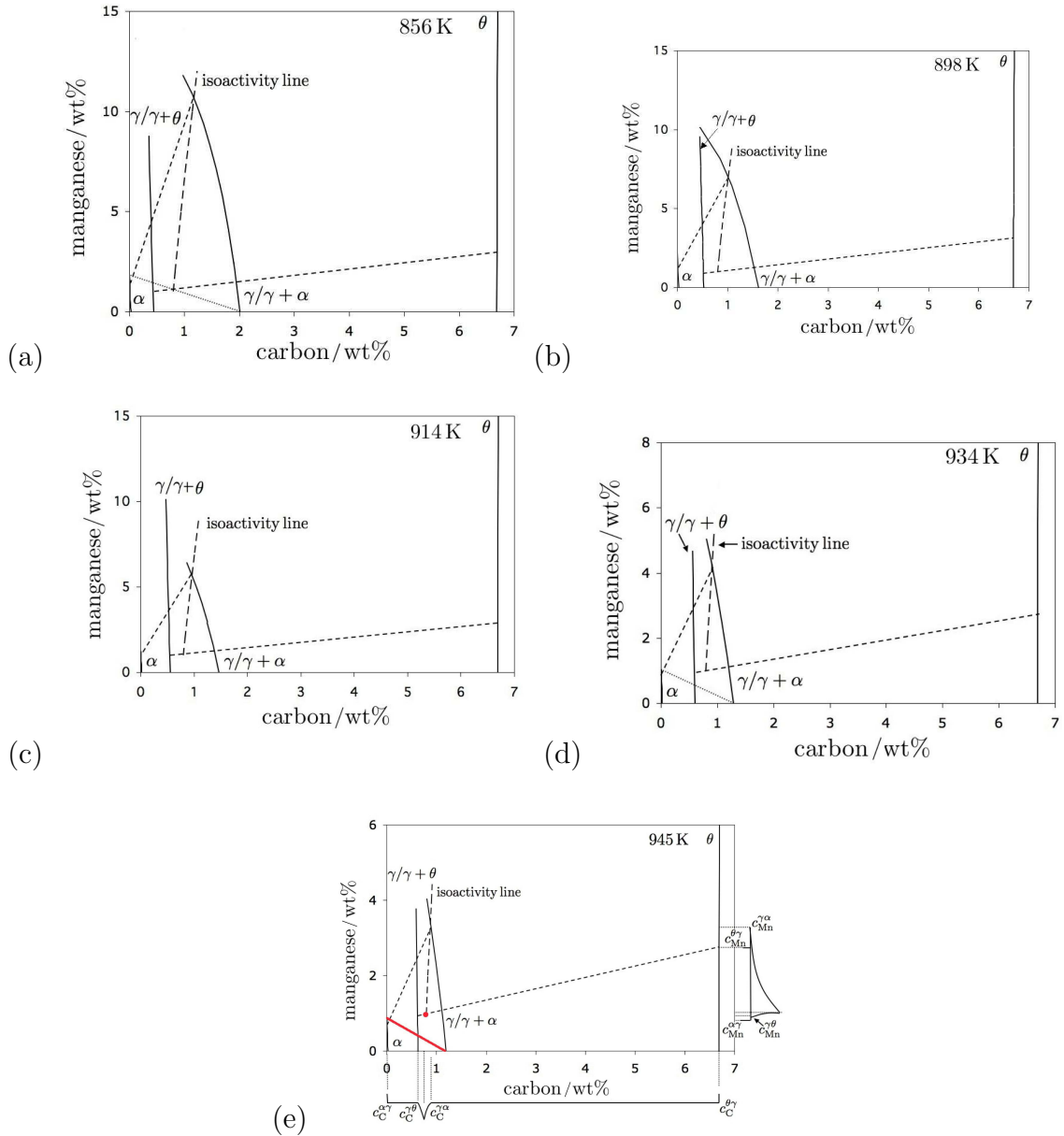
Figure 5.5: The case for partitioning local equilibrium transformation of Fe–0.8C–1Mn wt%, noting that strict P–LE is not possible since the carbon iso–activity line does not intersect the $\gamma + \theta/\gamma$ phase boundary. The alloy is indicated by the red dot and the red line divides the $\alpha + \gamma$ phase fields into the P–LE and NP–LE domains.

Table 5.1: Grain boundary diffusivities in Fe from literature. T_m is the melting temperature.

System	$\delta\, D_0$ $\mathrm{m^3\,s^{-1}}$	Q_B $\mathrm{kJ\,mole^{-1}}$	Ref.
Fe in γ-iron	0.77×10^{-13}	159	[101]
Fe in γ or α-iron	5.4×10^{-14}	155	[44]
Fe in γ-iron	9.7×10^{-15}	$75.4 T_\mathrm{m}\,/\,K$	[102]
Fe in γ-iron	9.44×10^{-15}	$83.0 T_\mathrm{m}\,/\,K$	[99]
Fe in γ-iron	1.5×10^{-14}	$74.5 T_\mathrm{m}\,/\,K$	[100]

diffusivity of the substitutional solutes due to the lack of experimental data associated with them. Fridberg *et al.* [44] suggested that the grain boundary diffusivity of substitutional solutes like Mn, Cr, Ni *etc.* can be reasonably approximated to the boundary self–diffusivity of iron as their atomic size is closer to Fe. Kaur *et al.* [98] have shown that the diffusivities in case of volume self–diffusion of metals with same crystal structure at the melting temperature are identical, irrespective of the melting temperature difference between these. Brown and Ashby [99] and Gjostein [100] showed that these correlations hold good in case of grain boundary self-diffusion also. They further evaluated that the grain boundary diffusion coefficient D_B, for all the metals would approach a value of about $1\text{-}3 \times 10^{-9}$ $\mathrm{m^2\ s^{-1}}$ at the melting temperature. James and Leak [101] experimentally determined the grain boundary diffusivity of Fe in γ-iron with a radioactive tracer and using sectioning and residual activity technique. Table 5.1 summarises the activation energies calculated based on the data of various researchers and they were in the range of 134-159 $\mathrm{kJ\,mol^{-1}}$ with the pre-exponential terms being of the order of $10^{-14} - 10^{-15}\,\mathrm{m^3\,s^{-1}}$.

5.5 Pearlite Growth Rate in Fe-C-Mn Steels

5.5.1 Assumptions

It is assumed that when the transfer of atoms across the growth front is not rate limiting; for a diffusion–controlled reaction, the compositions at the interfaces can be estimated from the existence of local equilibrium. In such a case, the compositions are given by tie–lines of the equilibrium ternary phase diagram so that the chemical potentials (μ) of the species are locally uniform:

$$\mu_{\text{Fe}}^{\gamma} = \mu_{\text{Fe}}^{\alpha} \qquad \text{and } \mu_{\text{C}}^{\gamma} = \mu_{\text{C}}^{\alpha} \qquad \text{and } \mu_{\text{Mn}}^{\gamma} = \mu_{\text{Mn}}^{\alpha}$$

$$\mu_{\text{Fe}}^{\gamma} = \mu_{\text{Fe}}^{\theta} \qquad \text{and } \mu_{\text{C}}^{\gamma} = \mu_{\text{C}}^{\theta} \qquad \text{and } \mu_{\text{Mn}}^{\gamma} = \mu_{\text{Mn}}^{\theta}$$

Since the kinetic theory for pearlite gives the growth rate as a function of inter-lamellar spacing rather than a unique velocity, it is assumed that the actual spacing adopted is the one which leads to maximisation of the entropy production rate [60]. The preceding discussion based on experimental observations indicates that substitutional solutes partition during the growth of pearlite even at the lowest of temperatures studied. Furthermore, none of the data are consistent with growth involving local equilibrium with negligible partitioning. In addition, only an approximation to the P–LE mode can apply if local equilibrium is to be maintained, since the iso–activity line for carbon does not in general intersect the $\gamma/\gamma+\theta$ phase boundary; it is necessary, therefore, to assume that the tie-line connecting cementite and austenite passes through the alloy composition.

The growth rate of pearlite is then calculated based on the above set of assumptions bearing in mind that substitutional solutes must diffuse, and that the easiest diffusion path for such solutes is through the interface. The substitutional solute flux through the volume of austenite has been shown to be negligibly small in comparison.

5.5.2 Activation energy for boundary diffusion

Whereas data for volume diffusion are readily available, those for boundary diffusion are not. Use was therefore made of experimental data on pearlite growth where interlamellar spacing have also been measured and reported. Such data are available for 1.0Mn wt% [46] and 1.08–1.8Mn wt% eutectoid steels [17]. The data from Ridley [46] were used to derive interfacial diffusion coefficients by fitting to the theory for boundary diffusion–controlled growth of pearlite [7]:

$$v = 12sD_{\mathrm{B}}\,\delta\left(\frac{c_{\mathrm{Mn}}^{\gamma\alpha} - c_{\mathrm{Mn}}^{\gamma\theta}}{c_{\mathrm{Mn}}^{\theta\gamma} - c_{\mathrm{Mn}}^{\alpha\gamma}}\right)\frac{1}{S^{\alpha}\,S^{\theta}}\left(1 - \frac{S_{\mathrm{c}}}{S}\right) \tag{5.3}$$

where v is the growth rate of pearlite, s is the boundary segregation coefficient for the γ/α and γ/θ interfaces, the values of which are difficult to determine experimentally and hence are not available. The thickness of the transformation interface, δ, is assumed to be of the order of 2.5 Å[78]. S^{α} and S^{θ} are the thicknesses of the ferrite and cementite platelets. In order to avoid any assumptions regarding the segregation coefficient, a lumped value of sD_{B} is evaluated from the experimental data of Ridley [46]. The critical interlamellar spacing S_{c} at which $v = 0$ was calculated from $S/S_{\mathrm{c}} = 2$ based on the a growth rate which leads to the maximum rate of entropy production [60, 64]. Phase equilibria were, throughout this work, calculated using MTDATA and the TCFE database [76] and the compositions are listed in Table 5.2.

Table 5.2: P-LE compositions of manganese at the interface. (The compositions are reported in wt%.)

Temperature K	$c_{\mathrm{Mn}}^{\gamma\alpha}$	$c_{\mathrm{Mn}}^{\gamma\theta}$	$c_{\mathrm{Mn}}^{\theta\gamma}$	$c_{\mathrm{Mn}}^{\alpha\gamma}$
856	10.84	0.87	3.02	1.52
898	7.0	0.97	3.08	1.45
914	5.78	0.92	2.84	1.05
934	4.36	0.94	2.84	0.86
945	3.29	0.95	2.76	0.67

94

Fig. 5.6 shows a plot of $\ln sD_B$ vs. $1000/T$, the slope and intercept of which yields the boundary diffusion coefficient for manganese:

$$sD_B = 2.81 \times 10^{-3} \exp\left(-\frac{164434\,\mathrm{J\,mol^{-1}}}{RT}\right)\,\mathrm{m^2\,s^{-1}} \qquad (5.4)$$

The activation energy determined using the above procedure corresponds to the pearlite–austenite interface and is slightly higher than those reported by the other researchers for the grain boundary self–diffusion. This is in line with the argument Bokshtein $et\,al.$ [39] had cited for the diffusion along the phase boundaries, which suggests that the phase boundary does not exist as a branched network as opposed to a grain boundary which is continuous, resulting in lesser material transport through the former.

5.5.3 Interfacial energy

The interfacial energy per unit area σ for the ferrite-cementite interface can also be derived from the kinetic data available for pearlite growth. The critical spacing at which growth ceases because all of the driving force is used up in creating the interfaces is given by equation 3.18 discussed in chapter 3. In order to avoid the assumption that entropy of transformation is independent of temperature as discussed previously, the enthalpy and entropy changes as a function of temperature have been calculated using MTDATA [76] and the same has been shown in Fig. 5.7. The critical spacing S_c is calculated from the experimentally measured interlamellar spacings S [46] and the graphical relation of S/S_c shown in Fig. 5.8. The ratio S/S_c is calculated assuming the maximum entropy production rate and is equal to 2 for the range of temperatures studied. This is unlike the previous study on Fe–C alloy [64], simply because with the substitutional solute it is only the flux through the interface which is relevant, whereas in the case of carbon, the proportions contributed by volume and interface diffusion vary significantly with temperature. The interfacial energy estimated in this way is shown in Fig. 5.9. For reasons which are not clear, the values thus calculated are somewhat higher than those reported for Fe–C but not

dramatically different.

It is important to note that in all of the analysis of experimental data (v, S) that follows, the interfacial energy does not appear explicitly since equation 5.3 requires only the ratio S_c/S. Given measured values of S and the fact that $S/S_c = 2$ means that S_c is defined. However, in order to make predictions of the growth rate in the absence of experimental data, it clearly is necessary to know the interfacial energy.
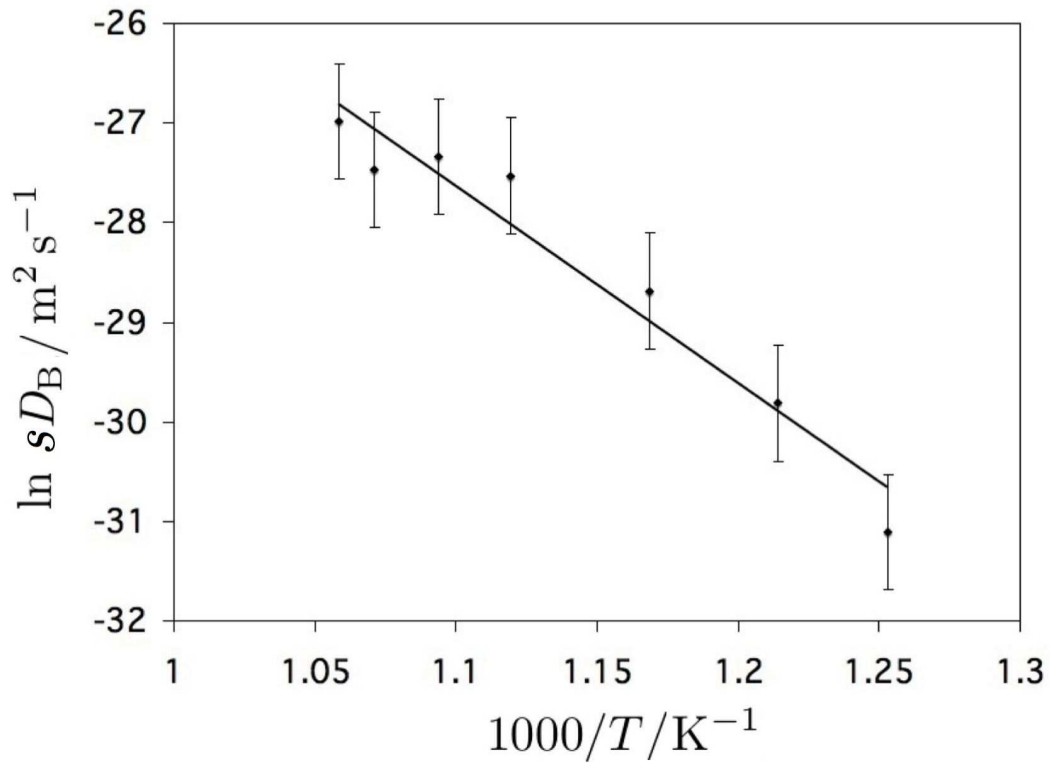
Figure 5.6: Arrhenius plot of sD_B versus inverse of temperature in Fe-1.0Mn-0.8C wt% steel for interface diffusion controlled pearlite growth. Error bars indicate the standard error of mean.
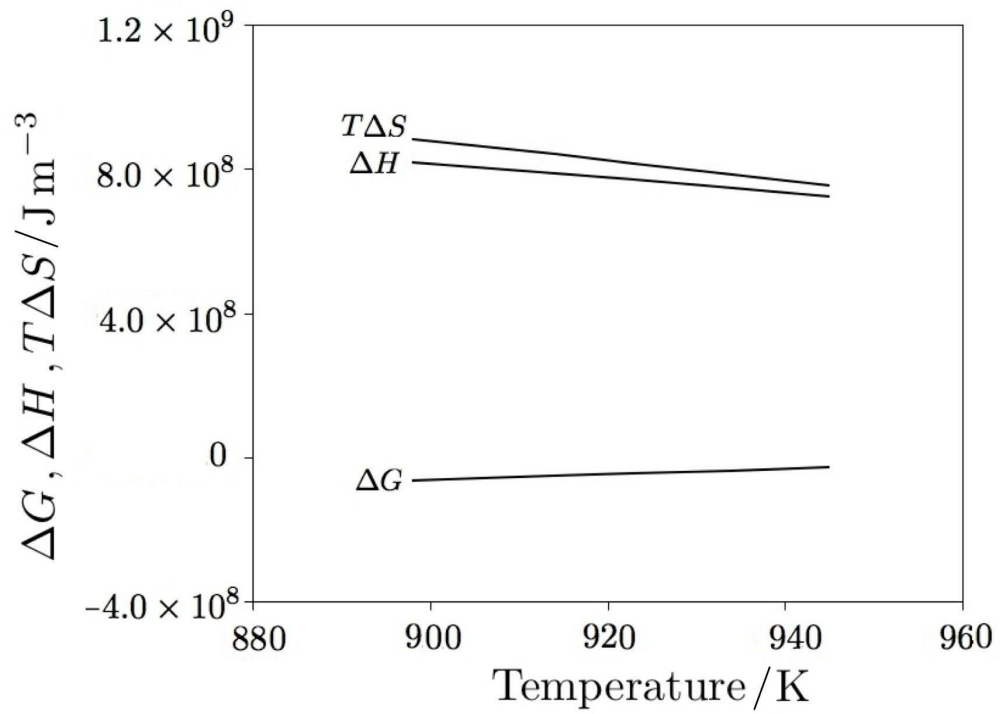
Figure 5.7: Free energy, enthalpy and entropy change as a function of temperature.
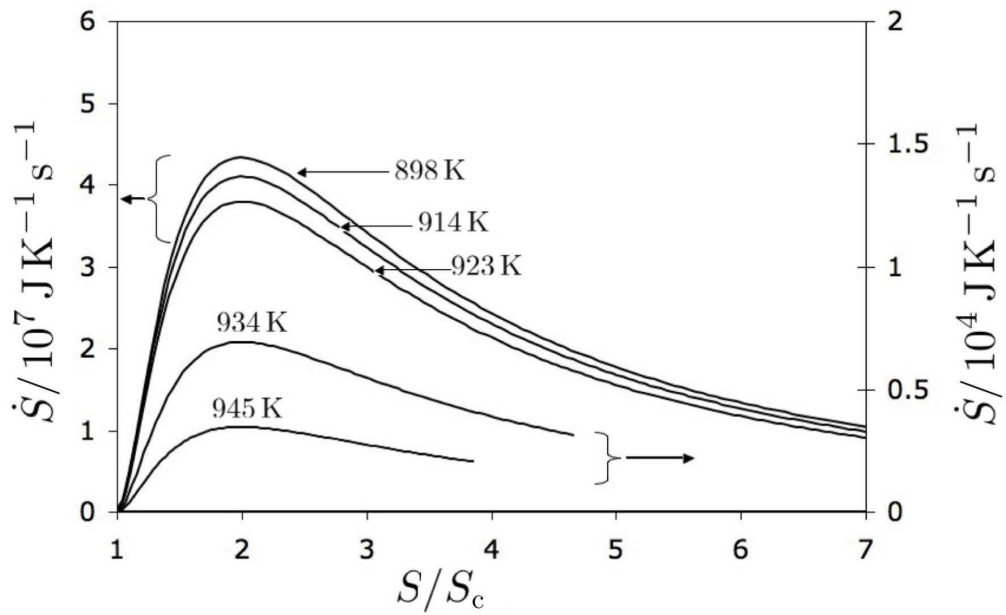
Figure 5.8: Variation in the entropy production rate as a function of the interlamellar spacing.
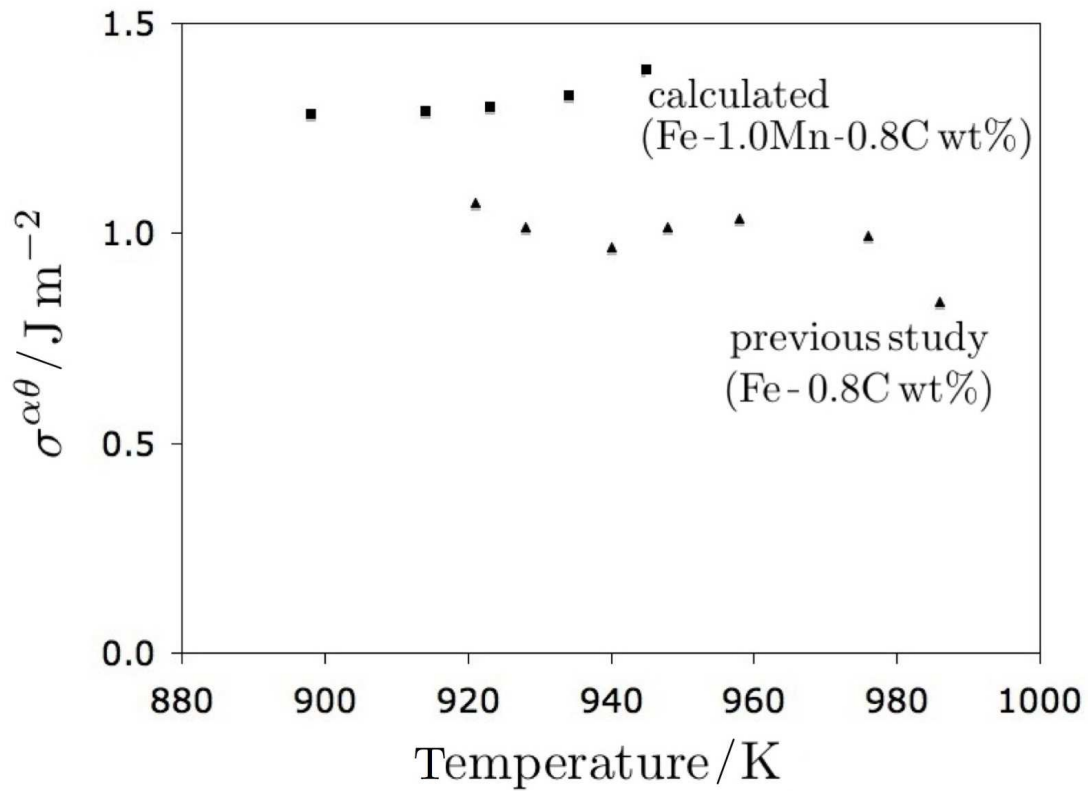
Figure 5.9: Ferrite-cementite interfacial energy compared with those from previous study for Fe-C steels [64].

5.5.4   Calculation of growth rate

The pearlite growth rate calculated assuming the partitioning local–equilibrium is shown in Fig. 5.10. There is a reasonably good match with the measured growth rate for 1.0Mn wt% steel [46]; that in itself is not surprising since the boundary diffusion coefficients and interfacial energies were derived using those data. The pearlite growth rate was also calculated for a steel containing 1.8Mn wt% and there seems to be a good fit with the experimental rates determined by [17] at low temperatures, although at higher temperatures the difference increases.

Figure 5.10: Pearlite growth rate as a function of temperature for Fe-1.0Mn-0.8C wt% and Fe-1.8Mn-0.69C wt%. Solid lines are calculated.

Assuming that partitioning local equilibrium governs the conditions at the transformation front, that the interfacial diffusivity derived here is generally applicable,

100

and that the maximum entropy production principle applies, the significant uncertainty in making predictions of the growth rate lies in the value of interfacial energy that must be used to determine interlamellar spacings. The extent of uncertainty may be assessed by using the maximum and minimum values determined from the Fe–1Mn–0.8C wt% system where the range is 1.28–$1.39\,\mathrm{J\,m^{-2}}$ with a mean value of $1.32\,\mathrm{J\,m^{-2}}$. Fig. 5.11 illustrates the difference these limits make to the growth rate of pearlite. It is suggested that in the absence of reliable data, it may be appropriate to use the mean value reported here accompanied by an error bar which is based on the range of $\sigma^{\alpha\theta}$.
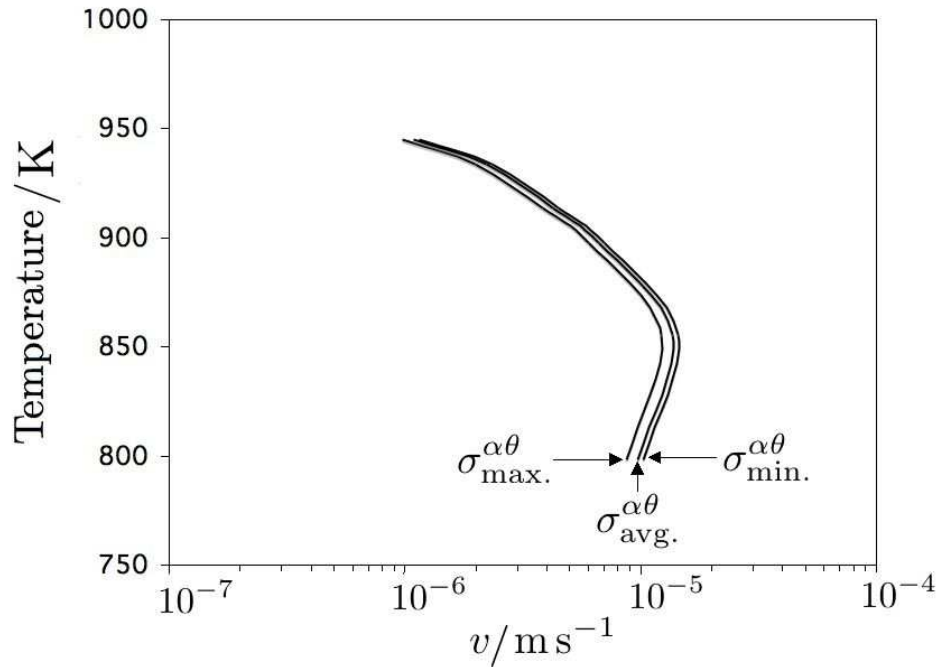
Figure 5.11: Sensitivity of the growth rate calculations to the α/θ interfacial energy.

5.6 Pearlite Growth Rate in Fe-C-Cr System

In order to extend the applicability of the theory discussed in this paper for steels containing Mn, the pearlite growth rate was calculated for Fe-0.82C-1.29Cr wt% based on the work of Razik *et al.* [18]. There is one complication when the data corresponding to 993 K and 1003 K are considered. Because the alloy has a carbon concentration which is hypereutectoid, the supercoolings at these particular transformation temperatures are not sufficient to permit ferrite to form until the carbon concentration of the austenite is reduced by the precipitation of cementite. Since both ferrite and cementite must be able to grow from austenite in order to form pearlite, it is assumed that this condition is satisfied when the austenite composition is reduced by the precipitation of cementite to the point where the $\alpha+\gamma/\gamma$ and $\theta+\gamma/\gamma$ phase boundaries intersect, as illustrated by the point 'A' in Fig. 6.6. The point 'A', which extrapolates to 'B' at the transformation temperature, is the composition of austenite assumed to decompose into pearlite when the supercooling is insufficient for the hypereutectoid alloy to permit the simultaneous precipitation. The average composition of the alloy is marked 'C' and has a carbon concentration which falls to the right of the extrapolated $\gamma + \alpha/\gamma$ phase boundary, making it impossible to simultaneously precipitate ferrite and cementite.

It was verified that none of the reported data are consistent with the negligible partitioning local equilibrium mode; all of the experiments involve transformation at low supersaturations so that the analysis again is based on partitioning local equilibrium. The boundary diffusivity of chromium, is, in the absence of data, assumed to be identical that of manganese; this is considered to be a good approximation [44]. The interfacial compositions are determined using MTDATA (TCFE database) [76] and the method described earlier for the steel containing Mn. The isothermal sections of Fe-C-Cr steel is shown in Fig. 5.13 along with the suitable tie-lines chosen. The interfacial compositions used for the calculation of pearlite growth rate are summarised in Table 5.3.

The interfacial energy has been determined for the steel containing Cr and it lies in the range of 0.52-0.89 $\mathrm{J\,m^{-2}}$ for the temperature range of 1003-933 K (Fig. 5.14).
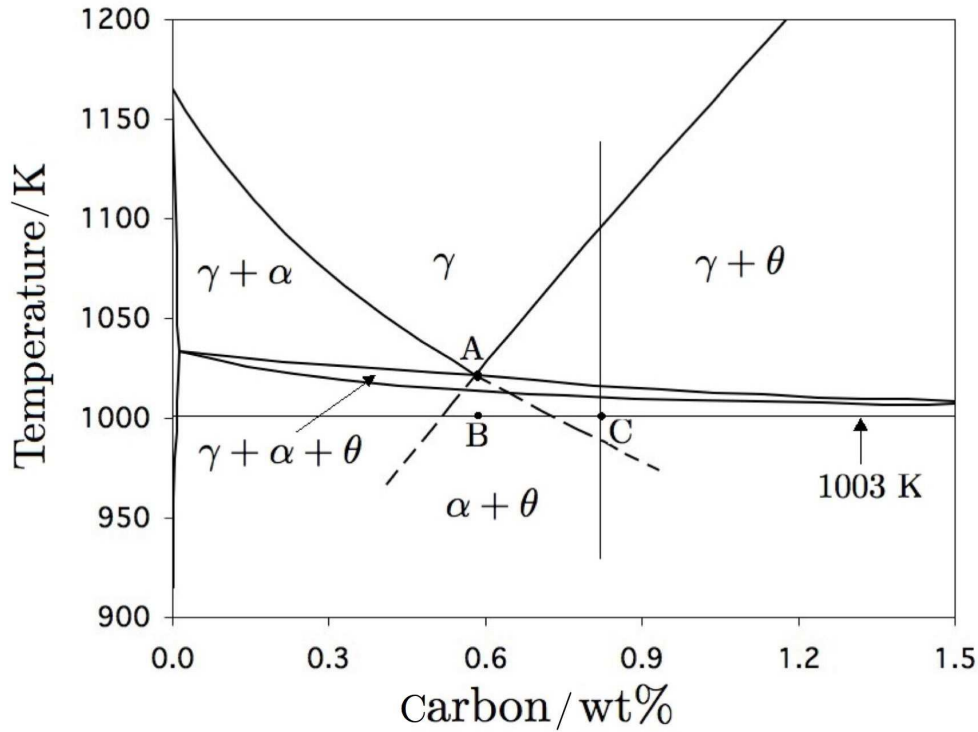
Figure 5.12: Isopleth section of Fe-Cr-C steel with the extrapolated phase boundaries.

The lower values of $\sigma^{\alpha\theta}$ obtained can be explained by the greater tendency of Cr to segregate.

It is observed that the growth rate estimated assuming the partitioning local equilibrium theory match measured values rather well as shown in Fig. 5.15. Razik *et al.* [18] in assessing their experimental data also calculated growth rates but not for the exact composition of the material studied, rather for an Fe–0.7C–1Cr wt% steel. Their calculations assume that chromium does not partition at all below the dashed horizontal line, so that pearlite growth is controlled by carbon diffusion alone. It is evident that such an analysis either greatly overestimates the growth rate when carbon is taken to diffuse through the interface, and under–predicts when carbon is taken to diffuse through the volume of the austenite ahead of the transformation front.

103
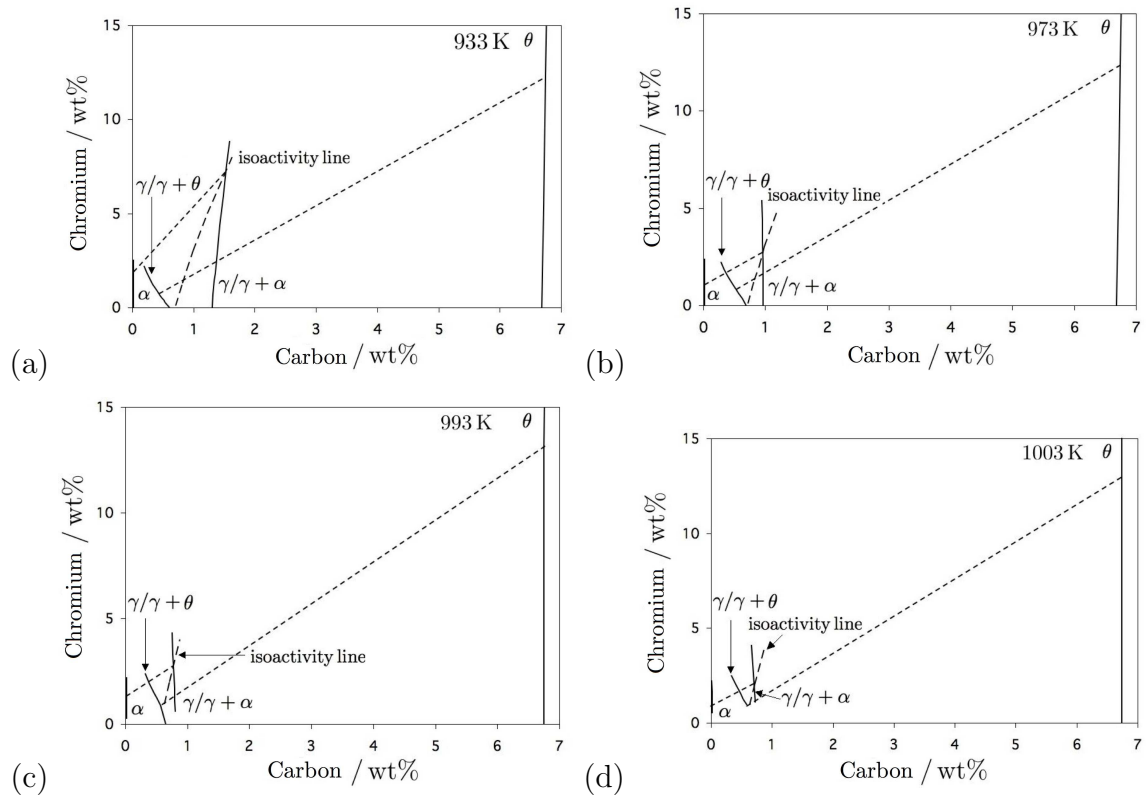
Figure 5.13: Isothermal section of ternary phase boundaries at various temperatures for Fe-C-Cr steel.
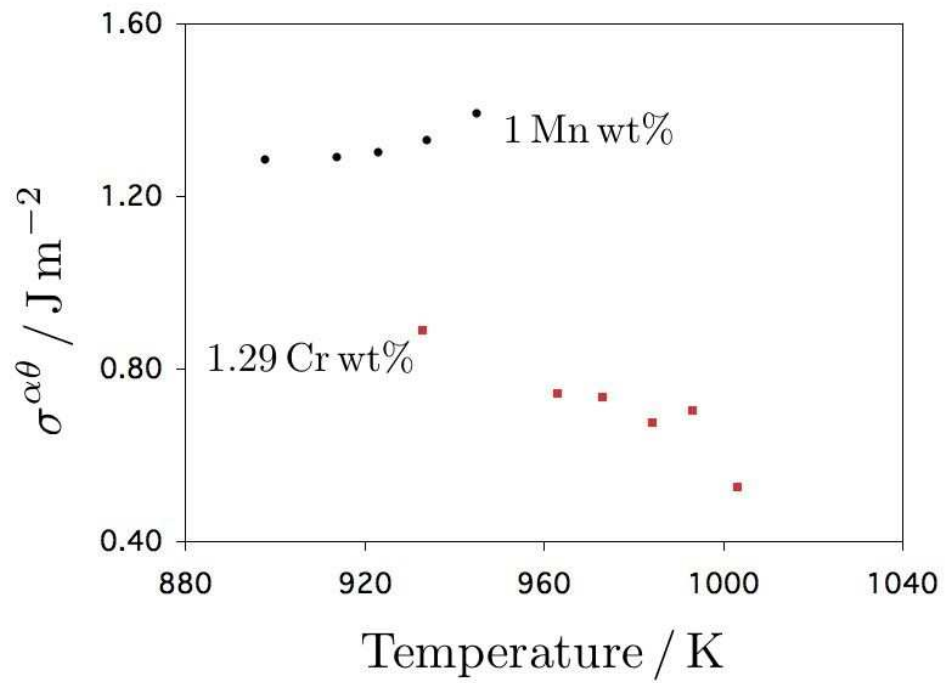
Figure 5.14: Comparison of ferrite-cementite interfacial energy for Fe-C-Cr and Fe-C-Mn steels.
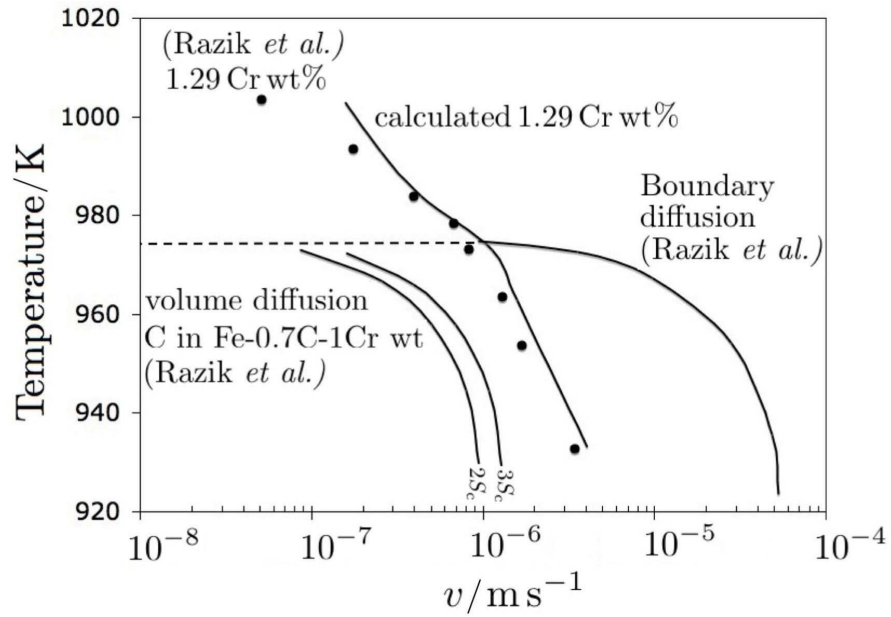
Figure 5.15: Comparison of calculated and experimental pearlite growth rate as a function of temperature for Fe-0.82C-1.29Cr wt%. The original calculations from [18] are included for comparison; the two values of $S/S_c = 2, 3$ for volume diffusion controlled growth correspond to the maximum growth rate and maximum entropy production criteria respectively. The dashed line represents their no–partition temperature.

Table 5.3: P-LE compositions of chromium at the interface. (The compositions are reported in wt%)

Temperature K	$c_{\mathrm{Cr}}^{\gamma\alpha}$	$c_{\mathrm{Cr}}^{\gamma\theta}$	$c_{\mathrm{Cr}}^{\theta\gamma}$	$c_{\mathrm{Cr}}^{\alpha\gamma}$
933	7.57	0.62	12.27	2.15
973	3.29	0.76	12.35	1.35
984	2.06	0.80	12.37	0.89
993	2.24	0.88	13.04	1.05
1003	2.11	0.93	13.05	1.06

For both the 1.8 Mn (Fig. 5.10) and 1.29 Cr (Fig. 5.15) alloys, the calculated growth rates at the highest of transformation temperatures is greater than those measured. It is possible in ternary steels for the transformation at high temperatures to occur where the three–phases $\gamma + \alpha + \theta$ exist in equilibrium, which would require the volume diffusion of substitutional solutes as the composition of the austenite changes during the course of transformation. This would result in a reduction in growth rate and an increase in interlamellar spacing [72, 103]. However, this is not the explanation for the observed discrepancy since in all cases the reported transformations occur in a phase field where only $\alpha + \theta$ are ultimately in equilibrium. The reasons for the discrepancy are therefore not clear.

5.7 Conclusions

It has been demonstrated that in circumstances where an analytical calculation of the growth rate of pearlite in ternary steels is useful, all of the published data are inconsistent with transformation in which the solute does not partition between the phases during transformation. Furthermore, even when partitioning is considered, none of the experimental data fall into the category of 'negligible–partitioning local equilibrium'. If local equilibrium is to be maintained then there is only one option possible, that in which the substitutional solute must diffuse over distances compa-

rable with the interlamellar scale of the pearlite structure. Since the diffusivity of substitutional solutes is much lower than that of carbon, the flux through the interface is by far the dominant mechanism for redistribution of atoms such as manganese or chromium. It is possible that the results can be extrapolated to other such substitutional solutes if pragmatic assumptions regarding interfacial energy and diffusivity are justified.

The method adopted here is capable of providing reasonable estimates of pearlite growth using an analytical equation due to Hillert, in combination with thermodynamic data and the assumption that the interlamellar spacing adopted is consistent with the maximum entropy production rate.

A number of difficulties have also been identified, for example, the fact that with hypereutectoid alloys there are circumstances when the simultaneous precipitation of ferrite and cementite is not possible when transforming at low supersaturations, so that it becomes necessary to allow the precipitation of cementite alone prior to the onset of pearlite. The growth rate is dependent on the α/θ interfacial energy and it is currently necessary when making predictions to assume approximate values derived from specific alloy systems. The dependence of interfacial energy on the chemical compositions at the transformation front is a rich and difficult area for future research.

Chapter 6

Divorced Eutectoid Transformation in Steels

6.1 Introduction

The theory discussed so far has been aimed specifically at the growth of lamellar pearlite in binary and ternary steels. However under a certain set of conditions, the pearlite may form as a mixture of spheroidised cementite surrounded by ferrite, also termed "a divorced eutectoid" structure. The name recognises the fact that there is no co-operation during growth, between the cementite and ferrite, as in the case of lamellar pearlite. Spheroidising annealing is a heat treatment which is used to achieve this structure, the primary objective being, the reduction in hardness to enable fabrication prior to the final hardening. The spheroidisation can be accomplished using two annealing treatments, namely, subcritical and intercritical with the latter used in the bearings industry for hypereutectoid steels. The subcritical treatment comprises heating in the region below the eutectoid temperature and holding for a prolonged duration in order to spheroidise the pearlitic structure, whereas in the case of intercritical annealing, the steel is heated in the region of austenite and cementite followed by slow cooling. The divorced eutectoid transformation (DET) relies on the presence of pre-existing fine cementite particles distributed in the austenite matrix

[104–106]. There is initially a competition between lamellar and divorced structure, while the steel is being cooled from the intercritical temperature. The formation of the divorced form is favoured when the spacing between the cementite particles is small (a function of low austenising temperature and time) and when the cooling rate is low.

This work described in this chapter discusses the theory of the divorced eutectoid transformation (DET) during the spheroidising annealing of bearing steels with special emphasis on predicting the transition region between pearlite and its divorced form in a rigorous manner for a binary and a multicomponent steel containing Cr, accounting for multiple flux paths and multicomponent diffusion.

6.2 Background

A typical spheroidising annealing cycle (Fig. 6.1) for producing a divorced eutectoid structure for a bearings steel usually consists of heating in the intercritical range of 1070-1100 K, holding there for 1-2 h, cooling at the rate of 15-25 K h^{-1} to 1025-1020 K, further slow cooling to about 950-965 K at cooling rates less than 10 K h^{-1} and finally air cooling to room temperature. As a result, the austenite with fine cementite particles transforms into ferrite and spheroidised cementite by the divorced eutectoid transformation (DET).

Honda and Saito [107] were the first to report the spheroidised structure. They heated various steels ranging from low to high carbon contents at temperatures above A$_1$, held there for 20 minutes followed by slow cooling to room temperature. They observed the microstructure to vary from a lamellar to a completely spheroidised form as a function of the austenising temperature, but the latter was found to persist at higher austenising temperatures in case of the hypereutectoid steels.

Oyama [104] gave a detailed account of events leading to the formation of the divorced eutectoid. The initial microstructure for the steel [1] consisted of a mix-

---

[1]Composition (wt%) C: 1.5, Mn: 0.5, Cr: 1.5, Si: 0.5
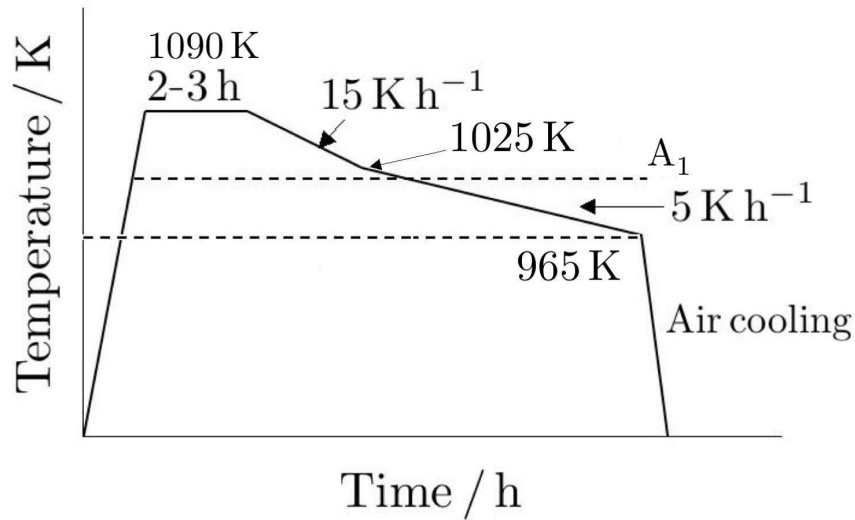
Figure 6.1: Schematic heat treatment for producing a divorced eutectoid structure in hypereutectoid steels. A_1 is the eutectoid temperature.

ture of pearlite and proeutectoid cementite. When this steel is heated within the inter-critical region, austenite forms in the regions of ferrite with much of the carbon coming from the dissolution of pearlitic cementite and the proeutectoid cementite. On holding at this temperature for a sufficient length of time, the ferrite disappears completely although some of the cementite from the pearlite still remains because the proeutectoid cementite also serves as a source of carbon. At this instance the distribution of carbon in austenite is non-uniform and away from equilibrium. The structure is ideal for the generation of divorced eutectoid, since there are a large number of closely-spaced cementite particles which simply grow during cooling and hence suppress the development of lamellar pearlite during cooling. When the soaking times are large enough, this might homogenise the distribution of carbon and coarsen the proeutectoid cementite, resulting in an increase in interparticle spacing. The divorced eutectoid will not form in such circumstances, and thus will be substituted by lamellar pearlite.

Verhoeven and Gibson [108] proposed a model for the divorced eutectoid formation wherein, the carbon partitioned as ferrite grows, is incorporated into the existing proeutectoid cementite as the ferrite-austenite boundary moves and the mechanism is illustrated in Fig. 6.2(a). During the course of transformation when the mixture of austenite and cementite is cooled below the eutectoid temperature, fluxes are created towards the cementite particles in both the austenite and ferrite, Fig. 6.2(b). If the γ/α interface advances with a velocity v, then the amount of carbon partitioned must equal that absorbed by cementite if the conditions of equilibrium were to be maintained at the interface:

$$\left(c^{\gamma\alpha} - c^{\alpha\gamma}\right)v = D_\gamma \frac{c^{\gamma\alpha} - c^{\gamma\theta}}{\lambda_\gamma} + D_\alpha \frac{c^{\alpha\gamma} - c^{\alpha\theta}}{\lambda_\alpha} \tag{6.1}$$

where λ_γ and λ_α represent the spacing of cementite particles on either side away from the interface. Verhoeven [109] studied the heat treatment conditions promoting the DET formation for SAE 52100 [1] steel. It was reported that the addition of Cr was the most effective way of reducing the final carbide particle size. This was attributed to the carbide formation/dissolution rate at the inter–critical holding temperature which is reduced by Cr addition.

Luzginova *et al.* [111] studied divorced pearlite formation in a hypereutectoid steel as a function of chromium concentration (0.5, 1.5, 2.5 and 3.5 wt %). The DET reaction was found to occur at smaller undercoolings (ΔT) as compared with the lamellar structure. It was observed that chromium promoted the divorced form at low austenitising temperature and when the cooling rate was reduced. Based on the theory proposed by Verhoeven [108], the transition line separating the DET from the lamellar pearlite as a function of undercooling and cementite particle spacing was calculated. It is unfortunate that the calculations of lamellar pearlite growth were for a binary Fe-C steel, which rather invalidates the analysis of the chromium effect.

---

[1]Composition (wt%) C: 1.03, Mn: 0.3, Cr: 1.28, Si: 0.23, P: 0.019, S: 0.014
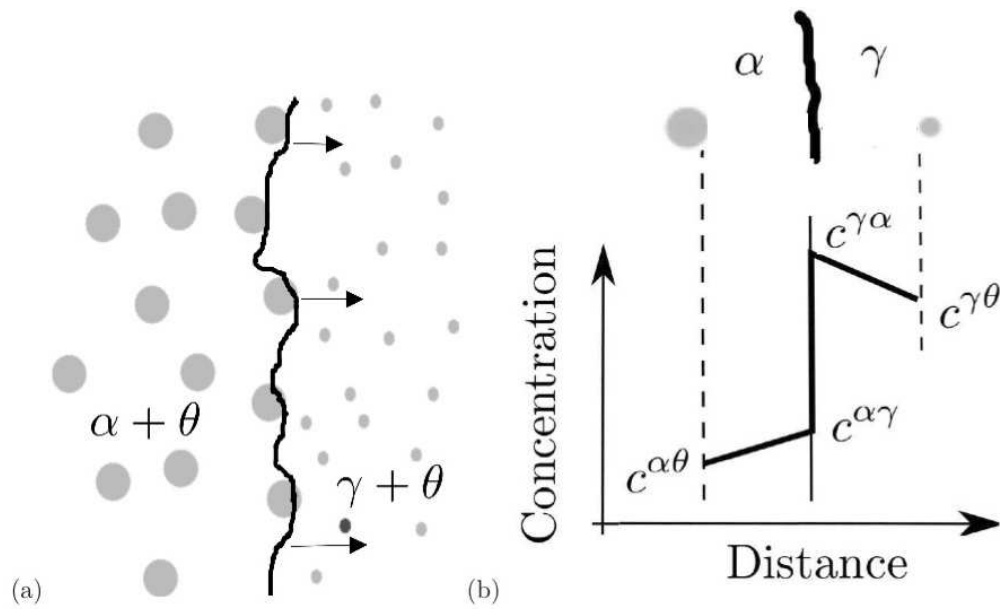
Figure 6.2: Schematic of (a) interface movement during the formation of divorced eutectoid and (b) concentration profile of carbon adjacent to the interface. $c^{\gamma\alpha}$ stands for concentration in austenite that is in equilibrium with ferrite and the other terms are interpreted similarly. Reproduced from Bhadeshia [110].

The objective of the current work was to revisit the theory for the binary as well as ternary systems taking into account the new theory proposed in the present work for the growth of lamellar pearlite [64, 112].

6.3 Divorced Eutectoid Transformation in Fe-C System

Verhoeven's approach [51] was used in order to calculate the velocity of the divorced eutectoid transformation front. For an undercooling ΔT at which ferrite first forms, the concentration differences in equation 6.1 can be determined from the Fe-C phase diagram [1] in order to obtain an approximate equation for the velocity:

$$v \approx \frac{2D_\alpha}{\lambda_\gamma + \lambda_\alpha} \frac{\frac{\Delta T}{27}\left[\frac{0.28}{D_\alpha/D_\gamma} + 0.009\right]}{0.75 + \frac{\Delta T}{27} \times 0.225} \tag{6.2}$$

where D_α and D_γ represent the diffusion coefficient of carbon in ferrite and austenite respectively. The diffusion coefficient of carbon in ferrite is based on the data of Smith [30]. The velocity, v was calculated as a function of carbide spacing. The corresponding growth in lamellar pearlite was estimated using the simultaneous volume and interface diffusion–controlled growth theory described in chapter 3. This calculation accounts for the concentration dependence of the diffusivity of carbon in austenite and assuming the maximum rate of entropy production criterion. The plot of rate of DET as a function of undercooling ΔT is shown in Fig. 6.3 for a variety of carbide spacings. Superimposing the growth rate of lamellar pearlite for an Fe-C alloy on this plot, shows that for each spacing, there is a unique undercooling where the transition from a divorced to a lamellar mode of growth occurs. This effectively means that lamellar growth is dominant above this undercooling. Figure 6.4 compares the boundary separating the divorced and lamellar structures

---

[1]The terms are evaluated from the phase diagram at 700°C. $c^{\gamma\alpha} - c^{\gamma\theta} \approx \Delta T(0.28/0.27), c^{\alpha\gamma} - c^{\alpha\theta} \approx \Delta T(0.009/27), c^{\gamma\alpha} - c^{\alpha\gamma} \approx 0.75 + \Delta T(0.225/27)$
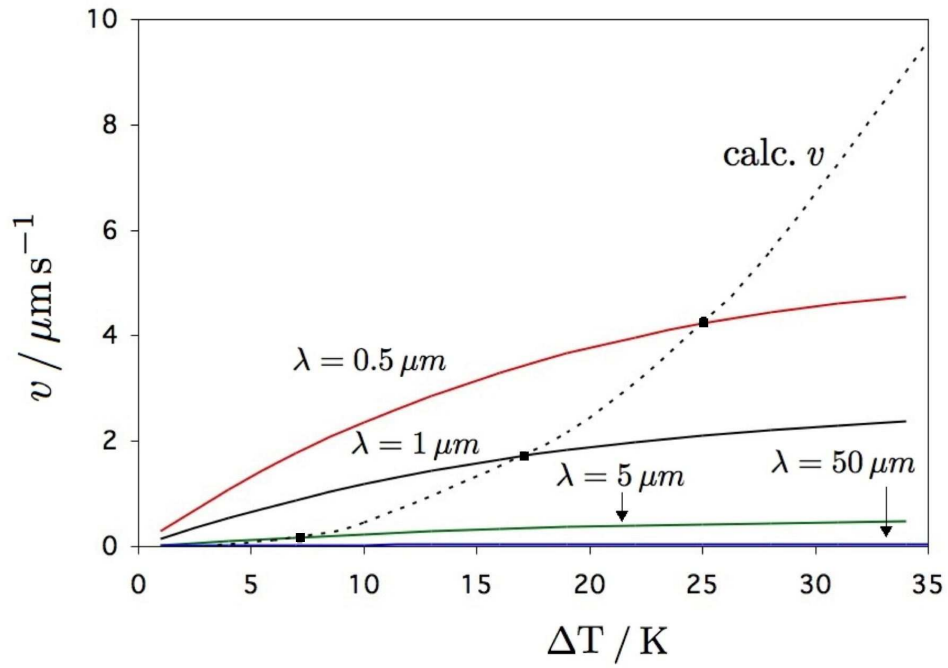
Figure 6.3: Plot of growth rate of pearlite (dotted line) superimposed on that of divorced eutectoid transformation (solid lines). The dots show the critical undercooling at a particular spacing above which the transition occurs from divorced to lamellar form.

for a Fe-C alloy, based on the simultaneous solution of the equations for divorced and lamellar modes of growth (graphically shown as the point of intersection of velocity of lamellar pearlite with the DET for appropriate spacing in the figure 6.3). It is observed that using the mixed diffusion–controlled growth of pearlite the curve shifts upwards, thereby expanding the domain of existence of the divorced form.
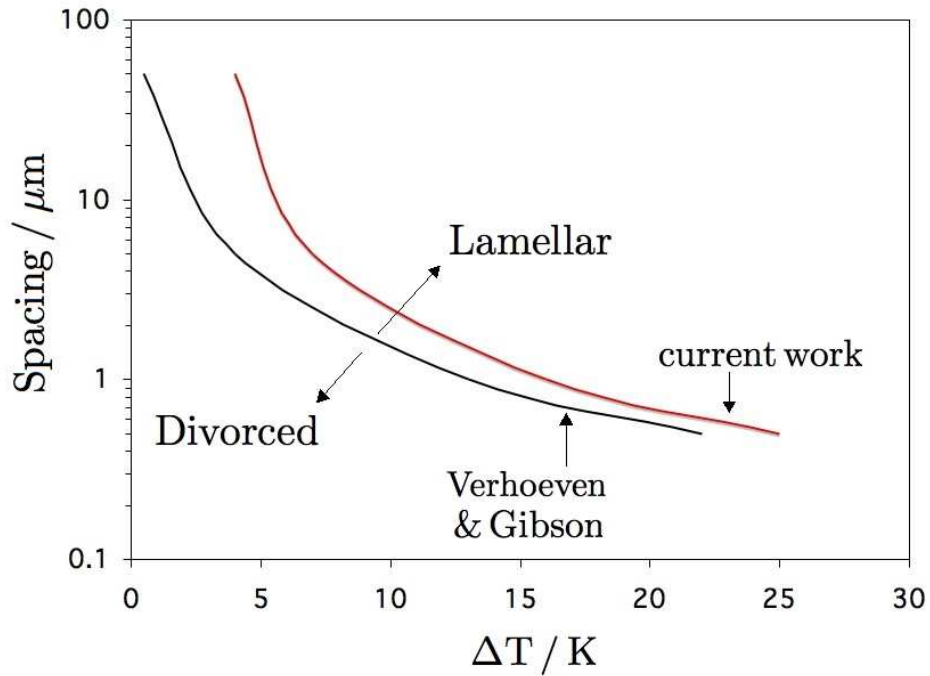
Figure 6.4: Transition line separating the divorced from the lamellar mode for a Fe-C alloy. The spacing refers to the distance between the carbide particles at the intercritical temperature and ΔT is the undercooling below the A_1 temperature.

Table 6.1: Chemical composition of the 1.5 wt% Cr steel used by Luzginova *et al.* [111]. All the compositions are in wt %.

C	Mn	Si	Cr
1.05	0.34	0.25	1.44

6.4 Divorced Eutectoid Transformation in Bearing Steels

The steels supplied to the bearings manufacturer are usually spheroidised in order to render them machinable and make them suitable for warm and cold-forming operations. The microstructure consists of relatively coarse cementite particles in the matrix of ferrite called the divorced eutectoid. The kinetics of spheroidisation depends on the carbon and chromium concentrations, higher carbon promoting the reaction by providing a greater density of nucleation sites, whereas chromium helps in reducing the interlamellar spacing of pearlite which is the starting microstructure. Once again for the calculation of velocity of the divorced eutectoid transformation front, the equation proposed by Verhoeven was used, the details of which have been discussed in the previous section. The composition of the steel used in the calculations is listed in Table 6.1.

The growth rate of pearlite was calculated based on Hillert's theory [7] and assuming partitioning local equilibrium:

$$v = 12kD_{\mathrm{B}}\,\delta\left(\frac{c_{\mathrm{Cr}}^{\gamma\alpha} - c_{\mathrm{Cr}}^{\gamma\theta}}{c_{\mathrm{Cr}}^{\theta\gamma} - c_{\mathrm{Cr}}^{\alpha\gamma}}\right)\frac{1}{S^{\alpha}\,S^{\theta}}\left(1 - \frac{S_{\mathrm{c}}}{S}\right) \qquad (6.3)$$

The partitioning local–equilibrium case corresponds to one in which the activity of carbon in the austenite ahead of the interface is almost uniform, thus allowing the flux of the slow diffusing chromium to keep pace. The activity of carbon in austenite for the alloy composition was calculated using MTDATA. The point of intersection of the carbon iso-activity line with the phase boundaries of $\gamma/\gamma + \theta$ and $\gamma/\gamma + \alpha$

gives the interfacial compositions of Cr in austenite in equilibrium with ferrite and cementite Fig. 6.5. Although the alloy under consideration is a multicomponent steel, it is reasonable to assume that diffusion of Cr through the phase boundary controls the growth of pearlite given the small concentrations of Mn and Si. In line with the work presented in chapter 5, for a Cr based steel, none of the data here are consistent with the negligible partitioning local equilibrium mode. The boundary diffusion coefficient for Cr was taken based on its applicability for ternary steels in chapter 5:

$$D_{\mathrm{B}} = 2.81 \times 10^{-3} \exp\left(\frac{-164434\,\mathrm{J\,mol^{-1}}}{RT}\right)\,\mathrm{m^2\,s^{-1}} \tag{6.4}$$

The interlamellar spacing was derived from the regression analysis of experimental data of Razik and co-workers [18] for steels containing Cr and the critical spacing was calculated assuming the maximum rate of entropy production criterion $S/S_{\mathrm{c}} = 2$.

For the hypereutectoid steel under discussion, at temperatures 995 K and above, the supercoolings are not sufficient for the simultaneous precipitation of ferrite and cementite. In such a case ferrite does not form until the carbon concentration of austenite is reduced by the precipitation of cementite. It is assumed that this condition is satisfied when the austenite composition is reduced by the precipitation of cementite to the point where the $\alpha + \gamma/\gamma$ and $\theta + \gamma/\gamma$ phase boundaries intersect, as illustrated by the point 'A' in Fig. 6.6. The point 'A', which extrapolates to 'B' at the transformation temperature, is the composition of austenite assumed to decompose into pearlite when the supercooling is insufficient for the hypereutectoid alloy to permit the simultaneous precipitation of $\alpha + \theta$. The average composition of the alloy is marked 'C' and has a carbon concentration which falls to the right of the extrapolated $\gamma + \alpha/\gamma$ phase boundary, making it impossible to simultaneously precipitate ferrite and cementite.

In case of a Cr based steel, the pearlite growth rate obtained was about an order of magnitude lower than that calculated by Luzginova *et al*. The difference arises because their calculations of lamellar growth are based on an equation derived originally for Fe-C alloy [51]. The effect of the Cr addition is only accounted for through the change in ΔT and the interfacial compositions. Hence the diffusion
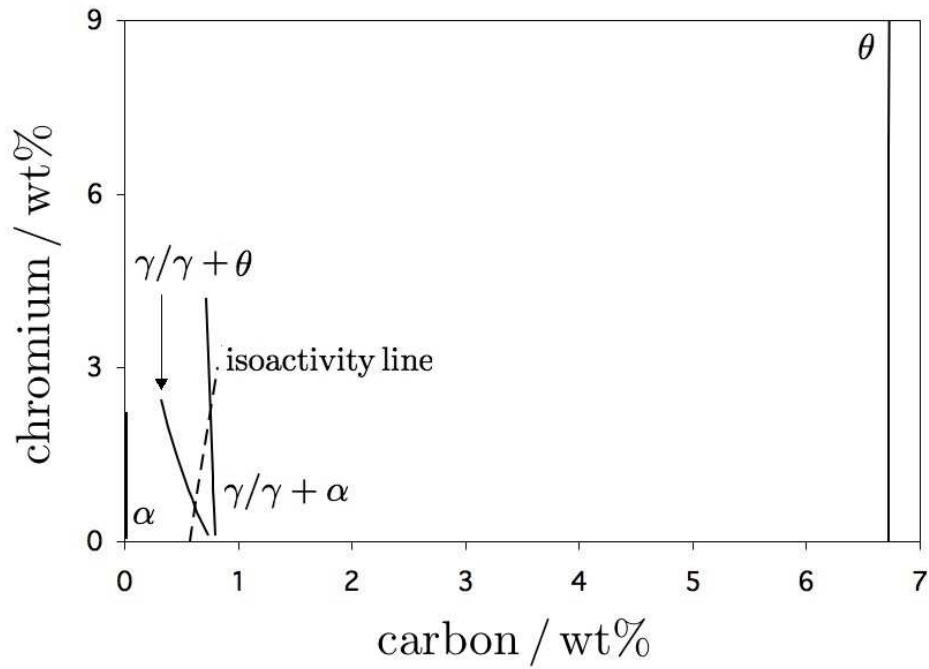
Figure 6.5: Isothermal section of a ternary Fe-C-Cr-Mn-Si system at 995 K.
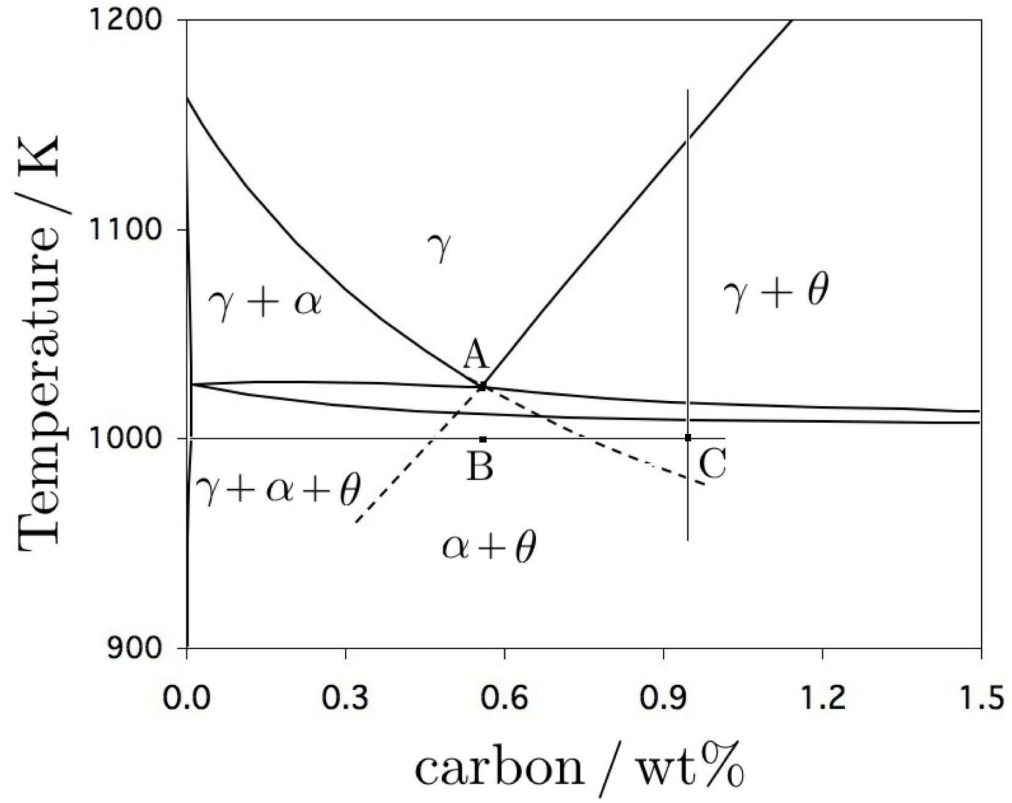
Figure 6.6: Isopleth section of Fe-C-Cr-Mn-Si steel with the extrapolated phase boundaries.

of the substitutional solute is entirely unaccounted for in their calculations, *i.e.*, a thermodynamic consequence of Cr. For a ternary system, the choice of tie-lines for determining the interfacial compositions should be based on both the $\alpha + \gamma$ and $\theta + \gamma$ phase fields using either the negligible partitioning local equilibrium or the partitioning local equilibrium approach discussed in chapter 5. Given that Luzginova *et al.* did not incorporate a kinetic effect for Cr, the interface compositions chosen from the phase diagrams will not satisfy the simultaneous flux equations similar to 5.1 and 5.2.

6.5 Determination of Carbide Particle Spacing

In order to evaluate the spacing between carbide particles as a function of the intercritical heat treatment temperature, the coarsening of spherical particles was first calculated using a procedure based on the work of Venugopalan and Kirkaldy [113]. The initial carbide particle size was assumed to be 0.4 μm consistent with Luzginova *et al.* [111].

$$\frac{dr}{dt} = \frac{8\,D_\mathrm{eff}\,\sigma\,V_\mathrm{m}}{81\,R\,T}\frac{1}{r^{*2}} \tag{6.5}$$

where r^* is the average cementite particle size after a certain time interval. The equation for the effective diffusivity in a multicomponent system is derived using the electrical analogy of resistances in parallel. This approach proves to be a useful one, especially since the system involves the simultaneous diffusion of the substitutional solutes:

$$\frac{1}{D_\mathrm{eff}} = \Sigma\,\frac{(1 - k_\mathrm{i})^2\,u_\mathrm{i}^*}{D_\mathrm{i}} \tag{6.6}$$

$$D_\mathrm{V} = 0.7 \times\,10^{-4} \exp\left(\frac{-286000\,\mathrm{J\,mol^{-1}}}{RT}\right)\ \mathrm{m^2\,s^{-1}} \tag{6.7}$$

Table 6.2: Parameters used in the calculation of spacing

Temperature K	f	u_{Cr}^*	u_{Mn}^*	k_{Cr}^*	k_{Mn}^*	D_{eff} $m^2\,s^{-1}$	r^* m	Spacing m
1093	0.0374	0.012	0.0033	9.25	2.01	$1.52{\times}10^{-17}$	$0.46{\times}10^{-6}$	$2.47{\times}10^{-6}$

D_V represents the volume diffusivity of the substitutional solutes in austenite and it can be taken to be identical for the elements under discussion.

$$u_i^* = \frac{u_i}{(1 + (k_i - 1)\,f)} \tag{6.8}$$

The subscript i refers to the solute element, f is the equilibrium volume fraction of cementite, u_i is defined as $u = x/(1 - x_c)$. The terms x and x_C are the mole fractions of the substitutional solute and carbon respectively. k_i is the partition coefficient between austenite and cementite calculated using MTDATA (TCFE database) [76]. The expression for u_i^*, the average alloy composition in austenite at the interface is determined based on the law of mixtures:

$$u_\gamma^* \,(1 - f_\theta) + u_\theta\, f_\theta = u_i \tag{6.9}$$

Table 6.2 shows the parameters used in the calculation of coarsening of the carbide particles. The effective diffusivity can be calculated using equation 6.6 and the parameters listed in Table 6.2. For practical purpose the volume diffusivities of substitutional solutes can be considered comparable to self-diffusion of Fe in the austenite [44]. The spacing between the carbide particles was calculated using an approximate approach for spherical particles deduced from quantitative metallography: [114].

$$\lambda = d \sqrt{\frac{\pi}{6f}} - 1 \tag{6.10}$$

The transition curve defined by plotting the calculated carbide particle spacings against the undercooling is shown in Fig. 6.7. It is observed that the curve shifts upwards as a result, which in effect would allow the divorced eutectoid structure to persist at much higher undercoolings for a given intercritical holding temperature as compared to those calculated by Luzginova *et al*.
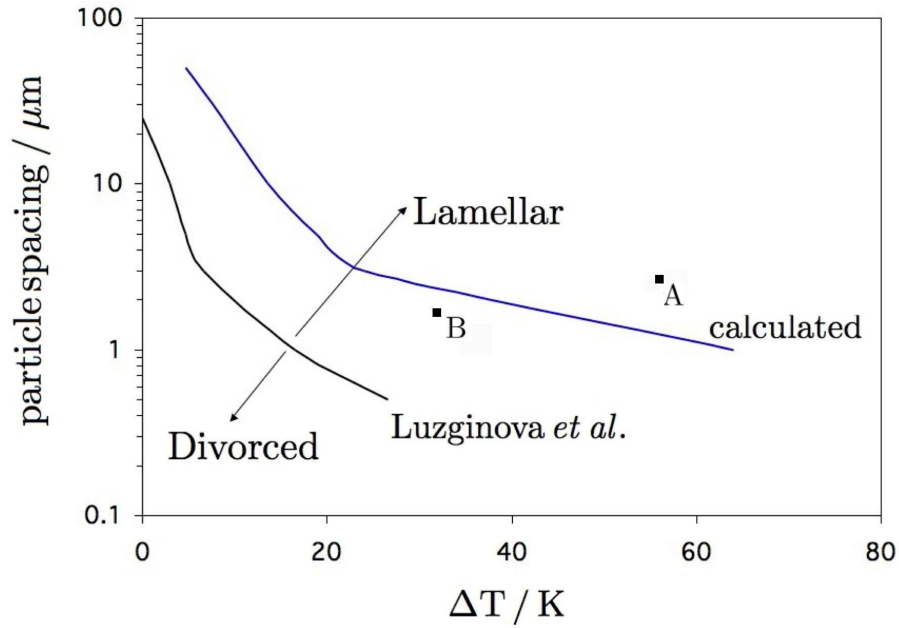
Figure 6.7: Comparison of calculated transition curve with the data of Luzginova *et al*. [111]. Points A and B correspond to the microstructure observed in Fig. 6.9(a) and Fig. 6.8(a) respectively.

6.6 Experimental Evaluation

The experimental data plotted by Luzginova *et al*. based on intercritical annealing treatment for the transition between DET and pearlite transformation may not be strictly valid since the calculated curve is based on isothermal transformation whereas

Table 6.3: Chemical composition of the steel used in the study. All the compositions are in wt %.

C	Mn	Si	Cr	Ni
0.98	0.30	0.25	1.50	0.18

their structures were generated by continuous cooling transformation. In order to confirm the validity of the calculations, a series of experiments was designed using a thermo-mechanical simulator. Cylindrical 8×12 mm samples were heated to a certain temperature in the intercritical region, undercooled below the A_1 line and allowed to transform isothermally. The actual composition of the steel used in the study is stated in Table 6.3. The temperatures were chosen so as to allow a varying degree of dissolution of cementite in the intercritical region and to assess the effect of different undercoolings. The samples were observed under the scanning electron microscope. A divorced eutectoid structure is favoured for specimens intercritically austenitised at 1073 K and 1050 K and isothermally held at 983 K and 933 K respectively. The relatively low intercritical temperatures ensure the presence of closely spaced fine cementite particles which on isothermal transformation just grow bigger on account of the net carbon transport as the ferrite-austenite transformation front progresses. The extent of formation of divorced (spheroidised) structure for the specimen transformed at 933 K is slightly lower as compared to that at 983 K, on account of higher undercooling, and is confirmed from the microstructure presented in Fig. 6.8(a and b).

In order to analyse the effect of higher intercritical temperatures (1123 K and 1103 K) on austenite decomposition, another set of experiments was performed where the specimens were transformed isothermally at 958 K and 933 K respectively. The higher austenitising temperature results in partial dissolution or coarsening of the pre-existing cementite particles, leading to increased spacings between them, and thus promoting the conditions for predominantly lamellar pearlitic structure,

Fig. 6.9(a and b). It is worth noting here that the higher spacing, λ, necessitates larger diffusion distances thereby making DET formation more difficult. The DET reaction dominates the lamellar pearlite at low undercoolings provided the austenising conditions are same. One common feature observed though, is the bimodal distribution of carbide particles owing to the presence of pro-eutectoid cementite on the grain boundaries and also the carbides growing intragranularly. The dilatation curves are shown in Figs. 6.10(a and b) for specimens austenitised at 1073 K and 1123 K respectively and both show the increase in strain as a result of expansion when the mixture of austenite and cementite transforms to either ferrite and spheroidised cementite or lamellar pearlite. In order to confirm the extent of spheroidisation in specimens treated at different temperatures, Vickers hardness measurements were done under a load of 10 kg and using a diamond pyramid indentor. The hardness data are presented in Table 6.4 and clearly show high values for the lamellar structure when compared to the divorced form.

The observed microstructures based on the isothermal treatment discussed above can be superimposed on the transition curve delineating the DET from the lamellar pearlite structure. According to the calculations done by Luzginova *et al.*, for the steel austenised at 1073 K and treated at 983 K, their predictions would suggest that the structure would lie in the lamellar pearlitic region. However the microstructure of this steel Fig. 6.8(a), consists of spheroidised carbides. The new transition curve based on the current work rightly predicts the microstructure to be that of divorced eutectoid. Similarly, the steel with a larger carbide spacing as a result of austenitising at 1123 K and holding at 958 K falls above the transition line owing to the lamellar structure. The experimental observations suggests that the divorced eutectoid structure exists over a larger domain than predicted by Luzginova *et al.* thus confirming the calculated transition line in Fig. 6.7.

6.7 Conclusions

It has been possible to redefine the transition boundaries separating the divorced eutectoid from the lamellar structure in case of Fe-C and a multicomponent steel con-

(a)

(b)
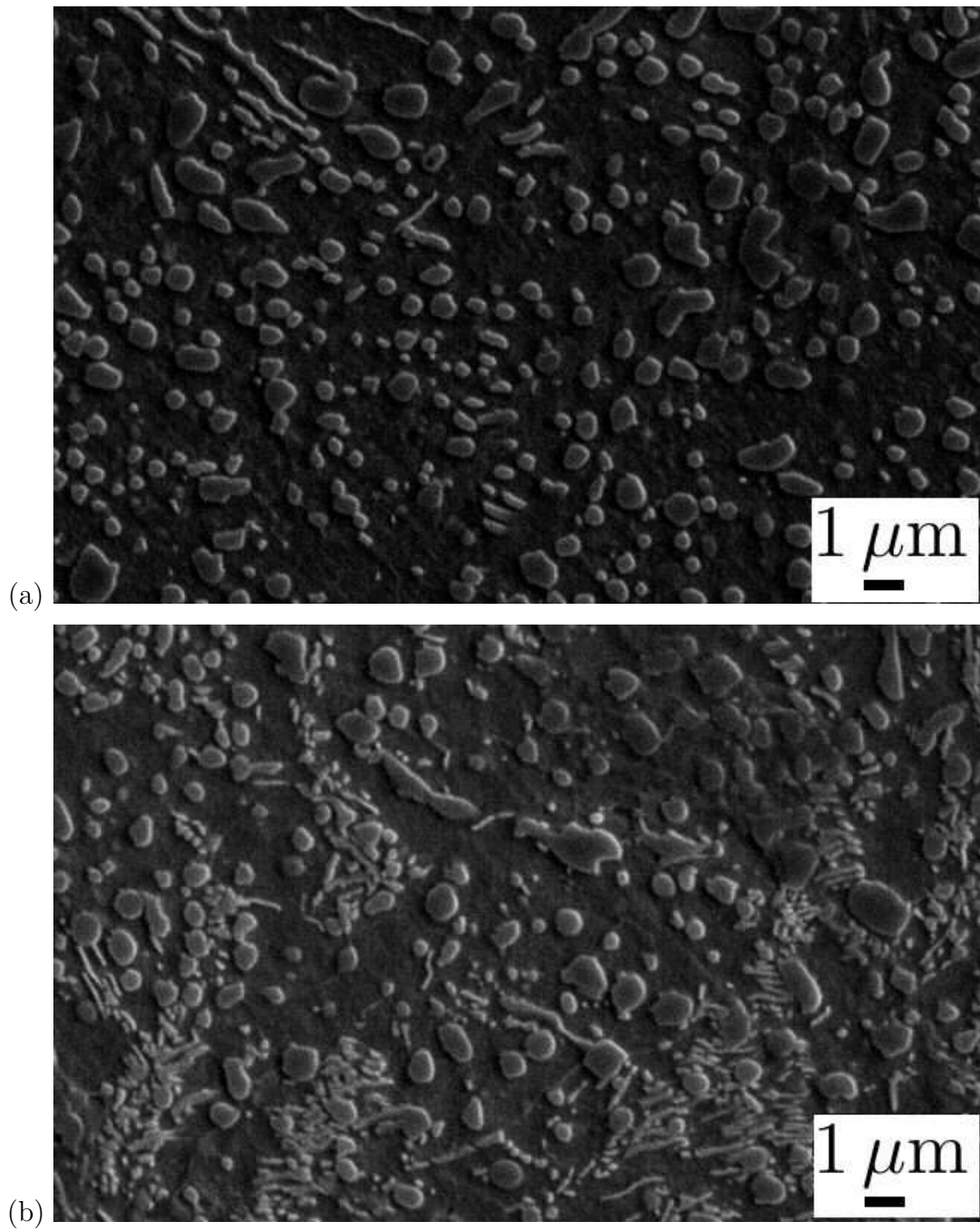
Figure 6.8: Microstructure showing divorced eutectoid structure obtained by (a) austenising at 1073 K and holding at 983 K. (b) austenised at 1050 K and held at 933 K.
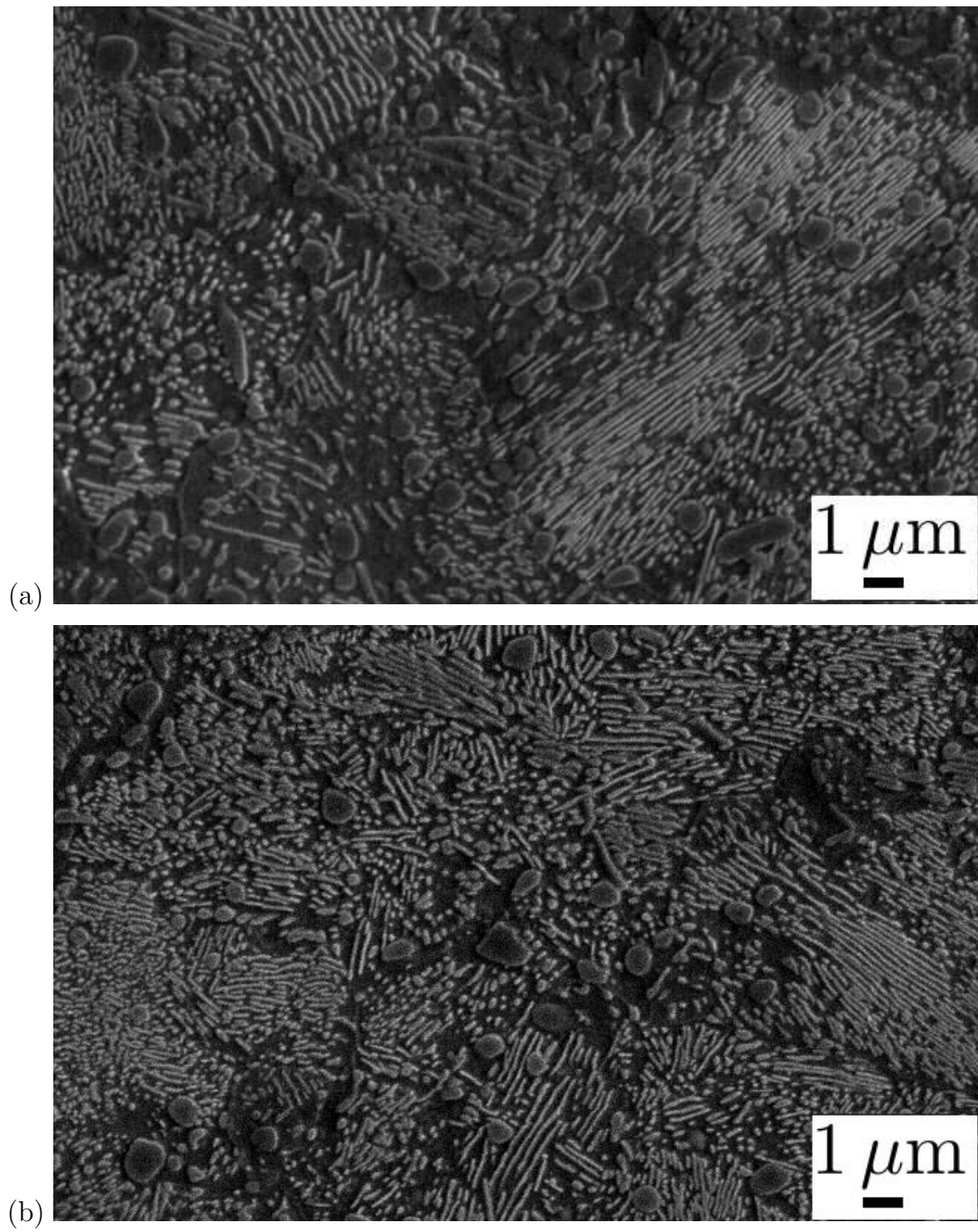
(a)

(b)
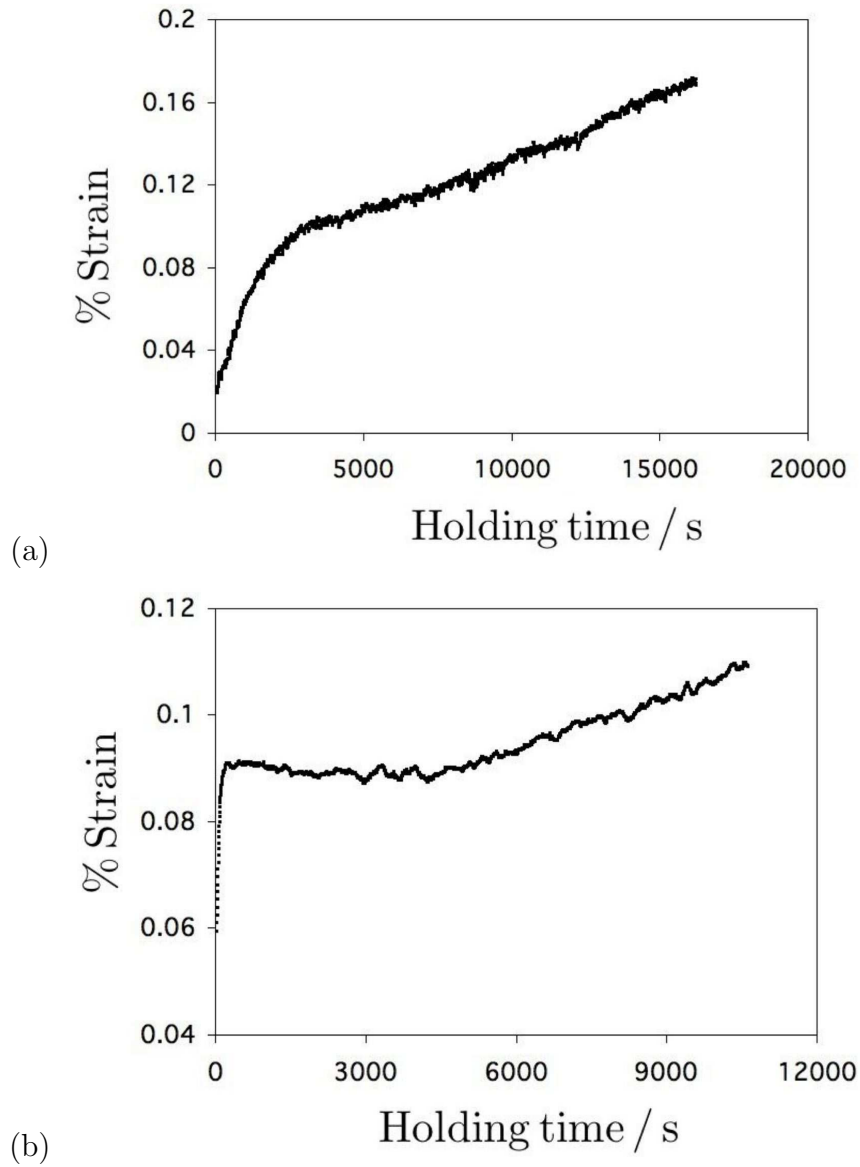
Figure 6.10: Dilatation curves for (a) Fig. 6.8(a) and Fig. 6.9(a).

128

Table 6.4: Vickers hardness data (10 kg load) for various heat treatments

Austenitising temperature K	Holding temperature K	Hardness HV
1073	983	198
1050	933	217
1103	933	280
1123	958	278

taining Cr. The method adopted here for the calculation of growth rate of lamellar pearlite in a multicomponent steel is based on the analytical treatment due to Hillert and modified for the interfacial compositions assuming partitioning local equilibrium and the maximum rate of entropy production criterion. The difficulties encountered during transformation at lower undercoolings where the simultaneous precipitation of ferrite and cementite is not possible, have been overcome in case of chromium containing steel using a new approach outlined. The calculations suggest that the transition line shifts significantly upwards in case of both the steels when compared with the work of previous researchers, thereby expanding the domain of the speroidised (DET) structure as a function of carbide spacing and undercooling and the same has been validated through the experimental data. This in turn has a potential to develop a more energy efficient spheroidising annealing process for steels requiring good machinability. The calculations also show that the presence of Cr enhances the process of spheroidisation by increasing the domain of existence of a divorced eutectoid structure, when compared with plain carbon steels.

Chapter 7

Conclusions and Scope for Future Work

General Conclusions

The work presented in the thesis describes the theory of pearlite growth and the divorced eutectoid transformation in binary and ternary steels. A simplified model has been proposed which combines the flux contributions from diffusion in the volume of austenite and the phase boundary to represent the mechanism of pearlite growth in Fe-C steels. It has been shown that the flux of carbon through the boundary between pearlite and austenite dominates at all but the highest of transformation temperatures. The maximum growth rate and entropy production criteria have been derived rigorously in the context of combined flux diffusion theory for the determination of critical interlamellar spacing, and it has been shown for the first time that the ratio of the nominal to critical spacing (S/S_c) is not constant but a variable quantity with respect to temperature. The ferrite-cementite interfacial energy has been deduced based on the calculated free energy values and assuming the maximum rate of entropy production as the optimum criterion. The theory leads also to a realistic value of the activation energy for interfacial diffusion of carbon which is less than that for volume diffusion in austenite and greater than for volume diffusion in ferrite. As

a consequence of this new theory, the match with the experimental data is better when compared with the previous work in spite of the fact that the considerations of equilibrium at junctions between interfaces are abandoned.

A third diffusion flux through the ferrite trailing behind the transformation front has also been incorporated in the mixed diffusion–controlled growth theory. The inclusion of flux through the ferrite indeed leads to an increase in the growth rate as compared to that in austenite alone. It has, however, been shown that combination of fluxes through austenite and the transformation front represent the experimental data rather well and given the lack of evidence of cementite thickening behind the transformation front, the third flux may be neglected in practice.

A more complex theory of pearlite growth in ternary steels containing either Mn or Cr has been discussed and it has been demonstrated that all of the published data are inconsistent with transformation in which the substitutional solute does not partition between the product phases. Furthermore, none of the experimental data fall in the category of 'negligible-partitioning local equilibrium'. It has been shown that these solutes must diffuse over distances comparable with the interlamellar spacing in pearlite. Although the diffusion coefficient of Mn or Cr is much smaller as compared with that of carbon, it has been demonstrated that the flux of these solutes along the interface is the rate controlling mechanism to allow for their redistribution between the product phases. A modified approach has been proposed to determine the interfacial compositions at the $\gamma/\gamma + \theta$ phase boundary, since the iso-activity line of carbon, in general does not intersect this boundary and it is therefore reasonable to assume that the tie-line connecting cementite and austenite passes through the alloy composition. The difficulty with respect to the simultaneous precipitation of ferrite and cementite has been highlighted for the hypereutectoid alloys at low supersaturations and the means to overcome this has been suggested. The importance of the α/θ interfacial energy as a function of composition in the accurate determination of interlamellar spacing and hence the growth has been emphasised.

The theories developed for the binary and ternary steels would be academic in nature unless they could be applied to an industrial scenario. The case of the divorced eutectoid transformation during the spheroidising annealing of bearing steels has been analysed quantitatively. Using a rigorous treatment it has been shown that there exists a wider window (than previously thought) for processing of these steels that would lead to an energy efficient process.

Scope for Future Work

The theory for pearlite growth in ternary steels could be applied to a multicomponent steel assuming that the diffusivities of substitutional solutes (like Cr, Ni, Mn *etc.*) are similar. But some work needs to be done in order to arrive at an effective diffusion coefficient which would account for the partitioning of various solutes during the growth of pearlite.

The theory for the pearlite growth rate discussed in this work assumes a constant interlamellar spacing and growth rate. However there are instances for *eg.* formation of divergent pearlite, where the spacing increases continuously leading to a decrease in growth rate as the transformation progresses. There is a potential for future work to account for this non-steady state behaviour in order to develop a unified theory.

The case of pearlite dissolution has been discussed briefly (Appendix A) and it has been shown that the dissolution kinetics are much faster as compared to that of pearlite formation owing to the higher temperatures involved in the former. It is still not clear whether it is the cementite in pearlite or the ferrite that dissolves first and whether the kinetics is governed by the diffusion of substitutional solute through the interface or the carbon. Some more work needs to be done in order to establish the exact mechanism, but it has been demonstrated that once this clear, the necessary theory should be readily deduced from the pearlite growth modes.

It has been thought that the theory for pearlite growth developed in this work can be integrated into the simultaneous transformation model that includes other phases and which would lead to the quantification of the microstructure for a range of steels.

Appendix A

Dissolution of Pearlite

Reaustenisation of steels is a common treatment employed during the processing of steels. This involves dissolution of the previously formed structure which may either be ferritic, pearlitic, bainitic or martensitic or a combination of these. It is expected that the pearlite dissolution kinetics should be much faster than growth owing to the higher temperatures involved in reaustenisation. Essentially the same equation employed for the growth of pearlite from austenite may be used for the dissolution, with appropriate adjustments of the local equilibrium conditions at the interfaces and of the diffusivity. The rates at which the ferrite and cementite lamellae are consumed by the austenite are assumed to be the same. The distance over which the diffusion occurs is the interlamellar spacing, which is determined during the original growth of pearlite. The concentration profiles for the austenite formation from pearlite are shown in Fig. 1.1. When the austenite is growing into ferrite, the carbon in the austenite becomes diluted at the γ/α interface. At the same time the carbon rich cementite rejects the carbon into the austenite.

In a Fe-4.77Mn-0.72C wt% steel it is observed that the dissolution rates are much faster as compared to the growth rate of pearlite, and the dissolution kinetics may either be governed by the C mixed-mode diffusion (through the volume of austenite and the austenite-pearlite interface) or the boundary diffusion of Mn, although the former mechanism seems to be much faster than the latter as shown in the Fig. 1.2. In order to experimentally validate the pearlite dissolution kinetics, the 5.0 Mn wt% steel was austenised at 1000°C, cooled to and isothermally held at 590°C for 1 h
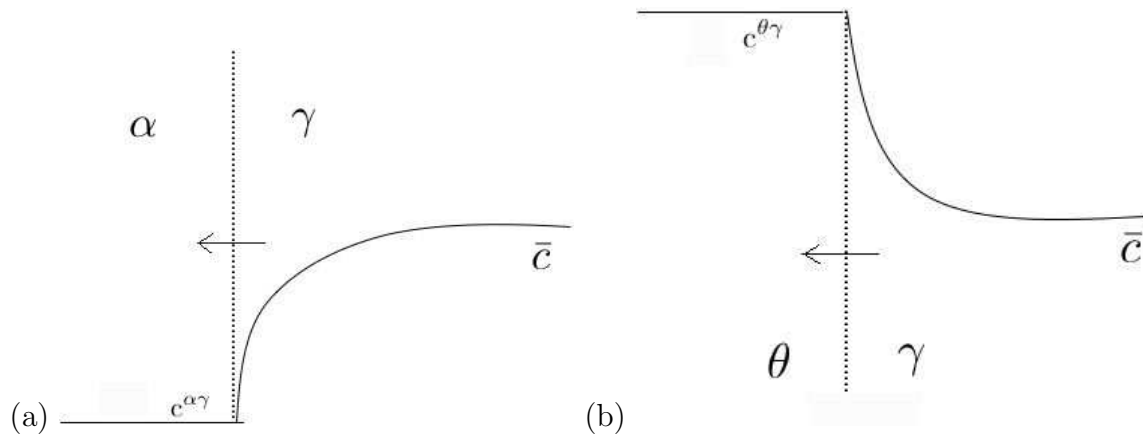
Figure 1.1: Schematic concentration profile for austenite growing into (a) ferrite and (b) cementite.

for complete transformation to pearlite. It was then reaustenitised at 800°C for 30 s and quenched to room temperature. The microstructure shows the presence of platelets of martensite, meaning that the pearlite dissolution was over in less than 30 s at 800°C leading to a completely austenitic structure which then transformed into martensite on quenching (Fig. 1.3).
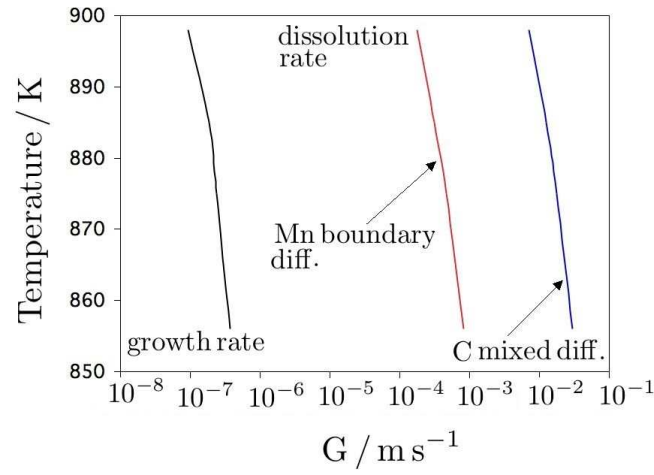
Figure 1.2: Comparison of calculated growth and dissolution rates of pearlite in a Fe-4.77Mn-0.72C wt % steel.
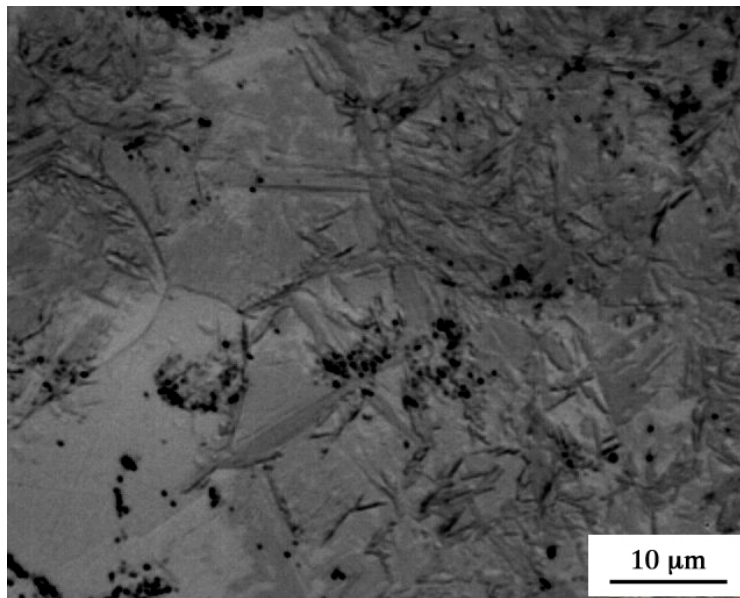
Figure 1.3: Microstructure showing martensite formed after quenching the reaustenised structure from 800°C (30 s hold) in a Fe-4.77Mn-0.72C wt% steel. Vickers hardness - 430 HV at 10 kg load.

Appendix B

Divergent Pearlite

In case of a Fe-4.77Mn-0.72C wt% steel, held at 625°C for 90 min., the pearlite transformation is incomplete and the microstructure shows colonies of pearlite, with the lamellae growing in a divergent manner, wherein the interlamellar spacing increases with time resulting in decrease in growth rate, Fig. 1.1. The formation of a divergent structure is a consequence of the alloy composition falling in the 3-phase $(\alpha + \theta + \gamma)$ region. The transformation in this region (Fig. 1.2) progresses wherein the the composition of austenite changes continuously in the region ahead of the growing pearlite thus necessitating volume diffusion of Mn and resulting in reduced growth rate.
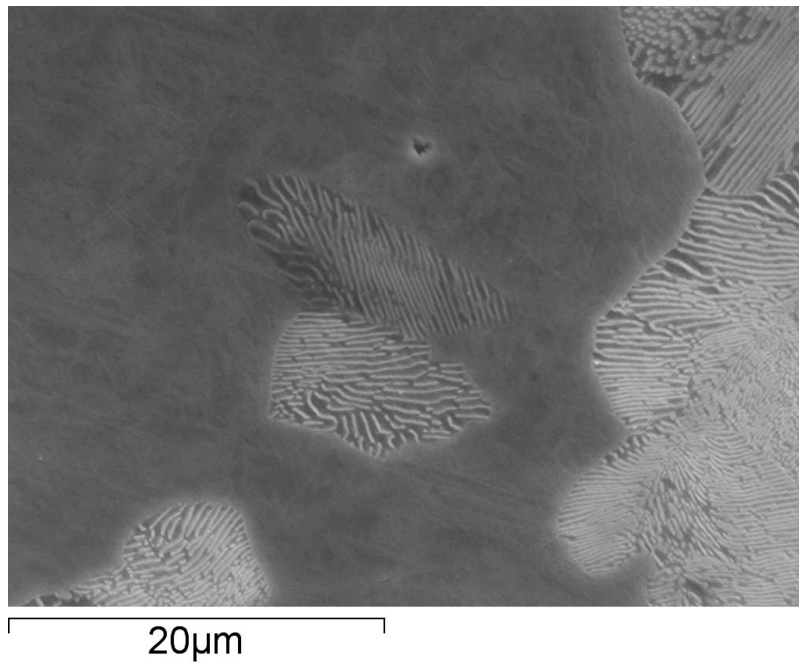
Figure 1.1: Micrograph showing divergent pearlite formation in a Fe-4.77Mn-0.72C wt% steel.
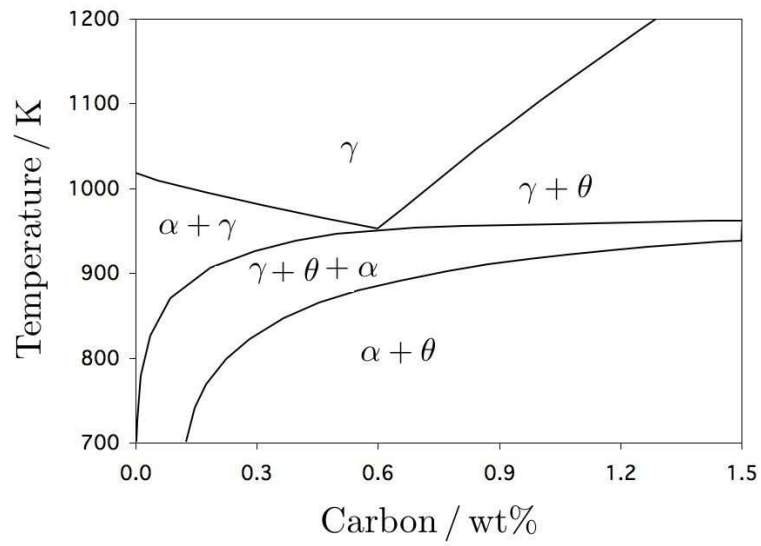
Figure 1.2: Isopleth section of Fe-C-Mn steel.

Appendix C

Program for Pearlite Growth in Binary Steels

1.1 Provenance of Source Code

Ashwin S. Pandit, Phase Transformations Group, Department of Materials Science and Metallurgy, University of Cambridge, Cambridge, UK.

1.2 Purpose

The program calculates the isothermal growth rate of pearlite in Fe-C steels.

1.3 Specification

Self-contained program written in fortran.

1.4 Description

The program calculates the isothermal growth rate of pearlite in Fe-C steel. The growth rate is calculated using a mixed diffusion of carbon through the austenite as well as the pearlite-austenite interface, thereby eliminating any assumptions regarding the diffusion paths taken by the solute.

1.5   References

1) R. H. Siller and R. B. McLellan, The application of first order mixing statistics to the variation of the diffusivity of carbon in austenite, Metallurgical Transactions, 1970, 1, 985-988.

2) W. W. Dunn and R. B. McLellan, The application of quasichemical solid solution model to carbon in austenite, Metallurgical Transactions, 1970, 1, 1263-126.

3) H. K. D. H. Bhadeshia, Diffusion of carbon in austenite, Metal Science, 1981, 15, 477-479.

4) H. K. D. H. Bhadeshia, MAP programs, http://www.msm.cam.ac.uk/map/steel/functions/cg-b.html.

5) R. Trivedi and G. M. Pound, Effect of concentration-dependent diffusion coefficient on the migration of interphase boundaries, J. Appl. Phys., 1967, 38, 3569-3576.

6) C. Zener, Kinetics of Decomposition of Austenite, Trans. AIME, 1946, 167, 550-595.

7) M. Hillert, The role of interfaces in phase transformations, 1970, In mechanism of phase transformations in crystalline solids. Monograph and Report series, no. 33, 231-247.

8) D. Brown and N. Ridley, Kinetics of the pearlite reaction in high-purity nickel eutectoid steels, J. Iron Steel Inst., 1969, 207, 1232-1240.

1.6   Parameters

Input parameters

argument in parentheses corresponds to the data type

carbon / wt%, (real)

Temperature / K, (real)

141

1.6.1   Input files

Input files :

fa_a_c.txt composition of carbon (column-3), iron (column-2) in austenite which is in equilibrium with ferrite at the interface as a function of temperature (column-1)
fa_f_c.txt composition of carbon (column-3), iron (column-2) in ferrite which is in equilibrium with austenite at the interface as a function of temperature (column-1)
ca_a_c.txt composition of carbon (column-3), iron (column-2) in austenite which is in equilibrium with cementite at the interface as a function of temperature (column-1)
ca_c_c.txt - composition of carbon (column-3), iron (column-2) in cementite which is in equilibrium with austenite at the interface as a function of temperature (column-1)
All the compositions in the files above are in mass fraction and the temperature is in K. The interfacial compositions are calculated using MTDATA (TCFE database).

1.6.2   Output parameters

Interlamellar spacing, lamda2 / m, (real)
Thickness of ferrite lamella, lamfe2 / m, (real)
Thickness of cementite lamella, lamce2 / m, (real)
Grain boundary diffusivity of carbon, dcgb4 / m^2 s^{-1}, (real)
Weighted average diffusivity of carbon, d$_a$vg/m^2 s^{-1}, (real)
Pearlite growth rate, velo / m s^{-1}, (real)

1.6.3   Output files

output.txt - gives the Temperature (in degree centigrade) and the growth rate in m s^{-1}

1.7 Program Listing

```fortran
program pearlite
integer loop,i,j,m,p,option,choice,w,p1,p2,p3,p4,r,s,t
real carbon,c_cem,c_fer
real coef,coef1,coef2,coef3,coef4,coe,coef5,coef7,d_coef
real af_ac,a_f_mn,c_f_mn
real tempf(1000),af_fe(1000),af_mn(1000),af_c(1000)
real tempf1(1000),ac_fe(1000),ac_mn(1000),ac_c(1000)
real tempf2(1000),fa_fe(1000),fa_mn(1000),fa_c(1000)
real tempf3(1000),ca_fe(1000),ca_mn(1000),ca_c(1000)
real df_cf,ddash1,ddash2,del_f,k,h,ddash,del_e,v1,v2
real v,v_gb,stor,stor1,st_mn,st_mn1,st_mn2,st_mn3
real k_gb,v3,v4,v5,st_c,st_c1
real c_f_c,c_fe(1000),c_c(1000),acti_c
real del_T,temp,teqm,teqm1,si_fc,slope,z1,df_av
real del_hm,del_vm,velo,delta,factor,lamda,lamfer,lamcem
real Mn,Cr,Si,f_fe(1000),f_c(1000),D(1000)
real eta,molfra,ans,d_avg,part_c,vcgb,dcgb,d_eff
real temp_1(1000),a_fe(1000),a_c(1000),temp_2(1000)
real temp_3(1000),a1_fe(1000),a1_c(1000),temp_4(1000)
real var1,var2,var3,var4,res1,res2,act,R1,CG,CG1
real var1_m,var3_m

del_f=21230
h=6.63E-34
z1=12
c_cem=6.67
c_fer=0.025
teqm=1000
open (unit = 22, file = 'fa_a_c.txt', status='old')
```

```fortran
      open (unit = 42, file = 'fa_f_c.txt', status='old')
      open (unit = 32, file = 'ca_a_c.txt', status='old')
      open (unit = 72, file = 'ca_c_c.txt', status='old')
      open (unit = 1,  file = 'output.txt', access='append')


c     ***********************************************************

      print *,'Enter the chemical composition:'

      print *,'Carbon'
      read *,carbon
      write(1,31)
31    FORMAT('----------------------------------------------')
      write(1,34),'Temperature','Growth rate'
34    FORMAT(X,A,7X,A)

      write(1,37),'(C)','(m s-1)'
37    FORMAT(4X,A,15X,A)
      write(1,38)
38    FORMAT('----------------------------------------------')

      do 61 loop=1,9
      print *, 'enter the temperature :'
      read *, temp
      If (temp .GE. teqm) then
      print *, 'Please enter temp lesser than teqm:'
      endif
c     ***********************************************************
      do 200 r=1,600
      read(22,*,end=201) temp_1(r),a_fe(r),a_c(r)
      if (temp_1(r) .EQ. temp) then
```

144

```
          var1=a_c(r)*100
c         a_c(r) is multiplied by 100 to convert mass fraction
        & into mass
          endif


  200     enddo
  201     endfile 22
          rewind 22


c         ************************************************************
          do 300 s=1,600
          read(42,*,end=301) temp_2(s),f_fe(s),f_c(s)
          if (temp_2(s) .EQ. temp) then
          var2=f_c(s)*100
c         f_c(p2) is multiplied by 100 to convert mass fraction
        & into mass

          endif


  300     enddo
  301     endfile 42
          rewind 42


c         ************************************************************
          do 400 t=1,600
          read(32,*,end=401) temp_3(t),a1_fe(t),a1_c(t)
          if (temp_3(t) .EQ. temp) then
          var3=a1_c(t)*100
c         a1_c(p3) is multiplied by 100 to convert mass fraction
        & into mass
          endif
```

```
   400        enddo
   401        endfile 32
              rewind 32
c             ****************************************************

              do 500 p4=1,600
              read(72,*,end=501) temp_4(p4),c_fe(p4),c_c(p4)

              if (temp_4(p4) .EQ. temp) then
              var4=c_c(p4)*100
c             c_c(p4) is multiplied by 100 to convert mass fraction
        & into mass
              endif

   500        enddo
   501        endfile 72
              rewind 72
c             ****************************************************


c             res1 and res2 calculates the diff. in interfacial
c             compositions in Fe–C alloy
c             ****************************************************
              res1=var1−var3
              res2=var4−var2


              call mol_frac_c(var1,var3,var1_m,var3_m)
c             calculates the mol_fraction of carbon in austenite
c             var1 is the carbon in austenite in wt%
```

```
          call  diff_calc (var1_m , var3_m , carbon , res1 , res2 , temp , d_avg )

c         calculates  the  pearlite  growth  rate  using  volume
c         diffusivity  of  C  in  austenite
c         call  boundary_diff_c (d_avg , temp , part_c , res1 , res2 , vcgb )
c         calculates  the  pearlite  growth  rate  using  boundary
c         diffusivity  of  C  in  austenite

          call  mixed_growth (temp , carbon , d_avg , res1 , res2 , velo )
          print  * ,'the  pearlite  growth  rate  in  m  s-1  is : ',  velo
          write (1 ,33) , temp-273, velo

  33      format ( f6 .1 , e22 .3 )

  61      enddo


          close (22)
          close (42)
          close (32)
          close (72)
          close (1)
c         close (113)
          stop
          end

c         *********************************************************

          subroutine  diff_calc ( var1_m , var3_m , carbon , res1 , res2 ,
     &  temp , d_avg )
          real  v1 , v2 , v , lamda , lamcem , lamfer , phi
```

```
          real  d_eff , delta
          delta=2.5e−10
          del_vm=7.1E−6
          del_e=8352
          k=1.38E−23

          call  phi_c ( del_e , k , temp , phi )
c         calculates  the  value  of  sigma : site  exclusion  probability ,
c         used  in  calculation  of  eta


          call  act_c ( var1_m , temp , del_e , acti_c )
c         calculates  the  activity  of  carbon  in  austenite  using  a
c         quasi  chemical  model : MAP

          call  DCG( var1_m , del_e , temp , R, slope )
c         calculates  the  differential  of  activity  of  carbon  in
      &  austenite

          call  DIFF( temp , var1_m , var3_m , del_e , acti_c , slope , phi , d_avg )
          end


c         ************************************************************
          subroutine  mol_frac_c ( var1 , var3 , var1_m , var3_m )
          real  wt_fe , fe_mol , c_mol , wt_fe1 , fe_mol1 , c_mol1
          wt_fe=100−var1
          fe_mol=wt_fe /55.8
          c_mol=var1 /12.01
          var1_m=c_mol /( fe_mol+c_mol )
          wt_fe1=100−var3
          fe_mol1=wt_fe1 /55.8
```

```
              c_mol1=var3/12.01
              var3_m=c_mol1/(fe_mol1+c_mol1)
              return
              end
c             ************************************************************
              subroutine lamda_crit_spa(teqm,temp,spac)
              real spac,del_T,del_hm,teqm,del_vm,del_HV,del_G,lamda2
              del_HV=(-2E6*temp)+2E9
              del_T=teqm-temp
              del_G=(8.09554e5*temp)-8.03332e08
              lamda2=1e-6/((-0.1627*temp)+162.74)
                spac=lamda2/(4.586e-35*exp(temp/12.8523)+2.03714)
              si_fc=-0.5*spac*del_G
              return
              end
c             ************************************************************
              subroutine lamella_thk(carbon,c_cem,c_fer,lamda,lamcem)
              real wt_frac_fer,vol_frac_fer,vol_frac_cem,r_fer
              real lamda,lamcem
              wt_frac_fer=(c_cem-carbon)/(c_cem-c_fer)
              vol_frac_fer=wt_frac_fer


c             densities of ferrite and austenite are nearly same
              vol_frac_cem=1-vol_frac_fer
              r_fer=vol_frac_fer/vol_frac_cem
              lamcem=lamda/(r_fer+1)
              return
              end


c             ************************************************************
              subroutine phi_c(del_e,k2,temp,phi1)
```

```
          real k2,phi1
          phi1=1-exp( (-del_e)/(k2*temp) )
c         print *, 'the value of phi is :',phi
c         print *, 'the value of temp is :',temp
          return
          end


c         *************************************************************


c         SUBROUTINE GIVING THE DIFFERENTIAL OF NATURAL LOGARITHM
c         (ACTIVITY OF CARBON IN AUSTENITE):
          subroutine DCG(var1_m,del_e,temp,R1,slope)
          real DG,DDG,var1_m,temp,slope,phi10
          R1=8.14
          phi10=1.0-EXP(-del_e/(R1*temp))
          DG=SQRT(1.0-2.0*(1.0+2.0*phi10)*var1_m+(1.0+8.0*phi10)
        & *var1_m**2)
          DDG=(0.5/DG)*(-2.0-4.0*phi10+2.0*var1_m+16.0*phi10*var1_m)
          slope=-((10.0/(1.0-2.0*var1_m))+(5.0/var1_m))
        & +6.0*((DDG+3.0)/(DG-1.0+3.0*var1_m)
        & -(DDG-3.0)/(DG+1.0-3.0*var1_m))
          return
          end
c         *************************************************************
c         FUNCTION GIVING THE NATURAL LOGARITHM (ACTIVITY
c         OF CARBON IN AUSTENITE):
          subroutine act_c(var1_m,temp,del_e,CG)
          real    var1_m,AJ,DG,EG,EG1,R,W,CG
          R=8.31
          AJ=1-EXP(-del_e/(R*temp))
          IF(var1_m .LE. 1.0e-10) THEN
```

150

```
           CG=LOG(1.0e−10)
           ELSE
           DG=SQRT(1.0−2.0∗(1.0+2.0∗AJ)∗var1_m+(1.0+8.0∗AJ)∗
      &    var1_m∗∗2)
           EG=5∗LOG((1−2∗var1_m)/var1_m)+6∗del_e/(R∗temp)
           EG1= (38575−13.48∗temp)/(R∗temp)
           CG=EG+EG1+6∗LOG((DG−1+3∗var1_m)/(DG+1−3∗var1_m))
           ENDIF
           RETURN
           END
c          ***************************************************************
c          subroutine GIVING THE CARBON DIFFUSIVITY IN AUSTENITE:
           subroutine DIFF(temp,var1_m,var3_m,del_e,acti_c,slope
      &    ,phi,d_avg)

           integer II,II2,II3
           real D(1000),CARB(1000)
           real X,THET,DASH,eta,R2,Z2,HH,KK,eta1,eta2,eta3,eta4
           real ACTI,DACTI,SIGMA,XINCR,var1_m,var3_m,acti_c,slope,
      &    phi,A5,ans,d_avg
           HH=6.6262e−34
           KK=1.38062e−23
           Z2=12
           A5=1.0
           R2=8.31
           DASH=(KK∗temp/HH)∗EXP(−(21230/temp))∗EXP(−31.84)
           XINCR=(var1_m−var3_m)/5
           DO 111 II=1,5
           CARB(II)=var3_m+(II−1)∗XINCR
           X=CARB(II)
           THET=X/(A5−X)
```

```
c               the var1 , var3 and X are to be expressed in mol fractions .

                ACTI=acti_c
                ACTI=EXP(ACTI)
                DACTI=slope
                DACTI=DACTI*ACTI
                DACTI=DACTI*A5/((A5+THET)**2)
                SIGMA=phi
                eta=A5+(Z2*(A5+THET))
                eta2=(A5-((A5+Z2/2)*THET)+(Z2/2)*(A5+Z2/2)*(A5-SIGMA)
          &     *THET**2)
                eta3=ACTI*(eta/eta2)
                eta1  =(A5+THET)*DACTI
                eta4=eta1+eta3
                D(II)=DASH*eta4
c               print *,'the dif coef in cm2/s and theta is:',D(II)
c               write(113,*), D(II), THET
   111          continue

                call TRAPE(var1_m , var3_m ,XINCR, II ,D, ans)
                d_avg=ans/(var1_m-var3_m)
                RETURN
                END
c               ************************************************************
                subroutine TRAPE(var1_m , var3_m ,XINCR, II ,D, ans)
                real  var1_m , var3_m ,XINCR,XX, sum ,D(1000) , ans1 , ans
                INTEGER Q, II
                sum=0
                do  999  Q=1, II −1
```

152

```
              XX=var3_m+(XINCR*Q)
              sum=sum+D(Q)


    999       continue
              ans=XINCR*(  (D(1)+D(5)/2)  +  sum  )
              return
              end
c             ************************************************************
subroutine  mixed_growth(temp,carbon,d_avg,res1,res2,velo)
              real  y5,spac2,dcgb3,dcgb4,dcgb5,velo1,velo2,velo,
              real  c_cem2,c_fer2,delta
              real  molfra,wt_fe2,fe_mol2,c_mol2,carbon,
              real  lamda2,lamce2,lamfe2,teqm,u
              c_cem2=6.67
              c_fer2=0.025
              teqm=1000
              delta=2.5e-10
              call  lamda_crit_spa(teqm,temp,spac2)
              lamda2=1e-6/((-0.1627*temp)+162.74)
              call  lamella_thk(carbon,c_cem2,c_fer2,lamda2,lamce2)
              lamfe2=lamda2-lamce2
              print  *,  'the  S  in  m  is:',lamda2
              print  *,  'the  S_fer  and  S_cem  in  m  are:',lamfe2,lamce2
              u=res1/res2
              wt_fe2=100-carbon
              fe_mol2=wt_fe2/55.8
              c_mol2=carbon/12.01
              molfra=c_mol2/(fe_mol2+c_mol2)
              y5=molfra/(1-molfra)
              dcgb4  =  8.5133e-5*exp(-96851/(8.312*temp))
              print  *,  'The  D_gb  of  carbon  in  m2  s-1  is:',dcgb4
```

153

```
      print *, 'The D_wei_avg of carbon in m2 s-1 is:',
    & d_avg*1e-4
      velo1=((2*d_avg*0.0001)+(12*dcgb4*delta/lamda2))*lamda2
      velo2=(1-(spac2/lamda2))*(res1/res2)/(lamfe2*lamce2)
      velo=velo1*velo2
      return
      end
c     ************************************************************
```

Appendix D

Program for Pearlite Growth in Ternary Steels

1.1 Provenance of Source Code

Ashwin S. Pandit, Phase Transformations Group, Department of Materials Science and Metallurgy, University of Cambridge, Cambridge, UK.

1.2 Purpose

The program calculates the isothermal growth rate of pearlite in Fe-C-X steels.

1.3 Specification

Self-contained program written in fortran.

1.4 Description

The program calculates the isothermal growth rate of pearlite in Fe-C-X steel. The growth rate is calculated based on the user inputs for interfacial compositions based on the tie-line selection from an isothermal section of a ternary phase diagram. The growth rate in ternary steels is controlled either by partitioning of substitutional solute (X) through the phase boundary (P-LE) or by carbon diffusion through the

austenite and the transformation interface involving negligible partitioning of X, (NP-LE).

1.5   References

1) R. H. Siller and R. B. McLellan, The application of first order mixing statistics to the variation of the diffusivity of carbon in austenite, Metallurgical Transactions, 1970, 1, 985-988.

2) W. W. Dunn and R. B. McLellan, The application of quasichemical solid solution model to carbon in austenite, Metallurgical Transactions, 1970, 1, 1263-126.

3) H. K. D. H. Bhadeshia, Diffusion of carbon in austenite, Metal Science, 1981, 15, 477-479.

4) H. K. D. H. Bhadeshia, MAP programs, http://www.msm.cam.ac.uk/map/steel/functions/cg-b.html.

5) R. Trivedi and G. M. Pound, Effect of concentration-dependent diffusion coefficient on the migration of interphase boundaries, J. Appl. Phys., 1967, 38, 3569-3576.

6) C. Zener, Kinetics of Decomposition of Austenite, Trans. AIME, 1946, 167, 550-595.

7) M. Hillert, The role of interfaces in phase transformations, 1970, In mechanism of phase transformations in crystalline solids. Monograph and Report series, no. 33, 231-247.

8) N. A. Razik and G. W. Lorimer and N. Ridley, An investigation of manganese partitioning during the austenite-pearlite transformation using analytical electron microscopy, Acta Metallurgica, 1974, 22, 1249-1258.

1.6 Parameters

1.6.1 Input parameters

argument in parentheses corresponds to the data type

Carbon / wt%, (real)

Manganese / wt% (real)

Chromium / wt% (real)

1) P-LE or 2) NP-LE

Eutectoid temperature / K, (real)

Transformation temperature / K, (real)

P-LE: Interfacial compositions of X at $\alpha/\gamma + \alpha$ and $\theta/\gamma + \theta$ phase boundaries based on the isothermal section of a ternary phase diagram

NP-LE: Interfacial compositions of C at $\alpha/\gamma + \alpha$ and $\theta/\gamma + \theta$ phase boundaries based on the isothermal section of a ternary phase diagram

1.6.2 Output parameters

Thickness of ferrite lamella, lamfe3 / m, (real)

Thickness of cementite lamella, lamce3 / m, (real)

P-LE: Pearlite growth rate, v_pl / m s^{-1}, (real)

NP-LE: Pearlite growth rate, v_npl / m s^{-1}, (real)

1.7 Program Listing

```
program pearlite
integer loop,i,j,m,p,option,choice,w,p1,p2,p3,p4,r,s,t
real carbon,c_cem,c_fer
real coef,coef1,coef2,coef3,coef4,coe,coef5,coef7,d_coef
```

```
real af_ac , a_f_mn , c_f_mn
real tempf(1000), af_fe(1000), af_mn(1000), af_c(1000)
real tempf1(1000), ac_fe(1000), ac_mn(1000), ac_c(1000)
real tempf2(1000), fa_fe(1000), fa_mn(1000), fa_c(1000)
real tempf3(1000), ca_fe(1000), ca_mn(1000), ca_c(1000)
real df_cf , ddash1 , ddash2 , del_f , k , h , ddash , del_e , v1 , v2
real v , v_gb , stor , stor1 , st_mn , st_mn1 , st_mn2 , st_mn3 , k_gb
real v3 , v4 , v5 , st_c , st_c1
real c_f_c , c_fe(1000) , c_c(1000) , acti_c
real del_T , temp , teqm , teqm1 , si_fc , slope , z1 , df_av
real del_hm , del_vm , velo , delta , factor , lamda , lamfer
real Mn, Cr , Si , f_fe(1000) , f_c(1000) ,D(1000) , lamcem
real eta , molfra , ans , ans2 , part_c , vcgb , dcgb , d_eff
real temp_1(1000) , a_fe(1000) , a_c(1000) , temp_2(1000)
real temp_3(1000) , a1_fe(1000) , a1_c(1000) , temp_4(1000)
real var1 , var2 , var3 , var4 , res1 , res2 , act ,R1,CG,CG1
real c_af , c_ac , c_fa , c_ca , v_pl , v_npl , spcr , var3_m , var1_m
real d_b
c         variables for storing interfacial compositions and
c         velocity in ternary steels
          del_f=21230
          h=6.63E-34
          z1=12
          c_cem=6.67
          c_fer=0.025

          open (unit = 1,   file = 'output.txt', access='append')

c         ********************************************************

          print *,'Enter the chemical composition:'
```

158

```
         print *,'Carbon'
         read *,carbon
         print *,'Manganese'
         read *,Mn
         print *,'Chromium'
         read *,Cr


c        User input for the mechanism of pearlite growth
         print *,'Enter : 1 P–LE or 2 NP–LE :'
         read *, choice

         print *,'enter the eutectoid temperature in K'
         read *, teqm

         do 61 loop=1,2
         print *, 'enter the temperature :'
         read *, temp

         If (temp .GE. teqm) then
         print *, 'Please enter temp greater than teqm:'
         endif

         If (choice .EQ. 1) then
         d_b=2.81e-3*exp(-164434/(8.31*temp))
         temp=temp-273
         lamda=10**(-2.2358+(0.09863*1.8)-log10((693-temp)/693))
     & *(1e-6)

         call lamella_thk(carbon,c_cem,c_fer,lamda,lamcem)
         lamfer=lamda-lamcem
```

```
          call PLE(temp,lamda,lamfer,lamcem,d_b,v_pl)
          print *,'the velocity of pearlite assuming P-LE is:
     & m2 s-1',v_pl
          elseif (choice .EQ. 2) then
          print *,'carbon in aus. in equilibrium with ferrite '
          read *,var1
          print *,'carbon in aus. in equilibrium with cementite '
          read *,var3

c         res1 calculates the diff. in interfacial compositions
c         in Fe-C alloy
c         ****************************************************
          res1=var1-var3
          res2=6.67-0.025

          call mol_frac_c(var1,var3,var1_m,var3_m)
c         calculates the mol_fraction of carbon in austenite
c         var1 is the carbon in austenite in wt%

          call lamda_crit_spa(teqm,temp,spac)
          lamda=spac*3
          call lamella_thk(carbon,c_cem,c_fer,lamda,lamcem)
          lamfer=lamda-lamcem

          call vol_diff(var1_m,var3_m,carbon,res1,res2,temp,ans2)
c         calculates the pearlite growth rate using volume
c         diffusivity of C in austenite

          call mixed_growth(temp,carbon,ans2,res1,res2,velo)
          print *,'the velocity of pearlite in NP-LE mode is:
     & m2 s-1',velo
```

```
            write (1 ,*) , temp −273 , velo
            else
            stop
            endif


61          enddo
            close (1)
            stop
            end
c           ***************************************************************

            subroutine  vol_diff ( var1_m , var3_m , carbon , res1 , res2 , temp , ans2 )
            real  v1 , v2 , v , lamda , lamcem , lamfer , phi
            real  d_eff , delta
            delta =2.5e−10
            teqm=1000
            del_vm =7.1E−6
            c_cem =6.67
            c_fer =0.025
            del_e =8352
            k=1.38E−23
            call  lamda_crit_spa ( teqm , temp , spac )
            lamda=spac *3

            call  lamella_thk ( carbon , c_cem , c_fer , lamda , lamcem )
c           calculates  the  thickness  of  ferrite  and  cementite  lamella
            lamfer=lamda−lamcem

            call  phi_c ( del_e , k , temp , phi )
c           calculates  the  value  of  sigma : site  exclusion
c           probability ,  used  in  calculation  of  eta
```

```
          call  act_c ( var1_m , temp , del_e , acti_c )
c         calculates  the  activity  of  carbon  in  austenite
c         using  a  quasi  chemical  model :MAP
c         print  *,'the  activity  is : ', acti_c

          call  DCG( var1_m , del_e , temp ,R, slope )
c         calculates  the  differential  of  activity  of  carbon
c         in  austenite
c         print  *,  'the  slope  is : ', slope

          call  DIFF ( temp , var1_m , var3_m , del_e , acti_c , slope , phi , ans2 )
          print  *,  'the  weighted  avg.  diff  coef  in  cm2/s  is : ', ans2
          return
          end



c         ****************************************************************
subroutine  mol_frac_c ( var1 , var3 , var1_m , var3_m )
          real  wt_fe , fe_mol , c_mol , wt_fe1 , fe_mol1 , c_mol1
          wt_fe=100−var1
          fe_mol=wt_fe /55.8
          c_mol=var1 /12.01
          var1_m=c_mol /( fe_mol+c_mol )
          wt_fe1=100−var3
          fe_mol1=wt_fe1 /55.8
          c_mol1=var3 /12.01
          var3_m=c_mol1 /( fe_mol1+c_mol1 )
          return
          end
c         ****************************************************************
```

```fortran
            subroutine lamda_crit_spa(teqm,temp,spac)
            real spac,del_T,del_hm,teqm,del_vm
            si_fc=0.60
            del_hm=4300
            del_vm=7.1E-6
            del_T=teqm-temp
c           print *,'the new teqm is:',teqm
            spac=2 * si_fc * teqm * del_vm / (del_T*del_hm)
            return
            end
c           ****************************************************************
            subroutine lamella_thk(carbon,c_cem,c_fer,lamda,lamcem)
            real wt_frac_fer,vol_frac_fer,vol_frac_cem
            real r_fer,lamda,lamcem,carbon
            wt_frac_fer=(c_cem-carbon)/(c_cem-c_fer)
            vol_frac_fer=wt_frac_fer

c           densities of ferrite and austenite are nearly same
            vol_frac_cem=1-vol_frac_fer
            r_fer=vol_frac_fer/vol_frac_cem
            lamcem=lamda/(r_fer+1)
            print *,'lamcem in sub is:',lamcem
            return
            end

c           ****************************************************************
subroutine phi_c(del_e,k2,temp,phi1)
            real k2,phi1
            phi1=1-exp( (-del_e)/(k2*temp) )
c           print *, 'the value of phi is :',phi
c           print *, 'the value of temp is :',temp
```

```fortran
      return
      end


c          FUNCTION GIVING THE DIFFERENTIAL OF NATURAL
c          LOGARITHM (ACTIVITY OF CARBON IN AUSTENITE):
      subroutine DCG(var1_m,del_e,temp,R1,slope)
      real DG,DDG,var1_m,temp,slope,phi10
      R1=8.14
      phi10=1.0-EXP(-del_e/(R1*temp))
      DG=SQRT(1.0-2.0*(1.0+2.0*phi10)*var1_m+
     & (1.0+8.0*phi10)*var1_m**2)
      DDG=(0.5/DG)*(-2.0-4.0*phi10+2.0*var1_m+16.0*
     & phi10*var1_m)
      slope=-((10.0/(1.0-2.0*var1_m))+(5.0/var1_m))+
     & 6.0*((DDG+3.0)/(DG-1.0+3.0*var1_m
     & )-(DDG-3.0)/(DG+1.0-3.0*var1_m))
      return
      end


c     *****************************************************************


c          FUNCTION GIVING THE NATURAL LOGARITHM
c          (ACTIVITY OF CARBON IN AUSTENITE):
      subroutine act_c(var1_m,temp,del_e,CG)
      real var1_m,AJ,DG,EG,EG1,R,W,CG
      R=8.31

      AJ=1-EXP(-del_e/(R*temp))
      IF(var1_m .LE. 1.0e-10) THEN
      CG=LOG(1.0e-10)
      ELSE
```

```
          DG=SQRT(1.0-2.0*(1.0+2.0*AJ)*var1_m+
     &    (1.0+8.0*AJ)*var1_m**2)
          EG=5*LOG((1-2*var1_m)/var1_m)+6*del_e/(R*temp)
          EG1= (38575-13.48*temp)/(R*temp)
          CG=EG+EG1+6*LOG((DG-1+3*var1_m)/(DG+1-3*var1_m))
          ENDIF
          RETURN
          END
c         ****************************************************************

c         subroutine GIVING THE CARBON DIFFUSIVITY IN AUSTENITE:
          subroutine DIFF(temp,var1_m,var3_m,del_e,acti_c,slope,
     &    phi,ans2)
          integer II,II2,II3
          real D(1000),CARB(1000)
          real X,THET,DASH,eta,R2,Z2,HH,KK,eta1,eta2
          real eta3,eta4,ans,ans2
          real ACTI,DACTI,SIGMA,XINCR,var1_m,var3_m
          real acti_c,slope,phi,A5
          HH=6.6262e-34
          KK=1.38062e-23
          Z2=12
          A5=1.0
          R2=8.31

          DASH=(KK*temp/HH)*EXP(-(21230/temp))*EXP(-31.84)
          XINCR=(var1_m-var3_m)/5

          DO 111 II=1,5
          CARB(II)=var3_m+(II-1)*XINCR
          X=CARB(II)
```

```
        THET=X/(A5-X)


c       the var1,var3 and X are to be expressed in mol fractions.
        ACTI=acti_c
        ACTI=EXP(ACTI)
        DACTI=slope
        DACTI=DACTI*ACTI
        DACTI=DACTI*A5/((A5+THET)**2)
        SIGMA=phi

        eta=A5+(Z2*(A5+THET))
        eta2=(A5-((A5+Z2/2)*THET)+(Z2/2)*(A5+Z2/2)*(A5-SIGMA)*
     &  THET**2)
        eta3=ACTI*(eta/eta2)
        eta1  =(A5+THET)*DACTI
        eta4=eta1+eta3
        D(II)=DASH*eta4

        write(113,*), D(II), THET
111     continue
        call TRAPE(var1_m,var3_m,XINCR,II,D,ans)
        ans2=ans/(var1_m-var3_m)
        RETURN
        END
c       ************************************************************
        subroutine TRAPE(var1_m,var3_m,XINCR,II,D,ans)
        real var1_m,var3_m,XINCR,XX,sum,D(1000),ans1,ans
        INTEGER Q,II
        sum=0
        do 999 Q=1,II-1
        XX=var3_m+(XINCR*Q)
```

```
              sum=sum+D(Q)
999           continue
              ans=XINCR*(  (D(1)+D(5)/2)  +  sum  )
              return
              end
c             ****************************************************************
              subroutine  mixed_growth(temp,carbon,ans2,res1,res2,velo)
              real  y5,spac2,dcgb3,dcgb4,dcgb5,velo1,velo2,velo
              real  c_cem2,c_fer2,delta
              real  molfra,wt_fe2,fe_mol2,c_mol2,carbon,lamda2
              real  lamce2,lamfe2,teqm
              c_cem2=6.67
              c_fer2=0.025
              teqm=1000
              delta=2.5e-10
              print  *,  'the  teqm  is:',teqm
              call  lamda_crit_spa(teqm,temp,spac2)
              lamda2=spac2*3
c             max.  entropy  production  criterion
              call  lamella_thk(carbon,c_cem2,c_fer2,lamda2,lamce2)
              lamfe2=lamda2-lamce2
              print  *,'the  value  of  lamce2,lamda2  is:',lamfe2,
        &  lamce2,lamda2

              wt_fe2=100-carbon
              fe_mol2=wt_fe2/55.8
              c_mol2=carbon/12.01
              molfra=c_mol2/(fe_mol2+c_mol2)
              y5=molfra/(1-molfra)
```

```
        dcgb4 = 2.961e−6∗exp(−72865/(8.31∗temp))
        print ∗, 'dcgb 4 is :',dcgb4,ans2
        velo1=((2∗ans2∗0.0001)+(12∗dcgb4∗delta/lamda2))∗lamda2
        velo2=(1−(spac2/lamda2))∗(res1/res2)/(lamfe2∗lamce2)
        velo=velo1∗velo2
        return
        end
c       ************************************************************
        subroutine PLE(temp,lamda3,lamfer3,lamcem3,d_b,v_pl)
        real v_pl1,c_af,c_ac,c_fa,c_ca,lamda3,lamfer3
        real lamcem3,v_pl
        real spcr,d_b
        delta=2.5e−10
        print ∗,'composition of X in aus. in equilibrium
&       with ferrite:'
        read ∗, c_af
        print ∗,'composition of X in aus. in equilibrium
&       with cementite:'
        read ∗, c_ac
        print ∗,'composition of X in ferrite in equilibrium
&       with aus:'
        read ∗, c_fa
        print ∗,'composition of X in cementite in equilibrium
&       with aus:'
        read ∗, c_ca
        spcr=lamda3/2
        print ∗,'lamda lamfer3 in ple are:',lamda3,lamfer3
        v_pl1=12∗d_b∗delta∗((c_af−c_ac)/(c_ca−c_fa))
        v_pl=v_pl1∗(1/(lamfer3∗lamcem3))∗(1−(spcr/lamda3))
        print ∗,'v is:',v_pl
        return
```

end

Bibliography

[1] H. C. Sorby. On the application of very high powers to the study of microscopic structure of steel. *J. Iron Steel Inst.*, 1:140–147, 1886. 1

[2] M. Hillert. The formation of pearlite. In H. I. Aaronson V. F. Zackay, editor, *Decomposition of Austenite by Diffusional Processes*, pages 197–237, New York, 1962. Interscience. 1

[3] M. V. Kral, M. A. Mangan, and G. Spanos and. Three-dimensional analysis of microstructures. *Materials Characterisation*, 45:17–23, 2000.

[4] M. D. Graef, M. V. Kral, and M. Hillert. A modern 3-D view of an old pearlite colony. *J. Metals*, 58:25–28, 2006. 1

[5] R. E. Smallman and R. J. Bishop. *Modern Physical Metallurgy and Materials Engineering.* Butterworth–Heinemann, 6th edition, 1999. 2

[6] C. Zener. Kinetics of decomposition of austenite. *Trans. AIME*, 167:550–595, 1946. 3, 25, 47, 52, 56, 59

[7] M. Hillert. The role of interfacial energy during solid state phase transformations. *Jernkont Ann.*, 141:757–89, 1957. 3, 23, 28, 94, 117

[8] M. Hillert. The mechanism of phase transformation in crystalline solids. pages 231–247, London, 1969. Institute of Metals. 3, 56

[9] N. Ridley. A review of the data on the interlamellar spacing of pearlite. *Metallurgical Transactions A*, 15A:1019–1036, 1984.

[10] J. W. Christian. *Theory of transformations in metals and alloys.* Part I. Pergamon Press, Oxford, U. K., 3rd edition, 2003.

[11] J. W. Christian. *The theory of trasformations in metals and alloys.* Part II. Pergamon Press, Oxford, U. K., 3rd edition, 2003. 3, 47

[12] J. H. Frye, Jr., E. E. Stansbury, and D. L. McElroy. Absolute rate theory applied to rate of growth of pearlite. *Trans. AIME*, 197:219–224, 1953. 3, 47, 66, 68

[13] D. Brown and N. Ridley. Kinetics of the pearlite reaction in high-purity nickel eutectoid steels. *J. Iron Steel Inst.*, 207:1232–1240, 1969. 48, 56, 63, 75, 78

[14] D. D. Pearson and J. D. Verhoeven. Forced velocity pearlite in high purity Fe–C alloys: part 1. experimental. *Metallurgical Transactions A*, 15:1037–1045, 1984. 3, 47, 50

[15] B. E. Sundquist. The edgewise growth of pearlite. *Acta Metallurgica*, 16:1413–1427, 1968. 3, 26, 45, 46, 47, 66

[16] M. Hillert. On theories of growth during discontinuous precipitation. *Metallurgical Transactions*, 3:2729–2741, 1972. 3, 23, 24, 27, 47, 48

[17] N. A. Razik, G. W. Lorimer, and N. Ridley. An investigation of manganese partitioning during the austenite-pearlite transformation using analytical electron microscopy. *Acta Metallurgica*, 22:1249–1258, 1974. 4, 35, 83, 84, 87, 94, 100

[18] N. A. Razik, G. W. Lorimer, and N. Ridley. Chromium partitioning during the austenite-pearlite transformation. *Metallurgical Transactions A*, 7A:209–214, 1976. 36, 83, 84, 87, 102, 103, 106, 118

[19] M. L. Picklesimer, D. L. McElroy, Jr. T. M. Kegley, E. E. Stansbury, and J. H. Frye. Effect of manganese on the austenite-pearlite transformation. *Transactions of the Metallurgical Society of AIME*, 218:473–480, June 1960. 4, 83

[20] J. W. Cahn. On the kinetics of the pearlite reaction. *Trans. A. I. M. E.*, 209:140–144, 1957. 9

[21] S. E. Offerman, L. J. G. W. van Wilderen, N. H. van Dijk, J. Sietsma, M. Th. Rekveldt, and S. van der Zwaag. In-situ study of pearlite nucleation and growth during isothermal austenite decomposition in nearly eutectoid steel. *Acta Materialia*, 51:3927–3938, 2003. 9, 10, 57

[22] W. F. Lange III, M. Enomoto, and H. I. Aaronson. Precipitate nucleation kinetics at grain boundaries. *International Materials Reviews*, 34:125–147, 1989. 9, 11

[23] P. C. Clemm and J. C. Fisher. The influence of grain boundaries on the nucleation of secondary phases. *Acta Metallurgica*, 3:70–73, 1955. 9, 13, 14

[24] H. I. Aaronson and J. K. Lee. Lectures on the theory of phase transformations. pages 165–229, 1999. 9

[25] S. E. Offerman, N. H. van Dijk, J. Sietsma, S. Grigull, E. M. Lauridsen, L. Margulies, H. F. Poulsen, M. Th. Rekveldt, and S. van der Zwaag. Grain nucleation and growth during phase transformations. *Science*, 298:1003–1005, 2002. 10, 63

[26] R. F. Mehl and W. D. Hagel. The austenite:pearlite reaction. In B. Chalmers and R. King, editors, *Progress in Metal Physics*, volume 6, pages 74–134, New York, 1956. Pergamon Press. 11

[27] J. W. Cahn and W. C. Hagel. Theory of pearlite reaction. In V. F. Zackay and H. I. Aaronson, editors, *Decomposition of Austenite by Diffusional Processes*, pages 131–192, New York, 1962. Intersciences. 12, 26, 29, 31, 66, 72

[28] R. F. Mehl and A. Dubé. The eutectoid reaction. In J. E. Mayer R. Smoluchowski and W. A. Weyl, editors, *In Phase Transformation in Solids*, pages 545–582, 1951. 14

[29] G. V. Smith and R. F. Mehl. Lattice relationships in decomposition of austenite to pearlite, bainite and martensite. *Trans. A.I.M.E.*, 150:211–226, 1942. 14

[30] C. S. Smith. Microstructure. *Trans. A. S. M.*, 45:533–575, 1953. 15, 114

[31] M. Hillert. Application of Gibbs energy-composition diagrams. *Lectures on the Theory of Phase Transformations*, pages 1–33, 1999. 15

[32] M. E. Nicholson. On the nucleation of pearlite. *Journal of Metals*, 6:1071–1074, 1954. 15

[33] K. C. Russell. private communication. August 1973. 16

[34] P. R. Engel. *The effect of interrupted quenching on the pearlite transformation.* PhD thesis, M.I.T, September 1973. 17

[35] F. B. Pickering T. Gladman, I. D. Mcivor. Some aspects of the structure-property relationships in high-carbon ferrite-pearlite steels. *J. Iron Steel Inst.*, 210:916–930, 1972. 16

[36] K. K. Ray and D. Mondal. The effect of interlamellar spacing on strength of pearlite in annealed eutectoid and hypoeutectoid plain carbon steels. *Acta Metallurgica et Materialia*, 39:2201–2208, 1991. 16

[37] B. L. Bramfit and A. R. Marder. A transmission electron microscopy study on the substructure of high purity pearlite. *Metallography*, 6:483–495, 1973. 18

[38] T. Takahashi, D. Ponge, and D. Raabe. Investigation of orientation gradients in pearlite in hypoeutectoid steel by use of orientation imaging microscopy. *Steel Research International*, 78(1):38–44, 2007. 18

[39] S. Z. Bokshtein. *Diffusion and Structure of Metals.* Metallurgiya Publishers, Moscow, 1973. 19, 22, 95

[40] J. Agren. A revised expression for the difusivity of carbon in binary Fe-C austenite. *Scripta Metallurgica*, 20:1507–1510, 1986. 20, 48

[41] R. Trivedi and G. M. Pound. Effect of concentration-dependent diffusion coefficient on the migration of interphase boundaries. *J. Appl. Phys.*, 38:3569–3576, 1967. 20, 54

[42] R. H. Siller and R. B. McLellan. The application of first order mixing statistics to the variation of the diffusivity of carbon in austenite. *Metallurgical Transactions*, 1:985–988, 1970. 20, 53

[43] H. K. D. H. Bhadeshia. Diffusion of carbon in austenite. *Metal Science*, 15:477–479, 1981. 21, 53

[44] J. Fridberg, L. E. Torndahl, and M. Hillert. Diffusion in iron. *Jernkont Ann.*, 153:263–276, 1969. 22, 36, 92, 102, 122

[45] S. Z. Bokshtein, S. T. Kishkin, and L. M. Moroz. Investigation of the structure of metals using radioiostopes. Technical report, Moscow, 1955. 22, 23

[46] N. Ridley. The pearlite transformation. In A. R. Marder and J. I. Goldstein, editors, *Phase transformations in ferrous alloys*, pages 201–236, Warrendale, PA, 1984. TMS-AIME. 25, 63, 94, 95, 100

[47] M.P. Puls and J.S. Kirkaldy. The pearlite reaction. *Metallurgical Transactions*, 3(11):2777–2796, 1972. 25, 64

[48] D. Cheetham and N. Ridley. Isovelocity and isothermal pearlite growth in a eutectoid steel. *J. Iron Steel Inst.*, 211:648–652, 1973. 25

[49] B. L. Bramfitt and A. R. Marder. Effect of cooling rate and alloying on the transformation of austenite. *Metallurgical Transactions*, 4:2291–2301, 1973. 26

[50] G. F. Bolling and R. H. Richman. Forced velocity pearlite. *Metallurgical and Materials Transactions B*, 1(8):2095–2104, 1970. 26

[51] J. D. Verhoeven and D. D. Pearson. Forced velocity pearlite in high purity Fe-C alloys. *Metallurgical Transactions*, 15A:1047–54, 1984. 26, 114, 118

[52] J. W. Cahn. The kinetics of cellular segregation reactions. *Acta Metallurgica*, 7:18–28, 1959. 26

[53] D. Turnbull. Theory of cellular precipitation. *Acta Metallurgica*, 3:55–63, 1955. 27, 47

[54] W. Seith and J. G. Laird. *Z. Metallkunde*, 24:193, 1932. 27

[55] K. Nakajima, M. Apel, and I. Steinbach. The role of carbon diffusion in ferrite on the kinetics of cooperative growth of pearlite: A multi-phase field study. *Acta Materialia*, 54:3665–3672, 2006. 30, 71, 72, 73, 79

[56] I. Steinbach and M. Apel. The influence of lattice strain on pearlite formation in Fe–C. *Acta Materialia*, 55:4817–4822, 2007. 31

[57] K. Hashiguchi and J. S. Kirkaldy. Pearlite growth by combined volume and phase boundary diffusion. *Scandinavian Journal of Metallurgy*, 13:240–248, 1984. 31, 51, 52, 57, 63, 65, 66

[58] D. Brown and N. Ridley. Rates of nucleation and growth and interlamellar spacings of pearlite in a low-alloy eutectoid steel. *J. Iron Steel Inst.*, 204:811–816, 1966. 31, 47, 63, 66, 67, 68

[59] M. Hillert. Swedish institute of metals research. Internal report, 1953. 32, 82

[60] J. S. Kirkaldy and R. C. Sharma. Stability principles for lamellar eutectoid(ic) reactions. *Acta Metallurgica*, 28:1009–1021, 1980. 93, 94

[61] G. R. Purdy, D. H. Weichert, and J. S. Kirkaldy. The growth of proeutectoid ferrite in ternary iron-carbon-manganese austenites. *Trans. TMS-AIME*, 230:1025–1034, 1964. 33

[62] D. E. Coates. Diffusional growth limitation and hardenability. *Metallurgical Transactions*, 4:2313–2325, 1973. 32, 82, 86, 87

[63] J. S. Kirkaldy. Diffusion in multicomponent metallic systems: I. phenomenological theory for substitutional solid solution alloys. *Canadian Journal of Physics*, 36:899–906, 1958. 33

[64] A. S. Pandit and H. K. D. H. Bhadeshia. Mixed diffusion-controlled growth of pearlite in binary steel. *Proceedings of Royal Society A*, 467:508–521, 2011. 33, 54, 71, 82, 94, 95, 99, 114

[65] R. C. Sharma and G. R. Purdy. Nucleation limitation and hardenability. *Metallurgical Transactions*, 4:2303–2311, 1973. 33

[66] S. A. Al-Salman, G. W. Lorimer, and N. Ridley. Pearlite growth kinetics and partitioning in a Cr-Mn eutectoid steel. *Metallurgical Transactions A*, 10A:1703–1709, 1979. 37, 85

[67] R. A. Ricks. Redistribution of substitutional alloying elements during formation of pearlite. In *Quantitative Microanalysis with High Spatial Resolution*, pages 85–89, March 1981. 37

[68] S. K. Tiwari and R. C. Sharma. The effect of alloying elements on pearlite growth. *Metallurgical Transactions A*, 16A:597–603, 1985. 37

[69] R. C. Sharma. PhD thesis, McMaster University, Hamilton, On, Canada, 1976. 37

[70] R. C. Sharma, G. C. Purdy, and J. S. Kirkaldy. Kinetics of the pearlite reaction in Fe-C-Cr. *Metallurgical Transactions*, 10A:1129–1139, 1979. 37, 83

[71] C. R. Hutchinson, R. E. Hackenberg, and G. J. Shiflet. The growth of partitioned pearlite in Fe-C-Mn steels. *Acta Materialia*, 52:3565–3585, 2004. 37, 40, 86, 89, 90

[72] J. W. Cahn and W. G. Hagel. Divergent pearlite in a manganese eutectoid steel. *Acta Materialia*, 11:561–574, 1963. 39, 107

[73] M. Hillert. An analysis of the effect of alloying elements on the pearlite reaction. In H. I. Aaronson, D. Laughlin, R. Sekerka, and C. Waymen, editors, *Solid-Solid Phase Transformations*, pages 789–806, Warrendale, Pennsylvania 15086, August 1981. The Metallurgical Society of AIME. 39

[74] H. K. D. H. Bhadeshia. Diffusional formation of ferrite in iron and its alloys. *Progress in Materials Science*, 29:321–386, 1985. 42, 50, 88

[75] K. A. Jackson and J. D. Hunt. *Trans. Amer. Inst. Min. (Metall.) Engrs.*, 236:1129–1139, 1966. 45

[76] Software. *MTDATA*. National Physical Laboratory (NPL), Teddington, UK, 2006. 48, 52, 54, 59, 63, 94, 95, 102, 122

[77] J. J. Kramer, G. M. Pound, and R. F. Mehl. The free energy of formation and the interfacial enthalpy in pearlite. *Acta Metallurgica*, 6:763–771, 1958. 48, 59, 62

[78] C. Capdevila, F. G. Caballero, and C. Garcia de Andres. Kinetics model of isothermal pearlite formation in a 0.4C-1.6Mn steel. *Acta Materialia*, 50:4629–4641, 2002. 48, 63, 94

[79] H. B. Aaron and H. I. Aaronson. Growth of grain boundary precipitates in Al-4%Cu by interfacial diffusion. *Acta Metallurgica*, 16:789–798, 1968. 50

[80] J. Goldman, H. I. Aaronson, and H. B. Aaron. Growth mechanisms of grain boundary allotriomorphs in Al-4%Cu at high homologous temperatures: Interfacial vs direct volume diffusion. *Metallurgical Transactions*, 1:1805–1810, 1970. 51

[81] Y. Suwa and Y. Saito. Two-dimensional grain growth with isotropic grain boundary energy, 1997. 52

[82] L. S. Darken. Diffusion of carbon in austenite with a discontinuity of composition. *Trans. AIME*, 180:430–438, 1949. 53

[83] C. Wells, W. Batz, and R. F. Mehl. Diffusion coefficient of carbon in austenite. *Trans. AIME*, 188:553–560, 1950. 53

[84] R. W. K. Honeycombe and H. K. D. H. Bhadeshia. *Steels: microstructure and properties*. Butterworth–Heinemann, London, U. K., 2nd edition, 1995. 57

[85] F. H. Buttner, H. Udin, and J. Wulff. *Trans. Amer. Inst. Min. (Metall.) Engrs.*, 191:1209, 1951. 62

[86] E. R. Funk, H. Udin, and J. Wulff. *Trans. Amer. Inst. Min. (Metall.) Engrs.*, 191(1206), 1951. 62

[87] S. K. Das, A. Biswas, and R. N. Ghosh. Volume fraction dependent particle coarsening in plain carbon steel. *Acta Metallurgica et Materialia*, 41(3):777–781, 1993. 62

[88] P. Deb and M. C. Chaturvedi. Coarsening behaviour of cementite particles in a ferrite matrix in 10b30 steel. *Metallography*, 15:341–354, 1982. 62

[89] A. G. Martin and C. M. Sellars. Measurement of interfacial energy from extraction replicas of particles on grain boundaries. *Metallography*, 3:259–273, 1970. 62

[90] M. Ruda, D. Farkas, and G. Garcia. Atomistic simulations in the Fe-C system. *Computational Materials Science*, 45:550–560, 2009. 62

[91] H. O. K. Kirchner, B. G. Mellor, and G. A. Chadwick. A calorimetric determination of the interfacial enthalpy of cu-in and cu-al lamellar eutectoids. *Acta Metallurgica*, 26:1023–1031, 1978. 62

[92] F. C. Hull, R. C. Colton, and R. F. Mehl. Rate of nucleation and rate of growth of pearlite. *Trans. AIME*, 150:185–207, 1942. 66, 68

[93] Robert C. Weast, editor. *CRC handbook of chemistry and physics*. CRC Press, Inc, Boca Raton, FL, 69 edition, 1988. 72

[94] R. B. McLellan, M. L. Rudee, and T. Ishibachi. The thermodynamics of dilute interstitial solid solutions with dual–site occupancy and its application to the diffusion of carbon in alpha–iron. *Trans. A.I.M.E.*, 233:1939–1943, 1965. 75

[95] H. K. D. H. Bhadeshia. Map programs. 75

[96] J. Chance and N. Ridley. Chromium partitioning during isothermal transformation of a eutectoid steel. *Metallurgical Transactions A*, 12A:1205–1213, 1981. 85

[97] D. E. Coates. Diffusion controlled precipitate growth in ternary systems I. *Metallurgical Transactions*, 3:1203–1212, 1972. 86, 87

[98] I. Kaur, Y. Mishin, and W. Gust. *Fundamentals of Grain and Interphase Boundary Diffusion*. John Wiley Sons LTD, 3rd edition. 92

[99] A. M. Brown and M. F. Ashby. Correlations for diffusion constants. *Acta Metallurgica*, 28:1085–1101, 1980. 92

[100] N. A. Gjostein. Short circuit diffusion. In *Diffusion*, pages 241–274, Metals Park, OH, 1973. American Society for Metals. 92

[101] D. W. James and G. M. Leak. Grain boundary diffusion of iron, cobalt and nickel in alpha-iron and of iron in gamma-iron. *Philosophical Magazine*, 12:491–503, 1965. 92

[102] W. Gust, S. Mayer, A. Bogel, and B. Predel. Generalised representation of grain boundary self-diffusion data. *Journal De Physique*, 46:537–544, 1985. 92

[103] J. Fridberg and M. Hillert. Ortho–pearlite in silicon steels. *Acta Metallurgica*, 18:1253–1260, 1970. 107

[104] T. Oyama, O. D. Sherby, J. Wadsworth, and B. Walser. Application of the divorced eutectoid transformation to the development of fine-grained, spheroidized structures in ultrahigh carbon steels. *Scripta Metallurgica*, 18:799–804, 1984. 110

[105] C. K. Syn, D. R. Lesuer, and O. D. Sherby. Influence of microstructure on tensile properties of spheroidised ultrahigh-carbon (1.8% C) steel. *Metallurgical and Materials Transactions A*, 25A:1481–1493, 1994.

[106] E. M. Taleff, C. K. Syn, D. R. Lesuer, and O. D. Sherby. Pearlite in ultrahigh carbon steels: Heat treatments and mechanical properties. *Metallurgical and Materials Transactions A*, 27A:111–118, 1996. 110

[107] K. Honda and S. Saito. *J. Iron Steel Inst.*, 102:261–269, 1920. 110

[108] J. D. Verhoeven and E. D. Gibson. The divorced eutectoid transformation in steel. *Metallurgical and Materials Transactions A*, 29A:1181–1189, 1998. 112

[109] J. D. Verhoeven. The role of the divorced eutectoid transformation in the spheroidization of 52100 steel. *Metallurgical and Materials Transactions A*, 31A:2431–2438, 2000. 112

[110] H. K. D. H. Bhadeshia. *Steels for Bearings*, chapter 7, page 40. SKF, 2011. 113

[111] N. V. Luzginova, L. Zhao, and J. Sietsma. The cementite spheroidization process in high-carbon steels with different chromium contents. *Metallurgical and Materials Transactions A*, 39A:513–521, 2008. 112, 117, 121, 123

[112] A. Pandit and H. K. D. H. Bhadeshia. Diffusion–controlled growth of pearlite in ternary steels. to be published in Proceedings of Royal Society A, 2011. 114

[113] D. Venugopalan and J. S. Kirkaldy. New relations for predicting the mechanical prperties of quenched and tempered low alloy steels. In D. V. Doane and J. S. Kirkaldy, editors, *Hardenability Concepts with Applications to Steels*, pages 249–268, Warrendale, PA, October 1977. The Metallurgical Society of AIME. 121

[114] Steel unversity website. 122